Negative Ions in Space

Published in:
Chemical Reviews

Document Version:
Publisher's PDF, also known as Version of record

Queen's University Belfast - Research Portal:
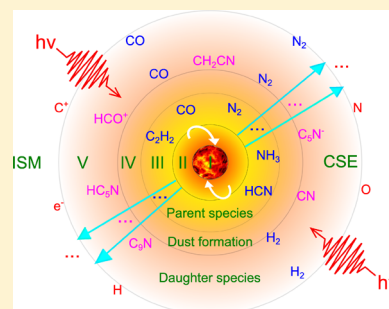Link to publication record in Queen's University Belfast Research Portal

Negative Ions in Space

Thomas J. Millar,*,† Catherine Walsh,‡,§ and Thomas A. Field‖

†Astrophysics Research Centre, School of Mathematics and Physics, and ‖Centre for Plasma Physics, School of Mathematics and Physics, Queen's University Belfast, University Road, Belfast BT7 1NN, U.K.

‡Leiden Observatory, Leiden University, P.O. Box 9513, 2300 RA Leiden, The Netherlands

§School of Physics and Astronomy, University of Leeds, Leeds LS2 9JT, U.K.

ABSTRACT: Until a decade ago, the only anion observed to play a prominent role in astrophysics was H^-. The bound−free transitions in H^- dominate the visible opacity in stars with photospheric temperatures less than 7000 K, including the Sun. The H^- anion is also believed to have been critical to the formation of molecular hydrogen in the very early evolution of the Universe. Once H_2 formed, about 500 000 years after the Big Bang, the expanding gas was able to lose internal gravitational energy and collapse to form stellar objects and "protogalaxies", allowing the creation of heavier elements such as C, N, and O through nucleosynthesis. Although astronomers had considered some processes through which anions might form in interstellar clouds and circumstellar envelopes, including the important role that polycyclic aromatic hydrocarbons might play in this, it was the detection in 2006 of rotational line emission from C_6H^- that galvanized a systematic study of the abundance, distribution, and chemistry of anions in the interstellar medium. In 2007, the Cassini mission reported the unexpected detection of anions with mass-to-charge ratios of up to ∼10 000 in the upper atmosphere of Titan; this observation likewise instigated the study of fundamental chemical processes involving negative ions among planetary scientists. In this article, we review the observations of anions in interstellar clouds, circumstellar envelopes, Titan, and cometary comae. We then discuss a number of processes by which anions can be created and destroyed in these environments. The derivation of accurate rate coefficients for these processes is an essential input for the chemical kinetic modeling that is necessary to fully extract physics from the observational data. We discuss such models, along with their successes and failings, and finish with an outlook on the future.

CONTENTS

1. INTRODUCTION: ANIONS IN ASTRONOMY

The origin of the absorption of radiation in the outer regions of cool stellar atmospheres was one of the major problems in astrophysics in the early years of the 20th century. Astronomers believed that the continuous opacity in the visible region of the spectrum was provided by metal atoms although with an unphysically large abundance, ∼1:50, with respect to hydrogen, compared to the observed ratio of ∼1:1000. In 1939, Wildt[1] calculated the absorption coefficient of H^- and showed that it dominated the visible opacity in stars, such as the Sun, with photospheric temperatures less than 7000 K and was consistent

with a metal/hydrogen ratio of 1:1000. In stellar atmospheres, the photoionization of metal atoms provides the electrons that form H⁻. Because the electron affinity of hydrogen is 0.75 eV, H⁻ provides continuum opacity at $\lambda < 1650$ nm.

The hydrogen anion also plays an extremely important role in the origin of structures in the early Universe. Once the Universe had expanded and cooled sufficiently to allow the protons and electrons to recombine to form atomic hydrogen—the so-called "recombination era", when the temperature was ~4000 K, or some 400 000 years after the Big Bang—H⁻ could form through radiative attachment[2]

$$H + e^- \rightarrow H^- + h\nu \qquad (1)$$

followed by associative detachment to form H_2

$$H^- + H \rightarrow H_2 + e^- \qquad (2)$$

The presence of H_2, even at a concentration as low as 1 ppm, has important consequences for the expansion of the Universe, because it is a very effective coolant through rovibrational and quadrupole rotational transitions, reducing the thermal pressure of the gas by over an order of magnitude and thereby dissipating its gravitational energy. If the cooling time is shorter than the expansion time, then regions of gas can undergo collapse to form stellar objects. Detailed calculations show that gas at 1000 K can form H_2 rapidly enough to allow gas masses of 10^6 $M_\odot$ (solar masses) to collapse and the first generation of stars in the Universe, the so-called "Population M" stars, to form.[3]

In 1973, Dalgarno and McCray[4] considered the role of anions, specifically H⁻, O⁻, C⁻, CH⁻, CH_2^-, CN⁻, and S⁻, in the formation of simple molecules in interstellar clouds. To be efficient in forming these anions, electrons must be relatively abundant to allow radiative attachment to form anions. The rate coefficients for electron attachment to these neutrals, however, are very small, typically less than 10^{-15} cm³ s⁻¹, and reactions involving these negatively charged species are generally unimportant compared to other gas-phase processes in interstellar clouds.

Sarre[5] subsequently discussed the formation of C_2^-, CN⁻, and C_2H^- and their likely detection in interstellar clouds. His criteria included (i) a high electron affinity, (ii) a low reactivity with abundant interstellar molecules (e.g., H_2), (iii) a high dissociation energy, (iv) a large dipole moment, and (v) a linear configuration to enhance the line intensity. His foresight allowed him to identify C_2H^- and CN⁻ as potentially observable molecular anions. He noted, for example, that C_2H^- could be formed by a number of reactions including proton transfer

$$H^- + C_2H_2 \rightarrow C_2H^- + H_2 \qquad (3)$$
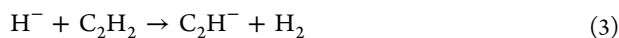
dissociative electron detachment, although this particular reaction is endoergic

$$C_2H_2 + e^- \rightarrow C_2H^- + H \qquad (4)$$

charge exchange with an anion

$$X^- + C_2H \rightarrow C_2H^- + X \qquad (5)$$

and radiative attachment[6]

$$C_2H + e^- \rightarrow C_2H^- + h\nu \qquad (6)$$

Although Sarre[5] briefly discussed the likely rotational spectrum of these ions, he did not calculate abundances. In 1981, Herbst[7] considered the production of more complex

ions, noting that radiative electron attachment to large neutral radicals with large electron affinities could be efficient. He took this early work one stage further by deriving a theoretical expression for radiative attachment rate coefficients (using phase-space theory) under typical interstellar conditions. He determined the radiative attachment rate, $k_{ra} \propto N_v(EA)$, where $N_v(EA)$ is the vibrational density of states of the anion at an internal energy equal to the electron affinity (EA). $N_v(EA)$ increases with increasing molecular size and electron affinity. Herbst[7] listed several potential molecules that can readily form anions through radiative attachment with rate coefficients close to the collisional limit ($\sim10^{-7}$ cm³ s⁻¹) at temperatures between 10 and 50 K: C_4H, C_3N, C_5N, C_7N, C_9N, C_2H_2CN, C_2H_3O, and $C_2H_3O_2$. Assuming reaction with H atoms as the dominant destruction mechanism for molecular anions under dense cloud conditions, Herbst calculated a typical steady-state anion-to-neutral ratio between ~0.01 and 0.1, that is, between ~1% and 10%.[7] This prediction was later borne out in astrophysical observations.

In 1996, Bettens and Herbst[8] included radiative electron attachment to C_n and C_nH ($n = 10-23$) in a model for fullerene formation in diffuse clouds, with destruction through photodetachment and reactions with H and C atoms. In 2000, this work was extended downward in size to linear carbon clusters with more than three atoms by Terzieva and Herbst[9] in response to suggestions that absorption by electronic transitions in species such as C_6^-, C_7^-, and C_8^- might be responsible for at least some of the 300 or so diffuse interstellar bands (DIBs). These have been observed, but still unidentified, in interstellar optical spectroscopy for nearly 100 years, although recently two DIBs near 960 nm were shown experimentally to be due to $C_{60}^{+\cdot}$.[10] Although it is now clear that these anions are not responsible for the DIBs—Rudkjøbing[11] had previously and erroneously suggested that H⁻ might be responsible for several DIBs—Terziera and Herbst showed that radiative attachment of electrons occurs in every collision for molecules with six or more carbon atoms.

The physical conditions in the clouds modeled by Bettens and Herbst and by Terziera and Herbst, namely, low densities and high UV radiation fields, meant that the abundances of anions were predicted to be small and undetectable.

The first work to predict observable column densities of anions was that of Millar et al.,[12] who, in 2000, used the chemistry of Bettens and Herbst[8] and the rate coefficients calculated by Terziera and Herbst[9] in a model of the circumstellar envelope (CSE) around the carbon-rich, asymptotic giant branch (AGB) star IRC+10216, an envelope that is now known to contain over 80 molecular species, including many linear carbon-chain species. In brief, Millar et al. predicted anion-to-neutral column density ratios of up to 25% and suggested that the C_nH^- species might be detectable by radio astronomy techniques.[12] As we shall see, this prediction was fulfilled in 2006 with the identification of C_6H^- in this CSE.[13] More complete details of the model calculations are provided in section 4.

In 1988, Lepp and Dalgarno[14] studied the chemistry of polycyclic aromatic hydrocarbons (PAHs) in dense interstellar clouds. Large molecules, such as PAHs, have long been postulated as possible carriers of the diffuse interstellar bands and, in particular, of the infrared emission features observed in the spectra of various objects.[15] Lepp and Dalgarno[14] included the formation of negatively charged PAHs through radiative electron attachment, adopting a rate coefficient equal to 6 ×

10^{-7} cm^3 s^{-1}.[16] They included destruction through mutual neutralization with all cations, M$^+$, with a rate coefficient on the order of $7.5 \times 10^{-8}(T/300)^{-0.5}$.[16] They assumed that associative detachment reactions with neutral atoms have a negligible rate at the low temperatures of dark clouds because these reactions have activation barriers. They found that, for moderate fractional abundances of PAHs, $\gtrsim 10^{-8}$, PAH$^-$ species became more abundant than electrons, essentially becoming the main charge carriers in dense clouds. They also determined that, at low PAH fractional abundances, $<10^{-8}$, $n(\text{PAH}^-)/n(\text{PAH}) \approx 1$. The anion-to-neutral ratio decreases as the PAH fractional abundance increases; however, even at large values, $\gtrsim 10^{-5}$, the anion-to-neutral ratio remains significant, $\sim 1\%$.

2. OBSERVATIONS

As mentioned in section 1, the first direct detection of an anion in space was the continuous absorption that H$^-$ provides in cool stars such as the Sun. At wavelengths longer than 1650 nm, the bound−free continuum disappears, and free−free transitions dominate with a cross section that increases with wavelength. In principle, this change in cross section should be observable at 1.65 μm, and observations of IR excess radiation in Be stars[17] were argued to be consistent with H$^-$. If so, H$^-$ should be detectable through resonance features near 113 nm in the far-UV. Early attempts to detect these features[18] gave an upper limit to the H$^-$ abundance that was about 5 times less than that derived from the IR observations.[17] Subsequently, Ross et al.[19] used the FUSE (Far Ultraviolet Spectroscopic Explorer) satellite to search for H$^-$ absorption toward a number of interstellar sources and planetary nebulae, but no detections were made, with upper limits in the column densities between 2 and 3 orders of magnitude larger than those predicted. Evidently, there is no expectation that astronomical lines from H$^-$ will be detectable in the near future.

The physical conditions in many astrophysical environments are extreme, compared with those here on Earth. Densities and temperatures are typically very low; number densities range from $n \approx 10$ cm^{-3} in the diffuse interstellar medium (ISM) to $\gtrsim 10^{10}$ cm^{-3} in the midplanes of protostellar disks. At a temperature of 100 K, these densities correspond to pressures of $\sim 10^{-16}$−10^{-7} mbar. Gas temperatures range from ~ 10 K in dense, dark molecular clouds to ≥ 1000 K in irradiated environments such as photon-dominated regions (PDRs) or the surfaces of protoplanetary disks. As such, the gas is in neither chemical, nor thermodynamic, equilibrium and is likely not at steady state, even over the long time scales often encountered in the ISM, $\gtrsim 10^4$ years.

Molecules are excellent probes of astrophysical environments. They emit (and absorb) radiation across the electromagnetic spectrum from ultraviolet (UV) wavelengths (nanometers) to radio wavelengths (centimeters) through electronic, vibrational, and rotational transitions. Molecules thus trace material across a large temperature range, from the coldest regions in space, ~ 10 K, to the hottest, $\gg 1000$ K. Astrophysicists exploit our knowledge of the chemistry of molecules to probe the physical and chemical conditions in astrophysical sources. Different combinations of physical conditions (e.g., gas temperature, gas density, UV radiation field) lead to the preferential formation of particular species, for example, products of photodissociation can be used to trace molecular gas that is irradiated by nearby stars. Observations of the line emissions from both the reactants and products of photodissociation (e.g., HCN and CN) can provide a measurement of the strength of the radiation field. In addition, observations of multiple line transitions of a single species can give estimates of the gas excitation temperature, observations of multiple isotopologues of a single species (e.g., ^{12}C^{16}O, ^{13}C^{16}O, and ^{12}C^{18}O) can reveal the optical depth of the emitting gas, and observations of multiple species in a particular region can reveal the underlying elemental composition of the source. Molecules are very powerful tools in astronomy, and physicochemical models play a vital role in the analysis and interpretation of astrophysical observations.

As mentioned in section 1, there have been a number of suggestions that anions might be responsible for some of the DIBs. Sarre[20] suggested that many of the DIBs might arise from electronic transitions involving dipole-bound states of anions. Tulej et al.[21] noted that five absorption bands in the optical spectrum of C$_7^-$ coincided with known DIBs, although this suggestion was refuted when high-resolution astronomical and laboratory spectroscopy became available. Sarre noted a close coincidence between the DIB at 803.79 nm and an absorption from the ground state of CH$_2$CN$^-$. Cordiner and Sarre[22] tested this hypothesis by obtaining spectra of eight stars and showed reasonable agreement between observations and laboratory measurements. Subsequently, Fortenberry et al.[23] calculated accurate rotational parameters for the anion. The presence of CH$_2$CN$^-$ in the diffuse ISM with sufficient abundance to produce the 803.79-nm DIB can thus be tested through future radio spectroscopic measurements.

The most sensitive method for detecting interstellar molecules in cold interstellar clouds is to search for rotational line transitions that exist in the radio and submillimeter regions of the spectrum and are thus amenable to the techniques of radio astronomy. Although more than 1000 anions are known in the laboratory, only two, OH$^-$ and SH$^-$, had measured rotational spectra before 2006. At that time, McCarthy et al.[13] reported the laboratory spectrum of C$_6$H$^-$ and recognized that these transitions corresponded to a set of harmonically related unidentified lines in the spectrum of IRC+10216[24] that had indeed been suggested to be C$_6$H$^-$ by Aoki.[25] In addition, McCarthy et al.[13] observed seven lines in IRC+10216 and two lines in the cold, dark cloud TMC-1, another rich source of carbon-chain molecules, and derived column densities and anion-to-neutral abundance ratios of 1−5% in IRC+10216 and $\sim 2.5\%$ and an overall column density of 10^{11} cm^{-3} in TMC-1, consistent with the predictions of Millar et al.[12] for IRC+10216. Brünken et al. later performed additional observations of C$_6$H$^-$ and its neutral counterpart, C$_6$H, in TMC-1, deriving an anion column density of 1.2×10^{11} cm^{-2} and an anion-to-neutral ratio of 1.6%.[26]

The ability of McCarthy and colleagues to measure rotational frequencies of hydrocarbon anions at centimeter and millimeter wavelengths[27] led to a rapid increase in their astronomical detection. In 2007, C$_8$H$^-$ was detected in TMC-1 by Brünken et al.,[26] with an anion-to-neutral ratio of 4.6%, and in IRC+10216 by Remijan et al.,[28] with a ratio of 2.6%, and C$_4$H$^-$ was observed in IRC+10216.[29]

Figure 1 shows the series of rotational transitions of C$_8$H$^-$ detected toward the dark cloud TMC-1,[26] and Figure 2 shows the characteristic double-peaked line profiles from its rotational transitions toward IRC+10216.[28] These double-peaked profiles indicate that the emitting volume of C$_8$H$^-$ is confined to a hollow shell, at least partially resolved at the spatial resolution of the telescope, in the outer circumstellar envelope. Subsequent laboratory measurements led to the detection of
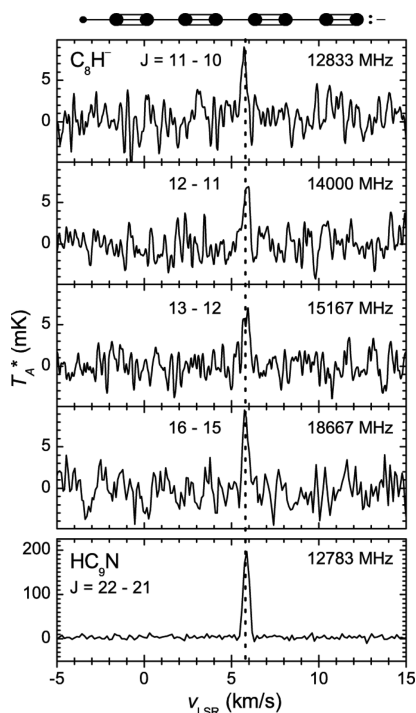
Figure 1. Rotational line profiles from C_8H^- anions in the cold dark cloud TMC-1.[26] Reproduced with permission from ref 26. Copyright 2007 IOP Publishing.

Figure 2. Rotational line profiles from C_8H^- anions in the circumstellar envelope of the carbon-rich AGB star IRC+10216.[28] Reproduced with permission from ref 28. Copyright 2007 IOP Publishing.

C_3N^- in IRC+10216,[30] and theoretical calculations were used to support the identification of 11 emission lines in IRC+10216 as C_5N^-.[31] Smaller anions are more difficult to detect, in part because of their very small radiative attachment rate coefficients, but CN^- has now been observed and a low upper limit for C_2H^- in IRC+10216 has been given.[32]

The presence of C_4H^- in the protostellar source L1527 was reported in 2008 by Sakai et al.[33] and Agúndez et al.[34] In more recent years, a number of authors have detected anions in a range of sources, most notably C_6H^- in dark clouds, prestellar cores and protostellar envelopes[35−38] including the first detection of C_4H^- in the dark cloud TMC-1.[38] Note that CN^-, C_3N^-, and C_5N^- remain undetected in dark clouds.

We present a summary of observed column densities and anion-to-neutral ratios and compare them to various model results (see section 4 for further details on the latter) in Table 1. A few simple conclusions can be drawn from the results in this table. The first is that, for the carbon-chain anions detected in interstellar clouds, anion-to-neutral abundance ratios are $\sim$1−5% for C_6H^- and C_8H^- and typically 2 orders of magnitude smaller for C_4H^-, presumably reflecting the smaller rate coefficient for electron attachment to C_4H. The second is that there is weak evidence that the ratio increases with molecule size, cf. C_4H^-, C_6H^-, and C_8H^- in TMC-1 and IRC +10216 and CN^-, C_3N^-, and C_5N^- in IRC+10216. Again, this is qualitatively consistent with an increase in the attachment rate coefficient for larger species.[6] Finally, in this section, it is worth pointing out that the anions C_4H^- and C_6H^- have been searched for unsuccessfully in photon-dominated regions[34,39] with upper limits on the anion-to-neutral ratios of 0.03−0.06%.

Titan, the largest moon orbiting Saturn and the second largest in the Solar System, is the only satellite with an extensive, dense atmosphere. The Voyager missions to Saturn revealed that Titan had an atmosphere composed predom-

inantly of N_2, similar to Earth.[50] The pressure at the surface is also similar, $\sim$1.5 bar; however, the surface temperature is much lower, $\sim$90 K.[50] Additional minor species identified through observations with the UVS (ultraviolet spectrometer) and IRIS (infrared interferometer spectrometer) instruments on Voyager included CH_4 and H_2 and a plethora of hydrocarbons and nitrogen-containing species: C_2H_2, C_2H_4, C_2H_6, CH_3C_2H, C_3H_8, C_4H_2, HCN, HC_3N, NCCN, and CH_3D.[51−55] The oxygen-containing molecules CO and CO_2 were also detected.[56,57]
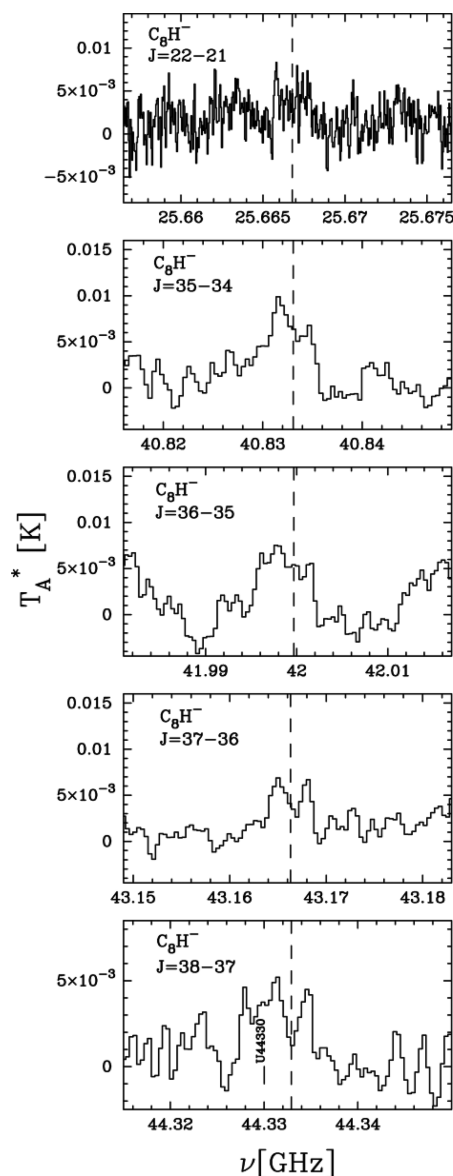
In recent times, the atmosphere of Titan has been under increased investigation because of the Cassini−Huygens mission. The ion neutral mass spectrometer (INMS) on Cassini revealed the presence of many molecular radicals and ions in the upper atmosphere of Titan.[58−60] These species are likely formed through the dissociation and/or ionization of N_2 and CH_4 by solar extreme-UV (EUV) and soft X-ray photons. The production of highly reactive radicals and ions drives a rich

Table 1. Anion Column Densities $(cm^{-2})^a$ and Anion-to-Neutral Ratios^b: Observations versus Model Results

source/model	C_2H^-	C_4H^-	C_6H^-	C_8H^-	CN^-	C_3N^-	C_5N^-	ref(s)
			Dark Clouds and Prestellar Cores					
TMC-1	≤2.2(11) [≤0.033%]	8(9) [0.0012%]	1.2(11) [1.6%]	2.1(10) [4.6%]	≤1.4(12) [≤3.0%]	≤7.0(11) [≤0.74%]	–	26, 30, 34, 35, 38
L1544	–	–	3.1(10) [2.5%]	–	–	–	–	39
L1512F	–	–	3.4(10) [4.0%]	–	–	–	–	39
Lupus-1A	–	4.4(10) [0.0088%]	6.5(10) [2.1%]	1.7(10) [4.7%]	–	–	–	36
L1251A	–	–	2.7(10) [3.6%]	–	–	–	–	37
L1512	–	–	2.0(10) [4.1%]	–	–	–	–	37
Millar et al., 2007	–	5.6(10) [0.13%]	1.4(11) [5.2%]	3.3(10) [4.2%]	–	–	–	40
Walsh et al., 2009	–	1.1(12) [0.92%]	1.0(12) [5.3%]	2.5(11) [4.0%]	2.9(10) [0.010%]	1.6(10) [0.15%]	6.5(10) [6.7%]	41
Cordiner and Charnley, 2012^c	6.6(8) [−]	2.0(11) [0.29%]	9.2(11) [2.3%]	7.3(11) [−]	7.1(9) [−]	8.6(9) [−]	3.5(10) [−]	42
Cordiner and Charnley, 2012^d	1.3(9) [−]	4.0(10) [0.42%]	1.1(10) [3.4%]	2.2(9) [−]	1.0(9) [−]	3.0(8) [−]	1.6(9) [−]	42
McElroy et al., 2013^e	3.1(10) [0.28%]	1.6(11) [0.76%]	4.2(11) [2.5%]	4.2(10) [1.8%]	2.0(10) [0.018%]	9.2(9) [0.54%]	3.4(10) [4.2%]	43
McElroy et al., 2013^f	–	1.4(10) [0.4%]	4.5(9) [3.2%]	1.2(8) [2.5%]	1.3(9) [0.0062%]	5.8(9) [0.69%]	–	43
			Protostellar Envelopes					
L1527	≤1.8(10) [≤0.0036%]	1.6(10) [0.011%]	4.8(10) [9.3%]	–	≤9.8(10) [≤0.2%]	–	–	34, 35, 44
Harada and Herbst, 2008	–	6.6(11) [8.5%]	5.9(10) [51%]	1.1(11) [46%]	–	3.3(11) [9.2%]	–	45
Cordiner and Charnley, 2012	3.5(9)	3.5(10) [0.33%]	1.0(10) [2.4%]	1.6(9)	1.2(10)	1.2(9)	1.3(10)	42
			Circumstellar Envelopes					
IRC+10216	≤7.0(10) [≤0.0014%]	7.1(11) [0.024%]	4.1(12) [6.2%]	2.1(12) [26%]	5.0(12) [0.25%]	1.6(12) [0.52%]	3.4(12) [13%]	28−32
Millar et al., 2000	–	–	–	2.7(13) [25%]	2.5(09) [0.00025%]	4.0(11) [0.125%]	1.3(13) [9.3%]	12
Millar et al., 2007	–	1.0(13) [0.77%]	1.7(14) [30%]	5.8(13) [28%]	–	–	–	40
Remijan et al., 2007	–	6.4(12) [3.8%]	2.7(13) [210%]	6.1(12) [240%]	–	–	–	28
Cordiner and Millar, 2009^g	2.3(10) [0.00037%]	2.1(13) [1.2%]	1.1(14) [7.3%]	2.1(13) [4.3%]	1.2(12) [0.046%]	7.7(11) [1.4%]	1.7(13) [6.8%]	46
Cordiner and Millar, 2009^h	5.5(10) [0.00098%]	2.5(13) [1.5%]	9.6(13) [7.4%]	2.0(13) [4.9%]	1.3(12) [0.059%]	9.0(11) [1.3%]	1.7(13) [7.1%]	46
Agúndez et al., 2010	6.8(10) [0.00038%]	2.0(11) [0.0089%]	1.8(14) [7.9%]	2.4(14) [32%]	8.4(12) [0.080%]	3.3(12) [0.43%]	3.9(13) [64%]	32
Woods et al., 2012	8.1(8) [0.000001%]	7.2(14) [5.9%]	8.2(14) [25%]	2.1(14) [20%]	3.0(12) [0.013%]	1.6(12) [0.42%]	1.3(14) [17%]	47
McElroy et al., 2013	1.5(10) [0.00015%]	1.3(13) [2.0%]	8.3(13) [15%]	2.9(12) [2.4%]	7.0(11) [0.017%]	1.0(12) [0.20%]	7.8(12) [22%]	43
Kumar et al., 2013	4.7(10) [0.00053%]	1.2(13) [2.2%]	6.8(13) [11%]	3.9(12) [2.3%]	7.0(11) [0.015%]	8.7(11)[0.13%]	8.2(12) [18%]	48
Millar, 2016^i	1.0(10) [0.00012%]	1.7(12) [0.15%]	6.7(13) [4.9%]	9.1(12) [1.5%]	1.8(12) [0.019%]	2.8(12) [0.11%]	1.7(13) [8.4%]	49

$^a a(b) = a \times 10^b$. ^{b}Square brackets contain the percentage anion/neutral abundance ratio where available. $^c n = 10^4$ cm^{-3}. $^d n = 10^5$ cm^{-3}. ^{e}Using the RATE12 gas-phase network. ^{f}Using the uva.kida.2011 gas-phase network. ^{g}Results from a "no shells" model. ^{h}Results from model with density-enhanced shells. ^{i}Results from a "clumpy" model of the envelope.

chemistry that produces hydrocarbons and N-containing species with observed latitudinal and diurnal variations in abundances.[61−63]

Coates et al. reported the detection of negative ions in Titan's atmosphere at altitudes between 950 and 1400 km using the electron spectrometer (ELS), one of the three sensors on the Cassini plasma spectrometer (CAPS).[64] The negative-ion density was estimated at ~100 cm^{-3} with masses within the range from 10 to ~10 000 amu/q. Further flybys and analyses demonstrated latitudinal and altitudinal dependence of the anion density with the heaviest anions found at high latitudes and low altitudes.[65] The detection of negative ions was considered surprising because early models predicted that the electron density and the abundances of parent neutrals were too low for efficient anion formation in the upper atmosphere and would instead be constrained to the lower ionosphere

where three-body electron attachment was expected to occur.[66−68]

Following the observational confirmation of molecular anions in Titan's ionosphere, Vuitton et al. concluded that cyano-containing molecules (−CN; e.g., C_3N and C_5N) and ethynyl-containing species (−C_2H; e.g., C_nH, n = 2, 4, 6, and 8) were likely candidates, as found in previous investigations into potential interstellar anions.[5,7]

Molecular anions were also detected in the coma of comet Halley. Chaizy et al. reported peaks in the mass spectrum, measured by the Giotto spacecraft, at 7−19, 22−65, and 85−110 amu/q at a distance of ∼2300 km from the nucleus.[70] They postulated some candidate species: CH^-, OH^-, CN^-, and heavier (possibly organic) HCON-containing molecules. Certainly, some of the molecular anions now identified in space fall within these mass ranges: C_2H^- (25 amu), CN^- (26 amu), C_4H^- (49 amu), C_3N^- (50 amu), and C_8H^- (97 amu).

3. CHEMISTRY OF ANIONS

A (nonexhaustive) list of the different mechanisms for the formation and destruction of negative ions is provided in Table 2. These mechanisms are primarily discussed as gas-phase processes, but they also occur on surfaces; surface processes are discussed in section 3.4.

Table 2. Mechanisms of Negative-Ion Formation and Destruction

Formation	
radiative electron attachment	$A + e^- \rightarrow A^- + h\nu$
collisional electron attachment	$A + e^- + C \rightarrow A^- + C$
dissociative electron attachment	$AB + e^- \rightarrow A + B^-$
ion-pair formation/polar dissociation	$AB + h\nu \rightarrow A^- + B^+$
electron-induced ion-pair formation	$AB + e^- \rightarrow A^- + B^+ + e^-$
collision-induced ion-pair formation	$AB + C \rightarrow A^- + B^+ + C$
Destruction	
photodetachment	$A^- + h\nu \rightarrow A + e^-$
electron-impact detachment	$A^- + e^- \rightarrow A + 2e^-$
associative detachment	$A^- + B \rightarrow AB + e^-$
collisional detachment	$A^- + B \rightarrow A + B + e^-$
mutual neutralization	$A^- + B^+ \rightarrow A + B$
Formation and Destruction	
charge transfer	$A^- + B \rightarrow A + B^-$
proton transfer	$A^- + HB \rightarrow AH + B^-$

3.1. Formation Mechanisms

The most important formation mechanisms included in Table 2 are initiated by attachment of a free electron. The energies of most free electrons in astrophysical environments will reflect local temperatures; in the range from 10 to 1000 K, the energy kT varies from ∼0.9 to 90 meV. Experiments and calculations in which free electrons strike atoms and molecules generally focus on electron energy ranges from 0 to ∼10 eV. Therefore, many experimental observations and calculated predictions of negative-ion formation occur at electron energies an order of magnitude above these kT values and might not be relevant to models of negative-ion formation. Most electron attachment experiments and calculations, however, are sensitive to processes that occur at 20 meV and lower electron energies, and results in this energy range can be useful.

Below, some processes where electron attachment occurs above energies that might be expected in astrophysical environments are considered because the physics of electron attachment is the same for electrons with energies from below 1 meV to energies up to and above 10 eV.

In the first step of electron attachment processes, a free electron, e^-, becomes attached to an atom or molecule, A, to form a superexcited metastable negative-ion state, A^{-*}, which can be represented by

$$A + e^- \rightarrow A^{-*} \tag{7}$$

Here, "superexcited" indicates that the anionic state is higher in energy than the ionization limit of the negative ion and can spontaneously lose an electron by autoionization, also called autodetachment

$$A^{-*} \rightarrow A + e^- \tag{8}$$

Hence, superexcited negative ions are often referred to as a "temporary negative ions" or "transient negative ions".[71]

A stable anion is formed following electron impact if the superexcited anion loses energy before it autoionizes; energy is lost by photon emission in radiative attachment, in collisions in collisional attachment, and for molecules by fragmentation in dissociative electron attachment. In dilute astrophysical environments, collisional stabilization will be negligible, except for atoms or molecules already adsorbed onto surfaces.

Thus, the rate of anion formation depends strongly on the lifetime of the superexcited anion. If the lifetimes of superexcited anions are short compared to photon emission lifetimes, the times between collisions, and the rates of molecular fragmentation, then the rates of anion formation will be very small. At particular electron energies, however, resonances can occur where the lifetimes of superexcited anions are long enough for significant rates of negative-ion formation to occur. More rigorously, if the rate of electron attachment is k_{att}, the rate of autodetachment is k_{det} and the rate of energy loss by, for example, photon emission is $k_{h\nu}$ then the rate of radiative electron attachment, k_{ra}, will be given by

$$k_{ra} = \frac{k_{att} k_{h\nu}}{k_{det} + k_{h\nu}} \tag{9}$$

If the rate of detachment, k_{det}, is significantly greater than the rate of photon emission, $k_{h\nu}$, then eq 9 can be simplified to give

$$k_{ra} = \frac{k_{h\nu}}{k_{det}} k_{att} \tag{10}$$

and it is clear that the ratio of the rate of energy loss, here photon emission, to autodetachment is critical to the rate of anion formation.

There is, in fact, a second mechanism for radiative attachment in which the electron emits a photon as it attaches to the atom or molecule. In this mechanism, a stable anion is formed immediately as energy is lost by photon emission during attachment. This mechanism is reviewed in section 3.1.2.

3.1.1. Electron Attachment. The two most important mechanisms for electron attachment are shape resonances and Feshbach resonances. In shape resonances, the shape of the potential in which the free electron moves while approaching the atom or molecule includes a barrier through which the electron can tunnel and behind which it can then become trapped. The clearest cause of a shape resonance is when an electron with angular momentum greater than zero approaches an atom or molecule. Figure 3 shows potentials for electrons
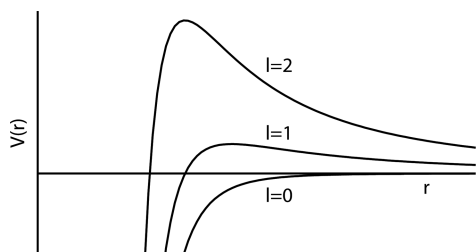
Figure 3. Schematic diagram to show potentials, $V(r)$, as a function of distance from an atom or molecule, r, for electrons with angular momenta $l = 0, 1, 2$. Centrifugal potential barriers are observed for $l = 1$ and 2 and also for higher values of l not shown here. $V(r)$ here was estimated as $V(r) = l(l + 1)/r^2 - 1/r^6$.
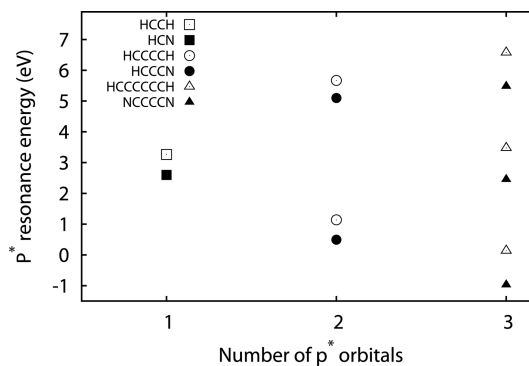

Figure 4. Energies of $^2\Pi$ shape resonances in electron attachment to acetylenic carbon-chain molecules predicted by semiempirical calculations.

with angular momenta of $l = 0, 1, 2$, approaching an atom or molecule. At short range, an attractive potential dominates, which is estimated here by a $-1/r^6$ term. At longer range, however, a repulsive "centrifugal" term that depends on $l(l + 1)/r^2$ will dominate if $l > 0$. The combination of these two potentials leads to the barriers visible for the cases with $l = 1, 2$ (and $l > 2$), but no barrier is observed for $l = 0$ as the centrifugal term is zero. Electrons that tunnel through these shape resonance barriers are, typically, trapped on femtosecond time scales, which are similar to the time scales for molecular vibration.

Particularly relevant here are shape resonances from attachment of electrons into π^* molecular orbitals. Linear carbon-chain molecules such as HCCH, HC_4H, HC_3N, C_4H, and NC_4N all have filled π-bonding and empty π^*-antibonding orbitals. For each CC or CN unit, there is one π orbital and one π^* orbital, which are mixed together or "conjugated" in molecules with multiple π and π^* orbitals. If a free electron attaches into an empty π^* orbital. then a $^2\Pi$-state anion will normally be formed from a $^1\Sigma$-state neutral, which requires p-wave electron attachment where $l = 1$ and, thus, where there will be a shape resonance. For example, the cyanoacetylene molecule, HC_3N, has two CC or CN units, and it has two π^* orbitals, which leads to two $^2\Pi$ shape resonances at different energies. Strictly speaking, for these linear molecules, each π and π^* orbital is, in fact, doubly degenerate so for each CC or CN unit there are two degenerate π orbitals and two degenerate π^* orbitals. These orbitals remain degenerate as long as the molecule is linear, but they will split if it is deformed.

Figure 4 shows calculated $^2\Pi$ resonance energies for a number of linear carbon-chain molecules, such as HC_3N, due to electron attachment into empty π^* orbitals in shape resonances. These energies were calculated with a semiempirical method[72,73] that is described below. Clearly, there is one shape resonance for each empty π^* orbital, but not shown in Figure 4 are the energies of Feshbach resonances that will also be present. Note that most of these resonances are well above the energies expected of free electrons in astrophysical environments, but the low energy predicted for the lowest $^2\Pi$ resonance for NC_4N is relevant here and discussed below.

In Feshbach resonances, the incoming electron excites the target before becoming attached to it. For example, in the case of the linear carbon-chain molecules discussed above, one of the electrons in the filled π molecular orbitals can be excited to a π^* orbital so that an anion is formed with two electrons in π^* orbitals and a vacancy in the π orbitals. Similar to Feshbach resonances are "core-excited" resonances, where the atom or

molecule is electronically excited as the electron attaches. The difference between Feshbach and core-excited resonances is that the energy of Feshbach resonances is lower than the energy of the excited neutral state formed by the attaching electron, whereas core-excited resonance energies are higher than the energy of the excited neutral state.

Atomic and molecular targets can be electronically excited, but in the case of molecules, there are also vibrationally and rotationally excited Feshbach resonances where the nuclear motion of the molecule is excited by the electron as it attaches to the molecule. Feshbach resonances can have significantly longer lifetimes than shape resonances.

There are other electron attachment resonance mechanisms. For example, the well-studied SF_6 molecule has a very large cross section for electron attachment close to zero electron energy, $\sim$2000 Å^2 at 1 meV electron energy,[74] due to s-wave attachment to give "excited vibrational levels" of the bound anionic ground state of SF_6^-.[75] These excited vibrational levels lie just above the energy of the neutral molecule plus a free electron. Thus, electron attachment close to zero energy leads to the formation of SF_6^{-*} superexcited anions. These SF_6^{-*} ions are so long-lived they can be detected mass spectrometrically on time scales of microseconds,[76−78] milliseconds,[79] and even seconds.[80]

The NC_4N molecule has been found to attach electrons with close to zero energy to form long-lived NC_4N^{-*} superexcited anions that have been detected on microsecond time scales.[81] It is possible that a similar attachment process is operating here to form a vibrationally excited state of a bound anionic ground state of NC_4N^- as for low-energy electron attachment to SF_6, but this has not been clearly established. One piece of evidence in favor, however, is the prediction of the calculations shown in Figure 4, which indicate that electron attachment into the lowest π^* orbital has a negative resonance energy, which indicates a bound anionic state. A clear difference in the attachment mechanisms to these two molecules, however, is that attachment to a $^2\Pi$ bound anionic state of NC_4N would be p-wave whereas SF_6 attachment is s-wave; the result of this difference would be that at close-to-zero electron energy, the attachment cross section will be orders of magnitude lower for NC_4N than for SF_6. The significance here of the NC_4N molecule is that it is a prototypical long-carbon-chain molecule similar to carbon-chain molecules observed in the interstellar medium. As with SF_6, the long lifetime of the negative ion suggests that the superexcited state can survive on long enough

time scales for photon emission and overall radiative electron attachment.

It is worth noting here that the s-wave attachment cross section to SF_6 has been observed to follow the expected $E^{-1/2}$ dependence, where E is the electron energy, down to energies of 20 μeV, which is below kT at 10 K.[74] Furthermore, the cross-sectional p-wave attachment to Cl_2 has been observed to follow the expected $E^{1/2}$ dependence down to energies of 1 meV.[82] These measurements confirm that the physics of electron attachment is the same over a wide range of electron energies.

Experimental techniques that can be used to observe electron attachment resonances and theoretical methods used in calculations of electron attachment resonances are listed in Table 3 with some representative references.

Table 3. Experiments and Theory Used to Investigate Electron Attachment

technique	ref(s)
Experimental Measurements	
electron transmission spectroscopy	72, 83–85
electron scattering measurements	75, 86, 87
electron energy loss spectroscopy	88, 89
negative-ion mass spectrometry with monochromatic electrons	90, 91
swarm experiments	92
FALP,[a] SIFT[b] flow-tube experiments	93
Theoretical Methods	
R-matrix	94
Schwinger variation	95, 96
complex absorbing potential	97, 98
semiempirical	72

[a]Flowing afterglow Langmuir probe. [b]Selected-ion flow tube.

Theoretical calculations of electron attachment resonances are significantly more difficult than calculations of ground and excited states of neutral atoms and molecules. The key difficulty is that superexcited states of a neutral atom or molecule plus an extra electron are inherently unstable with respect to dissociation into a free electron and the neutral target. Normally, one increases the size of a basis set to improve the accuracy of a calculation, and the energy of, for example, the ground state should converge toward the true value. If the same approach is taken for these electron attachment resonances, the extra electron will fill a diffuse orbital that fills most of the basis set, and the energy will converge to the energy of the neutral ground state. In effect, the problem being solved is the neutral target plus an electron confined to a box in three dimensions defined by the basis set. These states are "discretized continuum" wave functions and correspond to the electron traveling past the neutral target in the continuum and not attaching to it. It is necessary, therefore, to find a method of calculation that forces the electron to become attached to the target.

A simple method to consider first is a semiempirical method in which a small unrealistic basis set is chosen so that the discretized continuum states will be high in energy and, so, will not interfere with the calculation. The problem with this approach is that, because the basis set chosen is small, the energies will not be correct; this problem is overcome by scaling the energies calculated in a semiempirical manner by making several calculations under similar conditions for a group of similar targets including at least one target that has known resonance positions. A semiempirical linear scaling method is

used to move the calculated resonance positions for the known target to the true values already known, and then the same scaling procedure is used to scale the results for the other molecules with unknown resonance positions.[72,73] This semiempirical method was used to calculate the resonance energies shown in Figure 4.

More sophisticated methods calculate the electron scattering problem ab initio without the need for scaling; examples include the **R**-matrix, complex absorbing potential, and Schwinger variational methods. In the **R**-matrix method, space is divided into different spherically symmetric regions.[94] A calculation is done for an internal region that contains the target and an extra electron. Separate calculations are done outside this region for a free electron plus a simplified model of the target at the origin. Inner and outer calculations are then combined to determine the electron scattering, and resonance energies should be obtained close to their true values. An advantage of this technique is that the inner region needs to be calculated only once, whereas the outer part needs to be calculated once for each electron energy considered. Another way of addressing the issue of the scattering is to use a complex absorbing potential at some limit outside the target; this potential "absorbs" the wave function as it leaves the target and enables resonance energies to be calculated with normal variational methods.[97,98] The Schwinger variational method is another "more sophisticated" method in which, instead of directly solving the Schrödinger equation, the Lippmann–Schwinger equation is solved.[95,96] The Lippmann–Schwinger equation is a combination of the Schrödinger equation and scattering boundary conditions. A key benefit to this method is that it is particularly suited to scattering problems and trial scattering wave functions do not have to satisfy particular asymptotic boundary conditions. It is generally possible with these more sophisticated models to predict electron attachment resonance energies and cross sections for the formation of these superexcited states.

The energies of electron attachment resonances of HC_3N were calculated with the complex absorbing potential method by Sommerfeld and Knecht,[98] who also calculated the energies of neutral HC_3N, the dipole-bound state of HC_3N^-, and the valence-bound state of HC_3N^- ion in its bent equilibrium geometry. The resonance energies predicted by Sommerfeld and Knecht (0.7 and 6.2 eV) are close to the resonance energies predicted by the semiempirical calculations shown in Figure 4 (0.5 and 5.1 eV) and to the energies for the formation of negative ions in dissociative electron attachment to HC_3N (<1.6 and 5.1–5.6 eV). There is a thermodynamic limit to negative-ion formation at 1.6 eV, and only the high-energy tail of the lower resonance is observed; thus, the peak must lie below 1.6 eV. Complex absorbing potential calculations can be used to predict the lifetimes of superexcited anions from calculated resonance widths; for example, Sommerfeld and Knecht predicted a width of 0.15 eV for the lower resonance, which corresponds to a lifetime of 4 fs, and a width of 1.1 eV for the upper resonance.

Electron attachment to HC_3N was also calculated by Sebastianelli and Gianturco,[99] who reported calculations for HC_5N as well. For HC_3N, they predicted $^2\Pi$ resonances at slightly higher energies of 1.9 and 8.2 eV, but with widths similar to those obtained by Sommerfeld and Knecht, namely, 0.15 and 0.76 eV. The complexity of electron attachment resonance calculations should not be underestimated, particularly as the number of atoms in the target molecule increases.

Furthermore, the best calculations will consider multiple nuclear geometries or atomic positions and will ideally consider the resonances as potential energy surfaces (or curves in the case of diatomic molecules). Sebastianelli and Gianturco performed calculations at several different geometries, and their results are consistent with the fragmentation pathways of HC_3N observed in dissociative electron attachment experiments.[100]

In electron transmission spectroscopy and electron scattering measurements, a monochromatic electron beam passes through a sample with varying energy, and the transmitted electron current is recorded, which is analogous to optical absorption spectroscopy. The resonances widths observed are, of course, related to their lifetimes due to lifetime broadening. Thus, shape resonances are generally ∼250 meV wide or broader because of their short lifetimes, and Feshbach resonances are sharper features because of their longer lifetimes. In electron energy loss spectroscopy, the energies of electrons scattered by atoms or molecules are measured, and vibrational spectra, for example, can be obtained from the energy lost by electrons. If the energy of the incident electron is varied but the difference between the incidence and scattered electron energies is kept constant, resonances can be observed as variations in the probability of energy loss processes.[88]

Electron attachment resonances are observed directly in electron transmission, electron scattering, and electron energy loss measurements. By contrast, negative-ion mass spectrometric techniques and swarm and flow-tube measurements are indirect methods. For example, in negative-ion mass spectrometry with a monoenergetic beam of electrons, negative ions are observed that were formed by dissociative electron attachment at electron energies at which superexcited resonant states of the anion are formed. Negative ions cannot, however, be formed at all energies at which electron attachment resonances occur, for example, because the thermodynamic threshold for the formation of negative ions might lie above the energy of some resonant states.[73] Furthermore, when the negative-ion resonance states lie above the threshold for negative-ion formation, the intensity of negative ions as a function of energy will frequently be different from the profile of the electron attachment resonance, particularly when the resonance is broad: the "survival probability shift".[101,102] The survival probability shift is observed because of competition between electron autodetachment and dissociation of the superexcited anion state. In broad shape resonances, the higher the energy within the resonance, the higher the rate of autodetachment, and thus, the lower the probability of dissociation to give negative ions. The center of a resonance observed by negative-ion formation can be shifted below the center of the resonance observed by electron transmission spectroscopy by as much as, for example, 0.55 eV in the case of formic acid.[102] In swarm experiments, a "swarm" of electrons passes through the gaseous sample with a range of energies that are influenced by the application of electric fields. Although the electrons are not monoenergetic, it is possible to deconvolute the swarm results to derive electron attachment cross sections as a function of electron energy. In flow-tube techniques such as the flowing afterglow Langmuir probe (FALP) and selected-ion flow-tube (SIFT) techniques, there are multiple collisions, and free electrons are defined by a temperature rather than an energy. Swarm and flow-tube techniques have the great advantage that it is relatively straightforward to determine quantitative rate constants from their results, whereas with negative-ion mass

spectrometry, it is more difficult to obtain quantitative results, and frequently, relative cross sections and branching ratios have been published rather than absolute cross sections. A challenge in using data from swarm, FALP, SIFT, and other flow-tube experiments is that the collisions in the tube lead to significant rates of collisional attachment.

3.1.2. Radiative Electron Attachment. Radiative attachment to atomic hydrogen was presented in eq 1, and the importance of this process for the formation of H_2 in the early Universe was discussed above. It is possible to calculate the rate coefficient for radiative electron attachment to hydrogen atoms from the variation of cross sections with incidence photon energy for photodetachment of atomic hydrogen anions, which can be represented by

$$H^- + h\nu \rightarrow H + e^- \tag{11}$$

This photodetachment process is, of course, the reverse process of radiative electron attachment. McLaughlin et al.[103] combined experimental data and calculations to determine the photodetachment cross section for H^- over the widest possible range. They then used their photodetachment results to calculate radiative electron attachment rates. McLaughlin et al.[103] found that the rate constant for radiative attachment is 10^{-17} cm^3 s^{-1} at 10 K and rises with temperature to a maximum of ∼6 × 10^{-15} cm^3 s^{-1} at 10^5 K. This method of calculating radiative electron attachment avoids the need to determine the rates of electron attachment, autodetachment, and photon emission. In fact, this method of radiative attachment calculation determines rates of attachment for "direct radiative electron attachment" in which the photon is emitted as the electron attaches; direct radiative attachment is discussed further below.

In the case of the molecule SF_6, the lifetime of the superexcited anion formed upon attachment of electrons having energies very close to zero has been observed to be so long, up to seconds, that there is a significant rate of radiative electron attachment. The photon emission required from SF_6^-* to form the stable anion is in the infrared region because of the emission from the vibrationally excited superexcited anion. Rates of spontaneous emission can be calculated with the formula for the Einstein A coefficient; this formula includes a ν^3 (frequency-cubed) term, which dominates. In practice, the ν^3 term leads to typical lifetimes with respect to infrared emission in the millisecond range. Significant superexcited SF_6^-* anions have been observed with lifetimes of milliseconds and longer, so it is expected that significant numbers of stable SF_6^- ions will be formed by radiative electron attachment to SF_6.

Herbst and Osamura performed calculations of radiative electron attachment to $C_{2n}H$ ($n = 1-4$) molecules, as noted above in eq 6.[6] In their calculations, they examined the vibrational phase space occupied by superexcited anions formed in electron attachment to these molecules. As noted above, they predicted electron attachment rates close to the collisional rate. Their calculations, however, did not include detailed consideration of the electron attachment process by any of the methods described in section 3.1.1. Instead, they noted that molecules with large dipole moments can support dipole-bound anionic states close to the neutral ground state and predicted high rates of electron attachment with dipole-bound states acting as doorways to the formation of vibrationally excited ground-state anions, which can emit a photon to become stable.

Recently, Douguet et al.[104,105] performed calculations of radiative electron attachment to CN, C_2H, and C_4H that explicitly treated the electron attachment with the Schwinger

variational method. Furthermore, Douguet et al. pointed out that there is an additional mechanism of radiative attachment in which, as the electron attaches, a photon is emitted to give a stable anion product rather than a superexcited anion, which has to lose energy by photon emission. These authors defined direct radiative electron attachment (DREA) as the process in which the photon is emitted as the electron attaches and indirect radiative electron attachment (IREA) as a two-step process of electron attachment followed by photon emission from a superexcited anion. In the case of CN, Douguet et al. concluded that DREA is orders of magnitude larger than IREA and reported an overall rate of 7×10^{-16} cm^3 s^{-1} for radiative electron attachment. They predicted similar rates of 7×10^{-17} and 2×10^{-16} cm^3 s^{-1} for DREA to C_2H and C_4H, respectively. Douguet et al. noted that their direct radiative attachment rates for C_2H and C_4H are orders of magnitude lower than the indirect radiative attachment rates calculated by Herbst and Osamura[6] for these molecules. Ab initio calculation of photoemission from superexcited states is particularly challenging for polyatomic molecules, and Douguet et al. did not calculate indirect radiative electron attachment rates for C_2H and C_4H.

Very recently, the method of McLaughlin et al.[103] was used by Khamesian et al. to calculate rates for radiative electron attachment to CN, C_3N, and C_5N from their calculated photodetachment cross sections for CN$^-$, C_3N^-, and C_5N^-.[106] Their results indicated direct radiative electron attachment cross sections orders of magnitude lower than those predicted by Herbst and Osamura,[6] and although their results for CN were not exactly the same as the results of Douguet et al. described above,[104,105] they were of a similar order of magnitude. Again, however, the rate of indirect radiative electron attachment for these molecules was not calculated by Khamesian et al.

Carelli et al.[107] recently suggested that dipole-bound states might have a role in IREA. They calculated that, in the C_nN series for $n = 1, 3, 5, 7$, the molecule C_3N has a sufficiently large dipole moment, 3.0 D, to support dipole-bound states that could be formed as the first step of an IREA mechanism. It is interesting to note that Carelli et al. also calculated the dipole moments of the negatively charged analogues of these molecules, C_nN^-, and found large values such as 5.6 D for C_7N^-. The linear structure of these anions means that any anisotropy in the distribution of the electrons will give dipole moments that, as might be expected, strengthen significantly as the length of the molecule increases. The dipole moments of the anions are, of course, highly relevant to the rotational emission spectra through which they have been observed because the line strength is proportional to the square of the dipole moment of the molecule.

It is difficult to perform experiments to observe radiative electron attachment because of the long time scales of photoemission; an excellent vacuum is required to prevent the stabilization of superexcited anions by collisions with background gas particles on such long time scales. However, when superexcited anions are observed with long lifetimes in, for example, negative-ion mass spectrometers, radiative electron attachment can be deduced as in the case of SF_6 described above. An experimental investigation of electron attachment to linear NC_4N molecules found that NC_4N^-* superexcited anions with close-to-zero electron energies were observed on time scales of microseconds in a negative-ion mass spectrometer; it was proposed that some of these long-lived

superexcited anions might have sufficiently long millisecond lifetimes for radiative electron attachment.[81] The observation of long-lived NC_4N^-* is indirect evidence in support of Herbst and Osamura's prediction of radiative electron attachment to the linear molecules $C_{2n}H$.[6]

Khamesian et al. discussed the predictions of Herbst and Osamura and remarked: "Such a large cross section for electron capture could be justified for a system where the potential energy surfaces of the ground electronic states of the neutral molecule and the formed anion cross in the Franck−Condon region. However, for all carbon-chain anions observed in the ISM, the potential energy surfaces of the neutral molecule and the anion are almost parallel to each other, which implies that the electron capture cross section is small."[106] Here, we note, however, that, in the case of NC_4N, the anion states must cross the neutral state in the Franck−Condon region because of the experimental observation of long-lived NC_4N^-* anions formed in electron attachment with close-to-zero-energy electrons.[81] The calculated results presented in Figure 4 suggest that a bound anionic state of NC_4N^- exists in the Franck−Condon region as a result of electron attachment into the lowest π^* orbital of NC_4N. More sophisticated Schwinger variational theoretical calculations of electron attachment to NC_4N came to the same conclusion.[108] These theoretical predictions are in agreement with the experimental data. Significant rates of indirect radiative electron attachment can be anticipated. To date, NC_4N is the linear molecule with the most π^* orbitals that has been experimentally investigated by electron attachment. Perhaps other long linear carbon-chain molecules similarly form long-lived anions with close-to-zero-energy electron attachment. Therefore, we conclude that there are reasonable grounds to suspect that indirect radiative electron attachment can be a significant process for larger long-chain polyacetylenic molecules, which supports the predictions of Herbst and Osamura.[6]

Carelli et al. applied their molecular-scale calculations of electron attachment to molecules and used them to predict radiative electron attachment rates at different temperatures for polyaromatic hydrocarbons (PAHs)[109] and linear carbon-chain molecules.[110] They used these predicted rates to model anion abundances in the ISM.

3.1.3. Dissociative Electron Attachment. In dissociative electron attachment, superexcited molecular anions fragment to give one or more neutral particles and a fragment anion. The lifetimes of superexcited anions with respect to fragmentation can be as short as vibrational time scales, which are in the femtosecond range. Thus, fragmentation rates are generally orders of magnitude higher than the photon emission rates considered in radiative electron attachment. Therefore, rates of dissociative electron attachment are normally very much higher than radiative electron attachment rates. The contribution of dissociative electron attachment to negative-ion formation in astrophysical environments is, however, often restricted by the threshold electron energy required to form negative ions by this mechanism. For example, the threshold for the formation of C_3N^- from HC_3N, 1.3 eV, corresponds to kT at temperatures of ~15000 K;[73] such temperatures are orders of magnitude higher than average temperatures in dark molecular clouds, protostars, and cool circumstellar envelopes, for example. As a result, dissociative electron attachment can be significant only in regions where energetic electrons are present: In the Solar System, this would include Titan and cometary comae, and in

the interstellar medium, it would include protostellar winds, protoplanetary nebulae, and photon-dominated regions.

In the most simple dissociative electron attachment process, a molecule AB is broken into two molecular fragments A and B^- by dissociation of a single chemical bond between A and B

$$AB + e^- \rightarrow AB^{-*} \rightarrow A + B^- \tag{12}$$
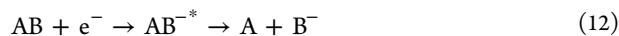
The threshold energy E_{th} for this process is given by

$$E_{th} = D(A{-}B) - EA(B) \tag{13}$$

where $D(A{-}B)$ is the energy of the chemical bond between A and B and $EA(B)$ is the electron affinity of B. These quantities can be thought of as the energy required to fragment the molecule and the energy released in attaching an electron to the molecular fragment B, respectively. For some molecular fragments B, the electron affinity is greater than the bond energy, and there is no energetic barrier to dissociative electron attachment. As an example, Herbst and Osamura[6] found that the dissociative electron attachment of acetylenic HC_6H to form C_6H^- is highly endothermic whereas the reaction of its carbene form H_2C_6 is exothermic. The formation of C_6H^- by this route thus depends on the abundances of the neutral isomers, which current astrochemical models are not able to predict. Note that the carbene form is detectable by rotational spectroscopy,[111] whereas the polyyne form is detectable by infrared (vibrational) spectroscopy only.[112]

Dissociative electron attachment can be investigated experimentally by negative-ion mass spectrometry with a monoenergetic electron source. Experimental issues can lead to differences in the data between different groups. For good electron energy resolution, the electrons should not be placed in strong electric fields; otherwise, they will be accelerated, and the resolution will be heavily reduced or destroyed. By contrast with a time-of-flight mass spectrometer, the best mass resolutions require large electric fields to extract the ions from the region where they are formed. These two contradictory requirements necessitate either a compromise electric field or pulsing, whereby electrons attach with minimal electric fields and ions are pushed out with large electric fields after the electrons have passed.[113] The overall result is that the collection efficiencies of different mass spectrometers can vary, leading to different results. If instead a quadrupole mass spectrometer is employed, then low electric fields can be used to extract negative ions. There still remains an issue, however, in that, with a low electric field, fragment ions formed in dissociative electron attachment with different initial kinetic energies will have different detection efficiencies, as fast-moving fragment ions can escape the weak electric field and not enter the mass spectrometer.

There is a good body of literature describing investigations of electron attachment to many different molecules. There are two issues, however, with including electron attachment data in chemical models. First, absolute values of dissociative electron attachment cross sections are not calculated in all investigations. Second, when absolute values are calculated, there can be variations between different research groups because of the ion collection issues described above.

In the case of dissociative electron attachment to acetylenic linear carbon-chain molecules, absolute cross sections have been reported for HCCH,[114,115] DCCD,[115] HC_4H,[114] HCN and DCN,[116] HC_3N,[117] and NC_4N.[81] For all of these molecules, the dissociative electron attachment processes are endothermic, so no anions are produced with close to zero

electron energy, except in the case of metastable NC_4N^{-*} discussed above. The energies of dissociative electron attachment for these molecules are in broad agreement with the predicted resonance energies shown in Figure 4.

Theoretical methods for the calculation of dissociative electron attachment are more difficult because it is necessary to calculate the potential energy curves or potential energy surfaces for superexcited anion states as a function of molecular vibrational coordinates and then to calculate the nuclear dynamics on the surfaces while allowing for autodetachment of the anion back to the neutral. A significant amount of work has gone into making such calculations for the dissociative electron attachment to H_2O with the calculation of potential energy surfaces[118] and then calculations with these surfaces to determine theoretical dissociative electron attachment absolute cross sections.[119] If the number of vibrational degrees of freedom considered is restricted, then it is possible to perform calculations for larger molecules; for example, dissociative electron attachment to CF_3Cl was investigated by considering two vibrational degrees of freedom.[120] Dissociative electron attachment has also been calculated for the acetylenic molecules HCCH,[121] HCN,[96,121] DCN,[96] and HC_3N.[121]

Calculations have also been performed for electron attachment to NC_4N,[108] NCCN,[122] and HC_4H[123] with multiple nuclear geometries to investigate potential dissociative electron attachment mechanisms. In the case of NC_4N, for example, evidence was found by Sebastianelli and Gianturco for dissociative electron attachment to yield CN^- and C_3N^- fragments, which were observed experimentally.[81] Cross sections from such calculations of electron attachment were used to determine rates of electron attachment to polyacetylenic molecules by Carelli et al.[124]

3.1.4. Ion-Pair Formation or Polar Dissociation. Anions are also formed in the fragmentation of molecules in which a positively charged fragment and a negatively charged fragment are formed. This process has been most studied for photon impact,[125] although electron-stimulated ion-pair formation was recently reported for acetylene.[126]

The threshold energy for ion-pair formation is similar to the ionization energy of the molecule. Comparison of the ionization and ion-pair formation processes

$$AB + h\nu \rightarrow AB^+ + e^- \tag{14}$$

$$AB + h\nu \rightarrow A^+ + B^- \tag{15}$$

leads to the observation that the ion-pair threshold, E_{ip}, is given by

$$E_{ip} = IP(AB) + D(A{-}B^+) - EA(B) \tag{16}$$

where $IP(AB)$ is the molecular ionization potential, $D(A{-}B^+)$ is the energy of the chemical bond between A and B in the AB^+ molecular ion, and $EA(B)$ is the electron affinity of B. Given typical bond energies and electron affinities, the ion-pair threshold will generally lie within a couple of electronvolts of the ionization energy, ~8−10 eV or higher, corresponding to radiation at UV or shorter wavelengths. Thus, this process is most likely to be important in energetic environments close to stars.

In the case of acetylene,[126] the ion pairs $H^- + C_2H^+$, $CH^- + CH^+$, and $C_2H^- + H^+$ have experimental appearance energies close to thermodynamic thresholds of 16.1, 19.4, and 16.1 eV, respectively.

Ion pairs can also be formed in collisions between neutral particles, typically, collisions between fast and/or excited atoms and neutral molecules. In these collisions, the energy required for ion-pair formation is provided by the kinetic energy of the fast atom and/or the electronic excitation energy of the atom.[127,128]

3.2. Destruction Mechanisms

3.2.1. Overview of Experimental and Theoretical Techniques. Stable anions in astrophysical environments are normally in their ground electronic states. In fact, for most atomic anions, only one electronic state is stable;[129,130] that is, all excited states lie above the energy of the neutral plus a free electron. The situation is similar for molecular anions, which "usually do not have bound excited electronic states".[131] The first point to note here is that it is possible to calculate the ground states of atomic and molecular negative ions with standard techniques because all of the electrons are bound and the systems lie below the neutral ground state. This is a considerable simplification compared to the difficulty in calculating the superexcited anion states that are formed in electron attachment. There are some systems, such as the nitrogen molecule N_2, in which the ground state of the anion lies higher in energy than the neutral ground state. For these systems, the difficulties of superexcited-anion-state calculations remain for the ground state of the anion, which, according to the terminology used here, is a superexcited anion ground state because it lies above the energy of the neutral plus a free electron. The calculation of stable negative-ion states is more difficult than calculations for similar states of neutral atoms and molecules because the highest occupied atomic or molecular orbitals are more diffuse than similar orbitals of neutral molecules; accurate calculations require larger basis sets than for neutrals and, in some cases, special basis sets.[131,132]

For experimental work, there are a number of challenges. For example, it is necessary to have stable reliable sources of negative ions, which are more difficult to produce than those for positive ions. Another difficulty, which is the same for both positive and negative ions, is the challenge of controlling low-energy beams of negative ions to mimic astrophysical conditions. At low energies, the space charge repulsion between like charges in particle beams makes this difficult. Furthermore, for low collision energies, it is important that any neutral collision partners not have significant kinetic energy. The issue of achieving low collision energies is not as difficult for electron processes, in which the thermal velocities of neutral molecules are not an issue because the mass of the electron is so much lower and collision energies are very close to the energy of the electron. One experimental solution to these issues is to use a cryogenically cooled electrostatic ion trap; this technique was developed by Gerlich et al.[133−135] Flow-tube methods in which the carrier gas undergoes expansion can also be used to achieve low temperatures.[136] Recent advances in cooling atoms and molecules in magnetic and electric field traps are particularly interesting from the point of view of studying low-temperature processes relevant to cold astrophysical environments,[137] but the trapping fields make it difficult to include charged particles in these experiments.

3.2.2. Photodetachment. Photodetachment has been observed experimentally for many atomic anions. Typically, negative-ion beams are photodissociated by laser radiation and sometimes synchrotron radiation; the photoelectrons are generally energy-analyzed, and these types of measurements have enabled accurate determinations of many electron affinities. Resonances observed in photodetachment cross sections measured as a function of photon energy have revealed the presence of many metastable superexcited states of atomic negative ions above the ionization threshold of the negative ion.[138] Génévriez and Urbain recently reported experimental absolute cross sections for photodetachment of H^-.[139]

Photodetachment of molecular anions is also an active line of research[132] through the measurement of photoelectron spectra, for example.[140,141] The recent observation of negative ions in the interstellar medium led to measurements of photodetachment of anions held in a radio-frequency ion trap for C_2H^-, C_4H^-, and C_6H^- anions.[142] These observations prompted theoretical calculations of photodetachment cross sections from C_2H^-, C_4H^-, and C_6H^- anions.[143] Overall good agreement between experiment and theory was found; this is particularly useful, as the experimental points confirm the usefulness of the theoretical data, which covers a wide range of photon energies.

Photodetachment data for CN^- and C_3N^- at 266 nm were incorporated into a model of the circumstellar envelope of the carbon-rich star IRC+10216; it was found that photodetachment by interstellar UV photons is the most important destruction mechanism for these anions in the circumstellar envelope.[48]

3.2.3. Electron-Impact Detachment. The calculation of electron-impact detachment is more complicated than the calculation of photodetachment or electron attachment processes, as two free electrons are released in the final state; an electron collides with an anion to give a neutral and two free electrons,[144] but it is possible to calculate absolute cross sections.[145] This process is, of course, the same as the electron-impact ionization of neutrals[146] but with the neutral target replaced by an anion. Ion storage rings have been used to investigate the electron-impact detachment of H^-, D^-, and O^- atomic anions,[138,147−149] for example. Electron-impact detachment of some molecular ions such as PO_n^-, with $n = 0−3$, has also been investigated.[150]

The relevance of electron-impact detachment to astrophysical environments will depend on the temperature of the electrons because there will, of course, be a threshold energy for electron-impact detachment, as electrons are bound in stable anions. In the case of CN^-, C_3N^-, and similar anions, the electron binding energy is ∼4 eV. The anion binding energy is, of course, equivalent to the electron affinity of the neutral molecule or atom.

3.2.4. Associative Detachment. A novel experiment to investigate the formation of H_2 molecules in associative detachment collisions between H^- and H, shown in eq 2 above, was recently described by Bruhns et al.[151,152] A beam of H^- ions at 10 keV energy was partially photodetached to leave a mixture of copropagating H^- ions and H atoms. The energy of the H^- ions was modified slightly just after dissociation to give accurate relative collision energies down to the millielectronvolt level. A particularly ingenious part of this experiment was the detection of the products. Electron detection would be particularly difficult because electrons would be formed, for example, in collisions of the ion beam with background gas and by atoms and ions hitting surfaces. Therefore, it was necessary to detect the H_2 product molecules and to have the signal not be swamped by the background H atoms also present in the beam. The solution employed was to first remove the H^- ions electrostatically. A fraction of the

remaining neutral H atoms and H_2 molecules were then ionized to give positive ions by charge stripping in a gas collision cell. H_2 molecules would give some H_2^+ ions with 20 keV energy, whereas H atoms gave H^+ with 10 keV energy. On this basis, a signal from the detection of 20 keV H_2^+ ions enabled the rate of associative detachment to be monitored.

This merged-beam method was also used to investigate and compare H_2 formation in associative detachment described by eq 2 through the equivalent process with deuterium in which D_2 is formed[153]

$$D^- + D \rightarrow D_2 + e^- \qquad (17)$$

Eichelberger et al.[154,155] measured the dissociative electron attachment of carbon-chain anions, including C_4H^- and C_6H^-, with H, N, and O atoms in a selected-ion flow-tube (SIFT) experiment. Although branching ratios of the product channels were measured for reactions with H atoms, this was not possible for N and O atoms. This is an important goal for future experiments, given that branching ratios are needed by models.

In another recent novel experiment, electrons generated in associative detachment were observed with an apparatus that combines an electron spectrometer with an ion trap.[156,157]

The technical challenges of these new experimental methods should not be underestimated.

3.2.5. Collisional Detachment.
Collisional detachment is an area in which there was significant experimental and theoretical work in the past, but it is a less active area of research now. One key source of experimental collisional detachment rate coefficients is from the analysis of electron swarm data.[158] Beam experiments in which single collisions are investigated have also been used.[159] A review of collisional detachment data suggests that collisional detachment dominates the inelastic collisions between negative ions and neutral atoms and molecules.[160] Theoretical treatments of collisional detachment include nonlocal resonance theory[161,162] and semiclassical investigations.[163]

Much research effort in the area has focused on collisional detachment processes of atmospheric interest. For example, it was recently found that electron detachment can play an important role in sprite ignition.[164] By contrast, the relevance of collisional detachment in astrophysical environments is less clear. As noted in section 3.2.3 with regard to electron-impact detachment, there will be threshold energies for collisional detachment processes, as electrons are bound in stable anions. For CN^- and C_3N^-, the threshold is ~4 eV, which corresponds to kT at ~45000 K. Thus, collisional detachment will be most important in astrophysical environments for weakly bound anions such as HCN^-. In the ground state of HCN^-, the extra electron is weakly bound in the dipole potential of the HCN molecule by only 1.56 meV.[165] Similar weakly (dipole) bound anions include anions of acetonitrile, CH_3CN^-, bound by 11 meV[166] and acetaldehyde, CH_3CHO^-, bound by 0.36 meV.[167]

3.2.6. Mutual Neutralization.
The importance of accurate cross sections for the mutual neutralization process

$$H^- + H^+ \rightarrow 2H \qquad (18)$$

for determining rates of molecular hydrogen formation was highlighted by Glover et al.[168] As noted above, an important mechanism for molecular hydrogen formation is the associative detachment between H^- and H shown in eq 2; Glover et al. pointed out that destruction of H^- by mutual neutralization will have affected the number density of H^- anions and, thus, the

rate of molecular hydrogen formation in the early Universe. In particular, Glover et al. highlighted the accuracy with which quantitative data were available for fundamental processes such as the mutual neutralization shown in eq 18 and the impact that this has on the uncertainty in predicted rates of molecular hydrogen formation in the primordial gas of the early Universe.

There is considerable experimental challenge in measuring quantitative data for mutual neutralization at well-defined collision energies as doing so generally requires the formation of stable, well-defined, copropagating positively charged and negatively charged ion beams. Adams and Smith made pioneering studies in this regard[169,170] using the flowing afterglow Langmuir probe (FALP) technique. They found that their measured rate coefficients reproduced the theoretical predictions of Hickman[171] to within a factor of a few at room temperature. The most recent experimental data for hydrogen anion and proton mutual neutralization were summarized by Urbain et al.,[172] who critically examined their data in comparison with previously reported experimental work. They conclude that their results are in agreement with ab initio calculations of Stenrup et al.[173] and theoretically calculated rate coefficients.[174] A newer experimental approach was developed in the group of Viggiano and Miller that allows mutual neutralization to be investigated in flow-tube experiments at well-defined temperatures.[175−177]

In addition to the $H^- + H^+$ system,[173] ab initio calculations have been performed on mutual neutralization for $F^- + H^+$ collisions.[178] The complexity of these ab initio calculations increases dramatically for systems with more than two atoms. An alternative approach to calculations can be made on the basis that the dynamics are dominated by long-range interactions. There is long-range attraction between the collision partners in mutual neutralization processes, but there is no long-range attraction (or repulsion) between the two neutral products after mutual neutralization. Therefore, there will be many curve crossings between the ionic reaction partners and neutral products, and the reaction will depend strongly on Landau−Zener interactions at these long-range crossings. Calculations with this simplified approach have been performed for mutual neutralization in $H^- + H_2^+$ collisions.[179]

3.3. Formation and Destruction Mechanisms: Ion−Molecule Reactions

In ion−molecule and ion−atom reactions, one anion is destroyed, and another is formed; we consider them all to be "ion−molecule" reactions even when they are strictly ion−atom reactions. Two examples of ion−molecule reactions are electron transfer and proton transfer between the ion and molecule, but there are additionally many other possible mechanisms. There have been a number of reviews of negative-ion−molecule reactions[180,181] and more general ion chemistry including negative ions.[182,183]

A wide range of experimental techniques can be applied to the investigation of ion−molecule reactions such as those involving ion traps, ion cyclotron resonance mass spectrometers, guided ion beams, and flow tubes.[184] The experimental information that can be obtained ranges from overall rate coefficients to detailed information about angular distributions of product ions formed in ion−molecule reactions. The theoretical methods applied to the calculation of anion−molecule reactions are similar to those used for neutral−neutral reactions and positive-ion−molecule reactions. As noted above, calculations are generally more demanding because of the

diffuse nature of the outer orbitals, which requires large basis sets. Thus, the repeated calculations at multiple geometries required to generate potential energy hypersurfaces over which negative-ion−molecule reactions proceed are a considerable challenge. For systems with more than four atoms, it is necessary to restrict some degrees of freedom in the calculations.[180]

3.4. Processes at Surfaces

The formation and destruction of negative ions on surfaces is not as well studied as processes in the gas phase. The charge on a molecule that is adsorbed on a surface might not be well-defined; however, electron-stimulated emission of anions from surfaces has been observed. For example, several investigations relevant to the irradiation of DNA have been reported by the group of Sanche.[185] Much of the focus on electron collisions with molecules on surfaces is concerned with the chemistry and processing that occurs on the surface induced by the electrons.[186] More relevant here is a recent investigation of low-energy electron impact on films of HCN, CH_3CN, and NH_2CH_2CN deposited on graphite at 90−130 K.[187] Ejection of H^- ions from the surface was observed by dissociative electron attachment. For these laboratory experiments, "low-energy" electrons generally have electron energies from ∼3 to ∼13 eV. Some demanding experimental measurements have been made with surfaces being struck by electrons with energies down to about 2−3 meV from an electron beam with an energy resolution of 2−3 meV generated by photoionization of argon gas.[188,189] In these experiments, it was found that neutral polar molecules with small dipole moments of 0.08−0.5 D, such as N_2O and toluene, deposited on surfaces at temperatures of ∼40−65 K can spontaneously align to give electric fields of ∼10^8 V m^{-1}; surface potentials of a few volts per 100 monolayers of adsorbed molecules have been observed.

Dissociative electron attachment has been less studied on surfaces than in the gas phase, but there was some success in reproducing experimental results[190] with theory[191] relatively recently for the model system of CH_3I on a Kr surface.

The process of collisional electron attachment shown in Table 2 is not considered important in most astrophysical environments, as pressures are far too low for this process to be significant. In contrast, however, for an atom or molecule adsorbed on a surface, the surface could act as the third body to stabilize a superexcited anion formed by electron attachment, and collisional attachment rates could be significant. Similarly, atoms and molecules in small clusters could be stabilized following electron attachment by collisions within the cluster. Theoreticians have exploited the similarity between cluster and surface environments by performing calculations of electron attachment to molecules in water-cluster environments[192] to simulate experimental measurements of electron attachment to molecules on water surfaces.[193] The calculations revealed that attachment cross sections were enhanced on the surface in part because multiple scattering by adjacent water molecules enhances the trapping of incident electrons and explains the significantly enhanced attachment cross section observed experimentally.

Ice mantles on interstellar grains do, however, show evidence of embedded ions, notably the presence of NH_4^+ and NCO^-. The latter ion has an infrared absorption band at 2165.7 cm^{-1} (4.62 μm) detected in the spectra of tens of deeply embedded young stellar objects.[194] This was identified unambiguously as NCO^- embedded in a strong hydrogen-bonded ice based on

isotopic substitution experiments. The gas-phase formation of the anion through the radiative association $CN^- + O$ was shown to have an extremely small rate coefficient at low temperatures,[195] less than 2.5×10^{-19} cm^3 s^{-1}, and the direct radiative electron attachment to NCO is also very slow.[196] Laboratory experiments indicate that the origin of the anion might be due to photon or cosmic-ray interaction[197] with the ice, although it has also been argued that the anion can be produced by low-temperature thermal reactions between HNCO and NH_3 in ice.[198]

Finally, negatively charged ions can also be formed in collisions of atoms[199,200] and positively charged ions[201] with surfaces. There is an ongoing challenge in the investigation of negative-ion formation processes at surfaces relevant to astrophysical environments.

4. CHEMICAL NETWORKS AND MODELS

4.1. Introduction

Calculations of chemical evolution in astrophysical environments typically employ chemical kinetics using a reaction network that describes the formation and destruction of each species. For physical conditions that remain constant in time, this amounts to an initial value problem in which the time evolution of all species is described by a set of ordinary differential equations (ODEs)

$$\frac{dn_i}{dt} = \sum_{jk} k_{jk} n_j n_k + \sum_l k_l n_l - n_i \left(\sum_{im} k_{im} n_m + \sum_p k_p \right) \text{ cm}^{-3} \text{ s}^{-1}$$

(19)

Here, k_{xy} and n_z represent the rate coefficients and number densities of species, respectively. The first and third terms represent the formation and destruction, respectively, of species i through two-body reactions, whereas the second and fourth terms represent the corresponding one-body reactions, e.g., photodissociation. This (often large) set of ODEs is solved using numerical methods, and calculation of the radiative transfer through the source model generates synthetic spectra that can be compared with observations.

Over the past 30−40 years, the community has collated chemical networks for use in such physicochemical models, using measured or calculated rate coefficients where available and estimated values otherwise. Modern gas-phase chemical networks typically contain some ≳6000 reactions involving ≳600 species and have expanded in size as the number of molecules detected in space has increased. The inclusion of grain-surface chemistry and/or isotopic fractionation can extend networks to in excess of ∼10 000 reactions, and it is only in the modern technological era that computing power has increased sufficiently for such calculations to be performed on a desktop computer.

The two most widely used gas-phase networks for astrochemical calculations are the UMIST Database for Astrochemistry (UDfA, http://www.udfa.net)[43,202−205] and the Kinetic Database for Astrochemistry (KIDA, http://www.kida.com).[206] The two networks have a similar ethos and originate from the need to describe the specialized chemistry that occurs at low temperatures, ∼10 K. There is much overlap between the current networks, with both including two-body reactions, photochemistry, and cosmic-ray-induced photochemistry. The latter arises from UV photons internally generated in molecular material through the excitation of H_2 molecules by cosmic rays.[207] UDfA typically employs measured
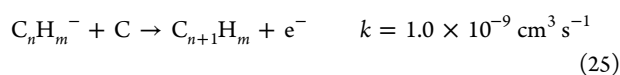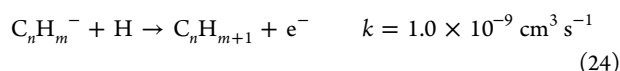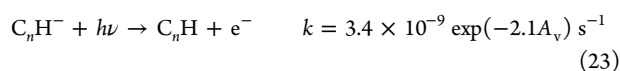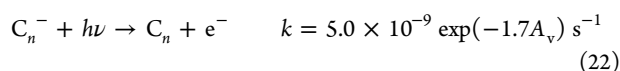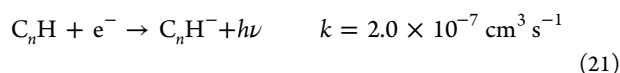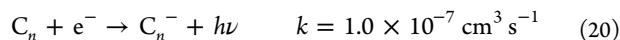
rate coefficients where available and also includes chemistry applicable at higher temperatures ($\gtrsim$100 K). KIDA is the modern version of the "New Standard Model", later renamed the Ohio State University (OSU) network, and was compiled primarily for use at low temperatures.[208−210] The modern version of KIDA now also includes high-temperature chemistry.[211] UDfA and OSU/KIDA have historically provided "complete" reaction networks for public use. However, KIDA also has a useful interface through which experts can recommend a rate coefficient based on an evaluation of all relevant and available data.

The recent releases of UDfA (RATE12)[43] and KIDA (kida.uva.2014)[212] were updated to include the chemistry of molecular anions following their discovery in space. In the remainder of this section, we describe the compilation of networks for anion chemistry and the models adopted for the different sources in which molecular anions have been observed and/or where they are expected to be abundant: dark clouds, protostellar envelopes, photon-dominated regions (PDRs), circumstellar envelopes (CSEs) of evolved stars, planetary atmospheres, and cometary comae. In Table 1, we present a summary of observed column densities and anion-to-neutral ratios compared with various model results.

4.2. Dark Clouds

Dark clouds are large ($R \approx 10-100$ parsecs), relatively dense ($n \approx 10^4$ cm^{-3}), cold ($T \approx 10$ K), and opaque ($A_v \approx 10$ mag) objects of molecular gas and dust within which young stars form. They exhibit a unique and rich chemistry depending on ion−molecule reactions driven by cosmic-ray ionization. This leads to large abundances of exotic molecules, including highly unsaturated long-chain hydrocarbon species, such as HC$_9$N. Table 1 lists the sources, anion-to-neutral ratios, and references for all anions detected in star-forming clouds to date.

The first comprehensive molecular anion chemistry was presented by Bettens and Herbst,[8] who included hydrocarbon anions, C_n^- and C_nH^-, in a chemical model of interstellar clouds. The network was restricted to anions with $10 \leq n \leq 23$ to focus on the formation of large carbon-chain molecules.[8,213] They included formation from radiative attachment and destruction through photodetachment and associative detachment with H and C atoms

$$C_n + e^- \rightarrow C_n^- + h\nu \qquad k = 1.0 \times 10^{-7} \text{ cm}^3 \text{ s}^{-1} \quad (20)$$

$$C_nH + e^- \rightarrow C_nH^- + h\nu \qquad k = 2.0 \times 10^{-7} \text{ cm}^3 \text{ s}^{-1} \quad (21)$$

$$C_n^- + h\nu \rightarrow C_n + e^- \qquad k = 5.0 \times 10^{-9} \exp(-1.7A_v) \text{ s}^{-1} \quad (22)$$

$$C_nH^- + h\nu \rightarrow C_nH + e^- \qquad k = 3.4 \times 10^{-9} \exp(-2.1A_v) \text{ s}^{-1} \quad (23)$$

$$C_nH_m^- + H \rightarrow C_nH_{m+1} + e^- \qquad k = 1.0 \times 10^{-9} \text{ cm}^3 \text{ s}^{-1} \quad (24)$$

$$C_nH_m^- + C \rightarrow C_{n+1}H_m + e^- \qquad k = 1.0 \times 10^{-9} \text{ cm}^3 \text{ s}^{-1} \quad (25)$$

Using a standard model of a dark cloud, they calculated anion-to-neutral ratios equal to ∼2.5% or 3.7% (depending on the underlying network) for all C_nH^- anions, $n \geq 10$. The highest fractional abundance, ∼10^{-12} (corresponding to a column density of ∼10^{10} cm^{-2}), was reached for $n = 10$ and decreased with increasing size of the anion.

Regarding smaller anions, Petrie[214] investigated potential routes to the formation CN$^-$. Early chemical networks included the formation of OH$^-$ and CN$^-$ through charge-transfer and proton-transfer reactions, for example, O$^-$ + HCN → CN$^-$ + OH, and destruction through associative electron detachment, for example, CN$^-$ + H → HCN + e$^-$.[202] Petrie estimated a radiative attachment rate for CN$^-$ equal to 1.4 × 10^{-17} cm^3 s^{-1} at a temperature of 10 K and concluded that radiative attachment is an unlikely formation mechanism for this anion under interstellar conditions. He considered other potential formation mechanisms, including charge transfer from PAH$^-$ species and dissociative attachment, and showed that these too were unlikely to lead to observable abundances of the anion under dark cloud conditions.

Ruffle et al.[215] extended the network from Bettens and Herbst to include C_nH_m anions with $n = 7-9$ and $m = 0$ and 1 to investigate the abundance of C_7^- in diffuse clouds, which was postulated at that time to be a possible carrier of numerous DIBs.[21] Ruffle et al. added the following associative detachment reaction

$$C_n + C_m^- \rightarrow C_{n+m} + e^- \qquad k = 1.0 \times 10^{-9} \text{ cm}^3 \text{ s}^{-1} \quad (26)$$
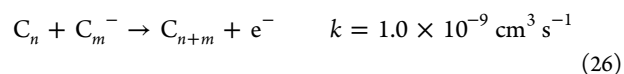
for all bare carbon chains with $n = 1-9$ and $m = 7-22$, in response to theoretical results suggesting that this reaction was highly exothermic for $n, m = 1-9$.[216] They were able to reproduce the relatively high fractional abundance of C_7^- (∼10^{-9} relative to hydrogen) required for the strong interstellar absorption bands attributed to this species, but only for very particular sets of conditions and only for relatively short periods of time.

Millar et al.[40] were the first to extend the anion chemical network down to $n = 4$, following the discovery of C_6H^- in TMC-1,[13] and thus considered the formation of the hydrocarbon anions C_4H^-, C_6H^-, and C_8H^- in dark clouds for the first time.[40] They assumed radiative electron attachment to the parent neutral as the main route to anion formation and calculated rates using the theory outlined in Terzieva and Herbst.[6,9] They included destruction through photodetachment, assuming a cross section, σ_{pd}, that depends on the photon energy, ϵ, and the electron affinity (EA) of the molecule in question

$$\sigma_{pd} = \sigma_0 (1 - \text{EA}/\epsilon)^{0.5} \text{ cm}^2, \qquad \text{EA} \geq \epsilon \quad (27)$$

They assumed $\sigma_0 = 1 \times 10^{-17}$ cm^2 and used the Mathis et al. prescription of the interstellar radiation field.[217] They also included additional gas-phase destruction routes through reactions with O atoms (in addition to associative detachment with H and C atoms) and mutual neutralization with C$^+$

$$C_nH_m^- + O \rightarrow C_{n-1}H_m^- + CO \quad (28)$$

$$C_nH_m^- + C^+ \rightarrow C_nH_m + C \quad (29)$$
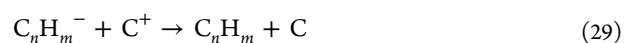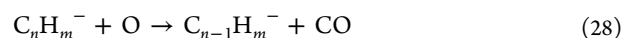
Rate coefficients from experimental measurements were employed where available.[154,218] The rate coefficient for mutual neutralization was taken to be that for mutual neutralization of carbon clusters, as used by Lepp and Dalgarno.[14]

Millar et al. determined anion-to-neutral ratios of 5.2% and 4.2% for C_6H^- and C_8H^-,[40] respectively, values that compare reasonably well with the values observed in the dark cloud TMC-1 (1.6% and 4.6%[13,26]). On the other hand, the prediction for C_4H^- was significantly larger than the value later observed (0.13%[40] versus 0.0012%[38]). C$_4$H has an

electron affinity similar to those of C_6H and C_8H, so the low anion abundance observed in dark clouds was considered surprising.[6] One difference between C_4H and its larger analogues is its relatively small dipole moment, 0.9 D, versus 5.5 and 6.3 D for C_6H and C_8H, respectively.[26] Cross sections for radiative attachment are enhanced for highly polar molecules ($\gtrsim$2 D) because of the presence of "dipole-bound" states (DBSs), which allow the electron to be loosely bound to the molecule.[140,219] DBSs can lie slightly below the neutral molecule in energy, creating Feshbach resonances in the continuum of the anion (see section 3.1.1). As discussed by Brünken et al.,[26] because C_4H has a small dipole moment, DBSs likely do not play a role in the formation of the anion through radiative attachment. Hence, the first step in the formation of the anion, electron capture and the formation of the temporary negative complex, is possibly very inefficient for C_4H. This is discussed further in section 4.5.

Following the detection of molecular anions in space, Wakelam and Herbst revisited the chemistry of negatively charged PAHs in dark clouds.[220] Following Lepp and Dalgarno,[14] they included the formation of PAH$^-$ species through radiative electron attachment and destruction through mutual neutralization

$$PAH^- + X^+ \rightarrow PAH + X \tag{30}$$

$$PAH^- + X^+ \rightarrow PAH + X' + H \tag{31}$$
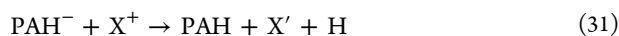
where X' represents the deprotonated cation. They termed the latter process "dissociative neutralization". They also included photodetachment through external photons, employing a typical cross section of $\sigma \approx 10^{-16}$ cm^2. Wakelam and Herbst found that PAH$^-$ species become more abundant than electrons beyond a time of ~160 years and, hence, are the dominant charge carrier.[220] They also determined that $n(PAH^-)/n(e^-)$ decreased as the fractional abundance of PAHs decreased, consistent with previous work.[14] Many molecules generally had increased abundances in models with PAH chemistry, including cyanopolyynes, HC_nN; organic molecules, such as HCOOH (formic acid) and CH_3OH (methanol); and carbon-chain molecules, such as CH_3CCH (methyl acetylene) and CH_3C_4H (methyl diacetylene). The calculations of Wakelam and Herbst[220] suggested that the inclusion of PAH chemistry has a catalytic effect, helping to build complexity. Current gas-phase networks tend to ignore PAH chemistry because PAHs likely vary considerably in size and resultant properties; nevertheless, models including the combined chemistry of PAH anions and smaller molecular anions, such as C_nH^-, should be investigated in the future.

The chemical model described by Millar et al.[40] was later updated and investigated in more detail by Walsh et al.[41] They extended the network to include the formation of C_nN^- species, following the detection of C_3N^- and C_5N^- in the circumstellar envelope of IRC+10216.[30,31] Herbst predicted that C_nN^- anions can also form efficiently through radiative electron attachment to the parent neutral molecule.[7] Walsh et al.[41] emplo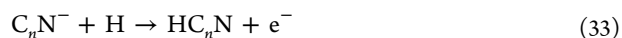yed the new radiative attachment rates calculated by Herbst and Osamura[6] and included the formation of C_3N^- through dissociative electron attachment to HNC$_3$, a metastable isomer of HC$_3$N[45,221]

$$HNC_3 + e^- \rightarrow C_3N^- + H \tag{32}$$

They included destruction through photodetachment (calculated as described previously) and through reaction with H, C,

and O atoms and mutual neutralization with abundant cations, such as C$^+$

$$C_nN^- + H \rightarrow HC_nN + e^- \tag{33}$$

$$C_nN^- + C \rightarrow C_{n+1}N + e^- \tag{34}$$

$$C_nN^- + O \rightarrow C_{n-1}N^- + CO \tag{35}$$

$$C_nN^- + X^+ \rightarrow C_nN + X \tag{36}$$

In the absence of any experimental measurements at the time, Harada and Herbst[45] and Walsh et al.[41] employed estimates of the rate coefficients in accordance with those assumed for the polyyne anions by Millar et al.[40] Walsh et al.[41] also expanded the chemistry for the bare carbon-chain and polyyne anions to include additional destruction through reaction with N atoms (using reaction channels and rate coefficients measured by Eichelberger et al. in 2007[155]) and through mutual neutralization with abundant cations. The inclusion of the destruction pathway through reaction with N also allowed additional formation pathways to the C_nN^- anions

$$C_nH_m^- + N \rightarrow H_mC_nN + e^-, \quad \text{for odd } n \tag{37}$$

$$C_nH_m^- + N \rightarrow C_{n-1}H_m^- + CN \tag{38}$$

$$C_nH_m^- + N \rightarrow C_{n-1}H_m + CN^- \tag{39}$$

$$C_nH_m^- + N \rightarrow C_{n-3}H_m + C_3N^-, \quad \text{for } n > 5 \tag{40}$$
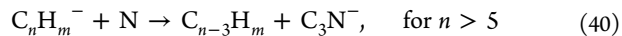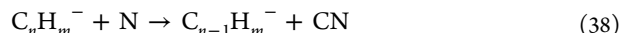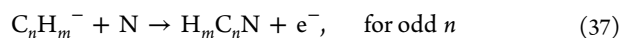
with the branching ratio to form the cyanopolyynes taken to be 0.5.[222]

Walsh et al. determined anion-to-neutral ratios of 5.3% and 4.0% for C_6H^- and C_8H^-, respectively.[41] These values are in good agreement with the earlier values from Millar et al.[40] and the values observed in dark clouds.[13,26,36,37,39] They also predicted an anion-to-neutral ratio for C_3N^- lower than the upper limit determined by Thaddeus et al. in TMC-1.[30] The ratio determined for C_4H^-, however, as found in earlier models, remained larger than the observed upper limit by more than 2 orders of magnitude.

The main goal of the work presented by Walsh et al. was to investigate the influence of the addition of anion chemistry on the existing gas-phase chemistry.[41] Work by Harada and Herbst modeling the envelope of the protostar L1527 hinted that molecular anions might have a catalytic effect on the production of larger hydrocarbon molecules.[45] Walsh et al. concluded that anion chemistry enhanced the production of the larger members of hydrocarbons, in particular, the families of C_n, C_nH, C_nH_2, and HC_nN molecules, with the relative enhancement increasing with increasing size of the molecule.[41] The effect was particularly significant for the cyanopolyynes (HC_nN), because the inclusion of anions increased the abundances sufficiently to improve the agreement with observation for the larger polyynes: HC_5N, HC_7N, and HC_9N.[210] The cyanopolyynes have a formation route through the reaction

$$C_nH_2 + CN \rightarrow HC_{n+1}N + H \tag{41}$$
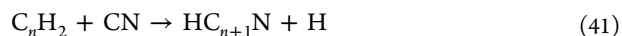
The C_nH_2 abundances are enhanced in the presence of anions through the reaction

$$C_nH^- + H \rightarrow C_nH_2 + e^- \tag{42}$$

which dominates the formation of the C_nH_2 species up to ~10^6 years.

Later, Cordiner and Charnley conducted a parameter-space investigation of anion chemistry in dark clouds for the first time,[42] in which they also included charge exchange between anions and dust grains, the freezeout of gas-phase material on dust grains, and desorption back into the gas phase through cosmic-ray heating of dust grains.[223,224] They investigated three different scenarios: (i) gas-phase only (model I), (ii) freezeout without desorption (model II), and (iii) freezeout with desorption (model III). For their "typical" dark cloud model, that is, at a density of 10^4 cm^{-3}, they found anion-to-neutral ratios of 0.29% and 2.3% for C$_4$H$^-$ and C$_6$H$^-$, respectively. They concluded that models that included freezeout and cosmic-ray-induced desorption are also able to reproduce the observed anion-to-neutral ratios with a reasonable degree of accuracy. This first parameter-based study demonstrated the sensitivity of the anion chemistry to various model assumptions including the effect of O atoms on the C$_6$H$^-$-to-C$_6$H ratio, with the potential (within model uncertainties) of using the ratio to probe the depletion of oxygen in dense clouds. We highlight here that much parameter space remains to be investigated, for example, temperature, initial elemental abundances, and the effect of grain-surface chemistry.

The latest release of the UMIST Database for Astrochemistry, RATE12, includes the chemistry of the families of molecular anions C$_n$H$_m^-$ (n = 1−10, m = 0, 1) and C$_n$N$^-$ (n = 1, 3, 5).[43] Updates since the compilation of the original anion network include newly measured photodetachment cross sections for hydrocarbon anions C$_2$H$^-$, C$_4$H$^-$, and C$_6$H$^-$ by Best et al.[142] and new experimentally measured rate coefficients for the reactions between C$_n$N$^-$ and H atoms by Yang et al.[225] McElroy et al.[43] also ran a typical dark cloud model to benchmark their network and to compare with previous releases of the database. They calculated anion-to-neutral ratios of 0.76%, 2.5%, and 1.8% for C$_4$H$^-$, C$_6$H$^-$, and C$_8$H$^-$, respectively. As found in previous models, these values (and the corresponding column densities) for C$_6$H$^-$ and C$_8$H$^-$ agree well with observations; however, the ratio for C$_4$H$^-$ remains about 2 orders of magnitude larger than that observed. McElroy et al.[43] also published results from a model using the full KIDA network available at that time, uva.kida.2011.[206] KIDA contains the anion chemical network compiled by Harada and Herbst in 2008.[45] The anion-to-neutral ratios calculated using KIDA for C$_4$H$^-$, C$_6$H$^-$, and C$_8$H$^-$ are 0.4%, 3.2%, and 2.5%, respectively. The largest disagreement between models and observations occurs for C$_4$H$^-$ where, in TMC-1, for example, its observed column density is about 10−100 times less than predicted (Table 1). This discrepancy indicates that the rate coefficients for radiative electron attachment used in these models[6] are too large. As discussed in section 3.1.2, the latest calculations[105] for C$_4$H give a value some 8 orders of magnitude lower than those used previously in model calculations. We included these latest radiative electron attachment rate coefficients in an update of the McElroy et al. model and found that n(C$_4$H$^-$) reduced by about a factor of 2 to about 8×10^{10} cm^{-2}, still an order of magnitude larger than the observed value. In this case, the formation of C$_4$H$^-$ is driven by the reaction[38]

$$C_5H^- + O \rightarrow C_4H^- + CO \qquad (43)$$

with a high rate coefficient based on laboratory measurements of C$_{2n}$H$^-$ + O (n = 1−3).[155] We also investigated the effects of the freeze-out of gas onto cold grain surfaces that Cordiner and Charnley showed can affect anion chemistry. We did find a short-lived phase in the chemical evolution, about 2×10^5

years, during which the C$_4$H$^-$ abundance was close to that observed. This is not likely to be the whole solution, as the overproduction of C$_4$H$^-$ also occurs in the circumstellar envelope of IRC+10216 in which freeze-out is unimportant (see Table 1 and section 4.5). Laboratory measurements of the C$_5$H$^-$ + O and the C$_6$H$^-$ + O reactions are encouraged. Finally, we note that both RATE12 and uva.kida.2011 predict column densities and ratios for CN$^-$ and C$_3$N$^-$ within the upper limits determined for TMC-1.

Figure 5 shows the time-dependent behavior of the major anions in a model of a dark cloud such as TMC-1 using the RATE12 network.
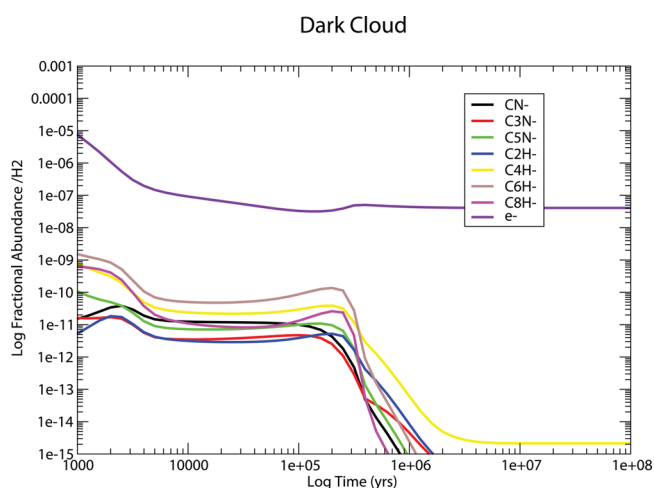
Figure 5. Time-dependent evolution of the fractional abundances of several anions and electrons in a chemical model of a cold dark cloud at 10 K.

4.3. Protostellar Envelopes

Stars form through the gravitational collapse of dense cores that form within dark molecular clouds, forming a protostar deeply embedded within a collapsing envelope of dust and gas.[226] Following the detection of C$_4$H$^-$ and C$_6$H$^-$ in the envelope of the low-mass protostar L1527,[34,44] with anion-to neutral ratios of 0.011% and 9.3%, respectively, Harada and Herbst modeled the chemistry in the envelope of this source.[45] The temperature they used was ∼30 K, higher than the typical temperature of dark clouds, ∼10 K, based on a suggestion from Sakai et al., who postulated that the surprising presence of carbon-chain molecules in the warm envelope of L1527 might be driven by the evaporation of CH$_4$ from ice mantles frozen onto dust grains.[35] This, in combination with a shorter time scale for collapse, leads to what they have termed "warm carbon-chain chemistry" (WCCC).[35] However, note that the rotational temperature derived from multiline observations of C$_6$H$^-$ lies closer to 10 than 30 K.[44]

Harada and Herbst modeled the time-dependent gas-phase chemistry in the envelope of L1527[45] and began their calculation with a significant fractional abundance of methane, CH$_4$, in the gas phase (∼3 × 10^{-6} with respect to the H number density) to simulate the WCCC proposed by Sakai et al.[35] Their model was able to reproduce the observed anion-to-neutral ratio for C$_6$H$^-$, ∼10%, at later times, between ∼10^5 and ∼10^6 years. This is despite the fact that their model overpredicts the abundance of the neutral molecule by more than an order of magnitude at all times beyond ∼10^3 years. The

results also showed that it might be possible for anions to become the main charge carrier under these conditions.[45] This is because the process of mutual neutralization is slower than the corresponding process of dissociative recombination (AB^+ + e^- → A + B, $k \approx 10^{-7}$ cm^3 s^{-1}). The addition of a large number of mutual neutralization reactions with abundant cations for each anion does not alter this result. This result is similar to that found in models in which PAH$^-$ ions are included.[14,220]

Cordiner and Charnley also ran a "L1527-like" cloud model, albeit using a lower temperature of 10 K.[42] They found that they could reproduce the observed abundances of C$_4$H, C$_6$H, and C$_6$H$^-$ to within a order of magnitude in a model that included freezeout in addition to gas-phase chemistry (model III). They attributed this result to the depletion of O atoms onto dust grains, which removed one of the main gas-phase destruction routes for carbon-chain molecules, allowing abundances of hydrocarbons to build up and persist for longer time scales. In particular, model II (freezeout without desorption) reproduced the relatively high C$_6$H$^-$/C$_6$H ratio observed in L1527 (∼10%), and they suggested that this scenario is an alternative to the WCCC postulated by Sakai et al.[35]

4.4. Photon-Dominated Regions

Photon-dominated regions (PDRs) are clouds of mainly neutral gas that are directly irradiated by UV photons emitted by nearby stars.[227] As the name suggests, UV photons dominate the physical and, thus, chemical structure. The photons heat the external layers of the cloud, and the wavelength-dependent penetration of photons leads to a characteristic stratified chemical structure.[227]

Millar et al. also investigated molecular anion chemistry in PDRs[40] using the Meudon PDR code[228] augmented with negative ions. Millar et al. assumed a fixed gas and dust temperature of 50 K, a total hydrogen density of $n(H) = 2 \times 10^4$ cm^{-3}, and parameters representative of the Horsehead Nebula: $G = 60G_0$ for the impinging radiation field (where $G_0 \approx 10^8$ photons cm^{-2} s^{-1} is the average interstellar radiation field), and $A_v = 10$ mag for the total exti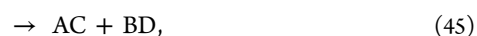nction to the cloud center.[40] Millar et al. found that significant abundances of anions are possible at low extinction, $A_v \approx 1.5–3$ mag. Because of the high abundance of electrons in this region, the radiative attachment rate is sufficient to overcome photodetachment at steady state. At lower extinctions, mutual neutralization with C$^+$ dominates the destruction of the anions. They also found that the anion-to-neutral ratios exceeded unity for anions with more than five carbon atoms. Their calculated fractional abundance for C$_4$H agreed well with that observed toward the Horsehead Nebula,[229] leading Millar et al. to conclude that C$_4$H$^-$ might be present in sufficient quantities to be observable in PDRs.[40] For the larger anions, they determined anion-to-neutral ratios of 4.7% and 17.5% for C$_6$H$^-$ and C$_8$H$^-$, respectively, indicating that these species might also be good targets. However, attempts to detect molecular anions in several well-studied PDRs proved to be futile.[34,39]

PDR models thus predict large abundances of molecular anions using the same chemical network as used in dark cloud models. The large disagreement between models and observations for PDRs might be related to the assumption of steady state adopted in the Meudon PDR code. Although a valid assumption in the lower extinction regions, as the visual extinction increases, chemical time scales generally become

longer, and the assumption breaks down. A test of the viability of the steady-state assumption would be to run a time-dependent PDR model, such as the UCL-PDR code, with anion chemistry included.[230,231] Alternatively, the disagreement might be related to the lack of experimental data available at that time for anion loss mechanisms important under PDR conditions: photodetachment and mutual neutralization. The photodetachment rate for anions in the chemical networks discussed thus far was estimated using eq 27 with a cross section of $\sigma \approx 10^{-17}$ cm^2 at threshold. Photodetachment cross sections for the C$_n$H$^-$ anions (n = 2, 4, and 6) have since been measured by Best et al.[142] They derived absolute cross sections at threshold of 7.7 × 10^{-18} cm^2 for C$_4$H$^-$ and 4.8 × 10^{-18} cm^2 for C$_6$H$^-$, reducing the photodetachment rates by a factor of 1.3 and 2, respectively, from those employed in the earlier models. Under steady-state PDR conditions, we would expect these new values to increase the anion-to-neutral ratios, rather than decrease them. The models also use a fixed rate coefficient for the process of mutual neutralization with abundant cations, and the networks include this reaction channel for each anion using a "typical" rate coefficient of $k = 7.5 \times 10^{-8}(T/300)^{-0.5}$ cm^3 s^{-1}.[232] The products are assumed to be the respective neutrals of the reactants (see reaction 24). For cations without a corresponding neutral, such as H$_3$O$^+$, the products are assumed to be the same as for the analogous process of dissociative recombination, for example, OH + 2H and H$_2$O + H. Mutual neutralization remains a poorly studied process, especially at the densities and temperatures typical of interstellar clouds. DESIREE (the Double Electrostatic Ion-Ring Experiment), currently under construction at Stockholm University, is designed specifically for the study of interactions between oppositely charged ions at low, well-defined relative velocities.[233] DESIREE will determine reaction rate coefficients and measure branching ratios for the various potential chemical pathways for the reaction of a molecular cation and anion[233]

$$AB^+ + CD^- \rightarrow AB + CD, \qquad (44)$$

$$\rightarrow AC + BD, \qquad (45)$$

$$\rightarrow A + B + CD, \qquad (46)$$

$$\rightarrow AB + C + D, \qquad (47)$$

$$\rightarrow A + B + C + D \qquad (48)$$

Currently, chemical networks include reaction 44 only or reaction 46 in the case of a cation without a neutral analogue, on the basis that mutual neutralization is a less exoergic process than dissociative recombination for the cation. Because channels that are able to decompose the anions into smaller fragments, thereby preventing easy recycling of the anion, can reduce the anion-to-neutral ratios below the upper limits observed in PDRs, the provision of experimental measurements is critical to our understanding. DESIREE was commissioned in 2014, and its first results have been released.[234]

4.5. Circumstellar Envelopes

The envelope of the carbon-rich AGB star IRC+10216 is the richest source of molecular anions found to date. All detected anions, C$_4$H$^-$, C$_6$H$^-$, C$_8$H$^-$, CN$^-$, C$_3$N$^-$, and C$_5$N$^-$, have been observed in this object.[13,24,28−32,235] Millar et al. were the first to include molecular anions in a chemical model of IRC +10216.[12] They added the carbon-chain anions C$_n^-$ and C$_n$H$^-$ ($n \geq 7$) using the network from Bettens and Herbst[213] and radiative attachment rates from Terzieva and Herbst.[9] They

employed a simple model for the CSE in which the gas is assumed to expand in a spherically symmetric manner with a constant velocity, 14 km s^{-1}, and mass-loss rate, 3×10^{-5} M$_\odot$ year^{-1}. The number density of the gas thus follows an r^{-2} distribution. The temperature profile was treated as a power law according to $T(r) = \max[100(r/r_i)^{-0.79}, 10]$ K, and the visual extinction through the envelope was determined using the method of Jura and Morris.[236] Figure 6 shows the typical

Figure 6. Schematic structure of the CSE for a C-rich AGB star, which is divided into six regions for modeling purposes: (I) degenerate C/O core and He/H burning shell, (II) convective shell, (III) stellar atmosphere in which parent species are formed, (IV) dust formation shell with an expanding envelope, (V) outer CSE where daughter species are formed primarily by photodissociation, and (VI) interstellar medium (ISM). Reproduced with permission from ref 237. Copyright 2014 EDP Sciences.

structure of a carbon-rich envelope[237] in which parent molecules, along with carbonaceous dust grains, are formed near the stellar surface. The parent molecules are injected at the innermost radius and are assumed to have formed in the photosphere of the star: CO, C$_2$H$_2$, CH$_4$, HCN, NH$_3$, N$_2$, and H$_2$S. The chemistry is now computed as a function of radius rather than time. Millar et al.[12] determined that molecular anions can reach large abundances in the outer regions of the circumstellar envelope, $r \gtrsim 10^{17}$ cm. They determined an anion-to-neutral ratio for C$_8$H$^-$ equal to 25%, which agrees very well with the ratio later observed by Remijan et al. (26%).[28]

Following the identification of C$_6$H$^-$ in IRC+10216,[24] Millar et al.[40] expanded their chemical model to include carbon-chain anions down to $n = 4$ (as was done for the dark cloud models, as discussed earlier). They determined anion-to-neutral ratios of 0.77%, 30%, and 28% for C$_4$H$^-$, C$_6$H$^-$, and C$_8$H$^-$, respectively. The value for C$_6$H$^-$ was large compared with the observed anion-to-neutral ratios available at that time (from 1% to 9% for C$_6$H$^-$[13,235]). Follow up observations of C$_6$H by Cernicharo et al.[29] further constrained the neutral column density to derive an anion-to-neutral ratio of 6.2%.

Millar et al.[40] found that the hydrocarbon abundances are sensitive to the initial assumed abundance of C$_2$H$_2$ (carbon-chain growth depends on the addition of available C$_2$ units). Remijan et al. revisited the model of Millar et al.,[40] following their detection of C$_8$H$^-$ in IRC+10216.[28] Using the same physical model, they calculated the abundance of carbon-chain

neutrals and anions for different models in which the initial fractional abundance of C$_2$H$_2$ (relative to H$_2$) was varied. They found that lowering their initial fractional abundance of C$_2$H$_2$ to 10^{-5} (relative to H$_2$) improved the agreement with the observed column densities for C$_6$H and C$_8$H and their respective anions. However, despite this improved agreement with observed column densities, their modeled anion-to-neutral ratios increased to ~2 and ~2.4 for C$_6$H$^-$ and C$_8$H$^-$, significantly worsening agreement with observation (8.6% and 26%, respectively).

Cernicharo et al. reported the detection of C$_4$H$^-$ in IRC +10216, deriving an anion-to-neutral ratio of 0.024%.[29] They also modeled the chemistry in the circumstellar envelope, employing the physical model described by Agúndez and Cernicharo,[238] which is similar to that described above from Millar et al.[12,40] Instead of employing theoretical radiative attachment rates, Cernicharo et al.[29] derived radiative attachment rates using the existing observations for C$_4$H$^-$ and C$_6$H$^-$. Assuming steady-state conditions and neglecting photodetachment, they expressed the anion-to-neutral ratio as

$$\frac{n(X^-)}{n(X)} = \frac{k_{ra}n(e^-)}{k_{ad}n(H) + k_{mn}n(Y^+)}$$

(49)

following Herbst.[7] If one assumes that $n(Y^+) = n(e^-)$, rearranging gives

$$k_{ra} = \frac{1}{n(e^-)} \frac{n(X^-)}{n(X)}[k_{ad}n(H) + k_{mn}n(e^-)] \text{ cm}^3 \text{ s}^{-1}$$

(50)

Cernicharo et al.[29] assumed $n(H)/n(H_2) = 10^{-4}$ and $n(e^-)/n(H_2) = 10^{-7}$ and used the observed anion-to-neutral ratios to derive radiative attachment rate coefficients equal to 2×10^{-10} and 5×10^{-8} cm^3 s^{-1} for C$_4$H and C$_6$H, respectively. Their estimate for C$_4$H was lower than that later calculated by Herbst and Osamura;[6] however, as already discussed, it is possible that the theory used to calculate the radiative attachment rate is inadequate for the smaller hydrocarbons. On the other hand, this simple approach derives radiative attachment rate coefficients for C$_6$H and C$_8$H that agree reasonably well with the theoretical values. We note here that care must be taken when deriving rate coefficients from observational results. In particular, the assumption that $n(Y^+) = n(e^-)$ was shown to be invalid because of the rapid capture of free electrons by carbon chains.[40] Often, the chemistry of the species in question is not completely defined, and important production and/or destruction routes can be neglected in chemical models.

Thaddeus et al. revisited this simple model following their detection of C$_3$N$^-$ in IRC+10216,[30] for which they determined an anion-to-neutral ratio of 0.52%. They derived a radiative attachment rate for C$_3$N equal to $1.9 \times 10^{-9}(T/300)^{-0.5}$ cm^3 s^{-1}, which is between a factor of 3 and an order of magnitude larger than that calculated by Petrie and Herbst[239] [$(2-4) \times 10^{-10}(T/300)^{-0.5}$]. Thaddeus et al. also explored the possibility that C$_3$N$^-$ has an additional route to formation through dissociative attachment to HNC$_3$, a metastable isomer of HC$_3$N (see reaction 32). Using the observed column density of HNC$_3$ in IRC+10216 (7×10^{11} cm^{-2}), they concluded that formation through dissociative attachment would require a rate coefficient of $\gtrsim 10^{-6}$ cm^3 s^{-1} to compete with radiative attachment to C$_3$N.

The same group of authors (Cernicharo et al.[31]) later identified C$_5$N$^-$ in the envelope of IRC+10216 with an anion-to-neutral ratio of ~55%, the largest of any detected anion to date. However, a reanalysis of the dipole moment of C$_5$N led to

a revised estimate for the neutral column density, leading to an anion-to-neutral ratio of 13%, more in line with the ratios observed for C_6H^- and C_8H^-. They added this species to their full chemical model of the circumstellar envelope using an estimated radiative attachment rate similar to that derived for the larger C_nH species, $2 \times 10^{-7}(T/300)^{-0.5}$ cm^3 s^{-1}. In the molecular shell of the envelope, they determined an anion-to-neutral ratio between 10% and 50%, agreeing reasonably well with the observed ratio.

A fully updated chemical model of IRC+10216 was presented in Cordiner and Millar,[46] in which they included the chemistry of all of the molecular anions detected at that time: C_4H^-, C_6H^-, C_8H^-, C_3N^-, and C_5N^-. They also included the chemistry of C_2H^- and CN^- following the measurement of their spectra in the laboratory.[240−242] Cordiner and Millar[46] also considered additional mechanisms to the formation of CN^- and C_2H^- through proton exchange of the dominant parent species (HCN and C_2H_2) with H^-

$$HCN + H^- \rightarrow CN^- + H_2 \tag{51}$$

$$C_2H_2 + H^- \rightarrow C_2H^- + H_2 \tag{52}$$
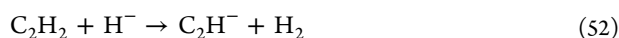
using rate coefficients from Prasad and Huntress[243] and Mackay et al.[244] This latter reaction, together with that of H^- and diacetylene to form C_4H^-, has been studied theoretically,[245] with both reactions having entrance channel barriers that give negligible reaction rate coefficients below 70 K but approach their Langevin values at higher temperatures. In the warm inner region of IRC+10216 where the density is high, H^- formation is relatively efficient, and the reactions proceed with rate coefficients on the order of 10^{-9} cm^3 s^{-1}. Because HCN and C_2H_2 are important parent species that form close to the photosphere of the star, H^- reactions do produce some CN^- and C_2H^-. Millar and Cordiner updated their physical model to include density-enhanced dust shells as revealed in scattered light images of IRC+10216[246] and first explored in models by Brown and Millar.[247] Cordiner and Millar[46] found that the inclusion of density-enhanced dust shells has a profound effect on the radial distribution of anions and their corresponding neutrals as a result of (i) the increased extinction of the interstellar radiation field and (ii) the increased efficacy of two-body reactions within the dust shells because of their higher density. However, the effect is minimal when the integrated column densities are determined. They achieved anion-to-neutral ratios of 1.5%, 7.4%, and 4.9% for C_4H^-, C_6H^-, and C_8H^-, respectively. They found improved agreement with the observed column densities of C_3N and C_3N^- and the corresponding anion-to-neutral ratio, even though they used the theoretical radiative attachment calculated by Petrie and Herbst,[239] which Thaddeus et al.[30] argued is too low to account for the observed abundance of C_3N^-. Cordiner and Millar[46] also included additional formation routes to the C_nN^- anions through the reaction between N atoms and hydrocarbon anions, $C_nH_m^-$ using the experimentally measured reaction rates from Eichelberger et al.[155] They found that these reactions improve the agreement with observations, especially for the N-containing anions. Their calculated values for C_2H^-, CN^-, and C_5N^- also agreed well with the observed values and upper limits.[29,32]

Agúndez et al.[32] detected CN^- in the envelope of IRC +10216 and also modeled the chemistry in the envelope, updating their chemical network to include much of the chemistry described by Walsh et al.[41] and Cordiner and

Millar.[46] They determined values in good agreement with observations and previous calculations. However, a fit to their observed line profiles suggested that CN^- was more centrally concentrated than predicted by their chemical model. The fit to the data suggested that the peak CN^- abundance is reached at a radius of $\sim 2 \times 10^{16}$ cm as opposed to that from the full chemical model, $\sim 5 \times 10^{16}$ cm. The chemical model included the formation route through HCN + H^-, which Agúndez et al. claimed contributes at most 0.2% toward CN^- formation in the inner regions of the envelope. Hence, the abundance and distribution of CN^- in IRC+10216 remains a challenge for modellers to explain.

In 2012, Woods et al. extended the theoretical investigation of anions in circumstellar envelopes to sources in the Large Magellanic Cloud (LMC) and Small Magellanic Cloud (SMC) to explore the chemistry of circumstellar envelopes at different metallicities.[47] Here, we discuss their anion results for galactic metallicity only (Milky Way, MW), for comparison with previous work and observations of anions in IRC+10216. For the generic MW model, they assumed an envelope expansion velocity of 20 km s^{-1} and a dust-to-gas mass ratio of 0.01, and they employed calculated abundances for the parent species computed assuming thermodynamic equilibrium (TE), which is valid for the conditions in the photosphere of the star. Consistent with previous models, they achieved reasonably good agreement with observed anion-to-neutral ratios for C_2H^-, C_8H^-, C_3N^-, and C_5N^-, despite overpredicting the column densities for C_8H^- and C_5N^- by about 2 orders of magnitude. These large column densities are likely due to the relatively large abundance of C_2H_2 used in the model.

McElroy et al. also ran a model of a CSE for the release of the recent version of the UMIST Database for Astrochemistry[43] to benchmark with previous releases of the database. The model used was that from Millar et al.,[12,40] and their results are included in Table 1. They obtained very good agreement with observations for C_2H^-, C_3N^-, and C_5N^-; however, they overpredicted the column densities and anion-to-neutral ratios for C_4H^- and C_6H^- and underpredicted the equivalent values for C_8H^- and CN^-. Followup work by Li et al. included the effects of self-shielding of N_2 photodissociation for the first time.[237,248] N_2 self-shielding reduces the available free atomic nitrogen in the outer envelope, where photodissociation becomes important for those molecules that do not self-shield. In general, the abundance of N-bearing daughter species is lowered. The results of Li et al. showed a general reduction in calculated column densities for the C_nN anions and a shift in the position of peak abundance inward toward the central star.[237,248] These results gave a slightly better agreement with observation for C_5N^- and a slightly worse agreement for CN^- and C_3N^-, compared with McElroy et al.[43] The influence of N_2 self-shielding on a CSE model including density-enhanced dust shells remains to be investigated.

Kumar et al.[48] recently measured the photodissociation rates of the CN^- and C_3N^- anions and investigated their effects on their radial distributions in IRC+10216. Figure 7 shows the radial distributions of the most abundant anions when the RATE12 network is used in conjunction with these new rates. This figure shows that the anion abundance becomes larger than the abundance of free electrons in the outer envelope in the range of $(3−6) \times 10^{16}$ cm, where C_6H^- carries the negative charge.

Because the real density distribution in IRC+10216 does not reflect that of an envelope expanding at constant velocity, we
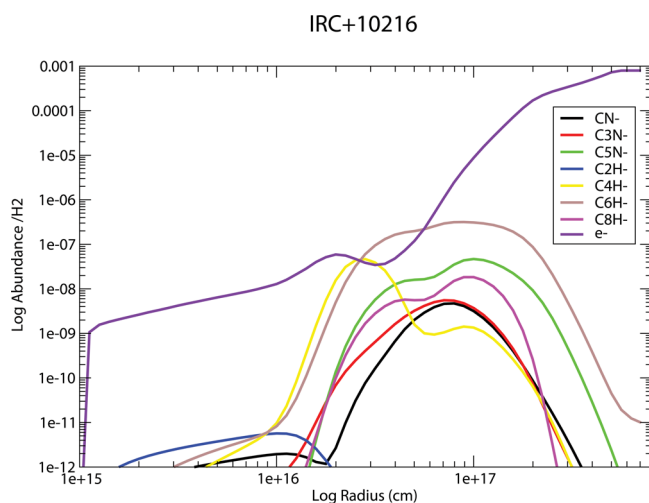
Figure 7. Radial distribution of the fractional abundances of the major anions and electrons in a chemical model of IRC+10216.

show in Figure 8 the effects of including a number of density-enhanced shells on an underlying $1/r^2$ density distribution.[46]
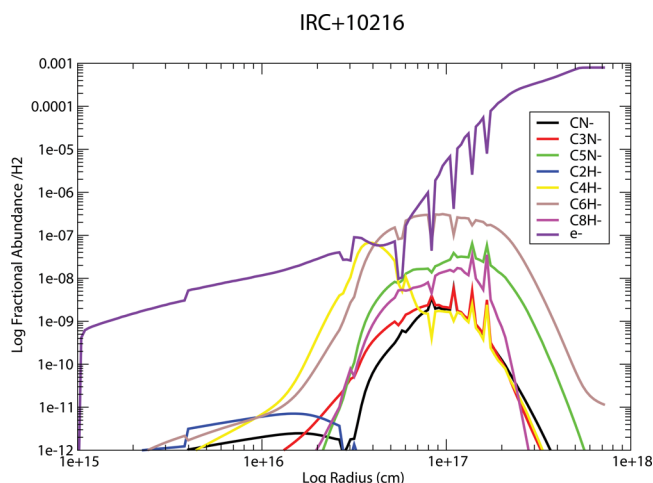

Figure 8. Radial distribution of the fractional abundances of the major anions and electrons in a chemical model of IRC+10216 in which high-density shells are included.

The primary effects of the higher-density shells are to increase the total extinction of the envelope to incoming UV photons from the interstellar medium and to decrease the collision times within the shells. Thus, parent molecules are not photodissociated as effectively in the shell model, and the rich gas-phase chemistry occurs slightly farther from the central star. In addition, the increased densities in the shells lead to peaks in the molecular abundances in the outermost shells but to a fall in the fractional abundances in the inner shells. The electron abundance falls within a shell because its abundance has an inverse proportionality to density because electrons are produced by a one-body process, photoionization, but destroyed by a two-body process, dissociative recombination with molecular cations.

The reasons for the differences between the different circumstellar models are difficult to analyze because each model employs a slightly different prescription of the physical structure of the envelope and different sets of parent molecular abundances. It has already been shown, for instance, that the

initial abundance of C_2H_2, in particular, has an effect on the calculated column densities of hydrocarbons.[28,40] Also, mutual neutralization has been shown to be an important destruction mechanism for anions in the envelope, and this remains a poorly understood process, as discussed earlier in the context of PDR models. In addition, the envelope of IRC+10216 has been shown to be highly complex, consisting of shells of material with a probable clumpy structure that can allow interstellar UV photons to penetrate the envelope to a deeper degree than heretofore believed. This is evidenced by the detection of gas-phase water in the inner envelope,[249] a very surprising observation in a carbon-rich AGB star, although shock chemistry might provide an alternative explanation. As such, simple models that assume smooth physical conditions through the envelope might be inadequate for comparison with observations of molecules that might be sensitive to the clumpy envelope structure. Millar[49] recently investigated the effect of clumps on chemistry, allowing some 2.5% of external UV photons to penetrate down to 10^{15} cm, in common with previous models.[250] We updated this model to include the latest radiative electron attachment data for CN, C_2H, and C_4H[105] and newly calculated rate coefficients for the H^- reactions with CN and HC_3N that produce CN^- and C_3N^-, respectively.[251] These deeply penetrating photons alter the radial distributions of the anions, for example, decreasing the peak fractional abundance of C_4H^- at 10^{16} cm and increasing abundances close to 10^{15} cm. Table 1 contains the resultant column densities. For most anions, the effects are negligible, but the column density of C_4H^- is now 1.7×10^{12} cm^{-2}, a factor of 10 less than that calculated by McElroy et al. and only a factor of 2.5 larger than that observed. We note, however, that the anion-to-neutral ratio is still an order of magnitude too large, indicating that the calculated column density of C_4H is an order of magnitude less than that observed. The issues for C_4H^- seen here and in the dark cloud models (section 4.2) are still not resolved. Indeed, there remains much to be understood regarding the chemistry of this intriguing CSE, and there is huge scope for further experimental and modeling efforts regarding the chemistry of anions.

4.6. Titan

There have been concerted efforts to model the chemical kinetics of anions in the atmosphere of Titan. Early models by Capone et al.[66,252] investigated the influence of cosmic-ray ionization on the ionization balance and chemistry in Titan's lower ionosphere. They included the negative ions H^- and CH_3^- and assumed formation through three-body electron attachment. They included destruction through photodetachment (important only for the dayside of the moon), associative electron detachment, and mutual neutralization. Although they concluded that ion–molecule chemistry, driven by cosmic-ray ionization of CH_4 and H_2, was likely to be important in the ionosphere, they predicted anion densities $\lesssim 10^{-4}$ times the cation density and deemed anion chemistry to be unimportant. Later, Borucki et al. extended the network to include the formation of anions through three-body electron attachment to radicals, such as NH_2, CH_3, CN, and C_2H.[67] However, they concluded that these radicals did not achieve sufficiently high abundances to efficiently form anions, predicting a maximum anion-to-cation ratio of 0.1, similar to other works at that time.[55,252]

Molina-Cuberos et al. used a parametric model in which they varied the abundance of electrophillic species in Titan's lower

atmosphere (<70 km) and computed the resulting abundances of cations, anions, and electrons.[68] For fractional abundances of electrophillic species above ~10^{-11}, they found that anions were the dominant charge carrier below an altitude of ~40 km. Such high abundances are adequate to significantly reduce the electron abundance and alter the electrical properties (e.g., conductivity) of the lower atmosphere. Borucki et al. then constructed a model in which they considered the influence of anions and charging of aerosols on the electrical properties of the lower atmosphere.[253] They included the formation of PAH⁻ ions following the work by Lebonnois et al. and Bakes et al. that showed that PAHs were a likely candidate for the composition of Titan's haze layer.[254,255] They found that the inclusion of anions and charged aerosols substantially reduced the abundance of electrons, namely, the ionization degree of the gas. They also computed that the charge state of aerosols changed from mainly positive during the day to mainly negative during the night, whereas the PAHs remained mainly neutral during the day and negative at night, in accordance with the earlier work by Bakes et al.[255] This work was the first to conclude that anions had a potentially important role in Titan's atmosphere.

Vuitton et al. included the chemistry of these molecular anions in a chemical model of the ionosphere for the first time,[69] extending an earlier model used to investigate the chemistry of ions, nitrogen-bearing species, and benzene in the ionosphere,[59,256,257] to compute the abundance of molecular anions at altitudes between 700 and 1200 km. They included much of the anion chemistry already discussed in this review, using typical or measured rate coefficients for each process. They also included additional reactions: formation through ion-pair production (i.e., $AB + h\nu \rightarrow A^- + B^+$) with cross sections of ~10^{-23}–10^{-19} cm² and destruction through proton transfer (or hydrogen abstraction, i.e., $AH + B^- \rightarrow A^- + BH$), using the Langevin (collisional) rate for all reactions without measured rate coefficients. Vuitton et al.[69] solved the chemistry in the ionosphere as a function of altitude, assuming steady state, that is, $dn_i/dt = 0$, a valid assumption in planetary atmospheres, given the short chemical time scales. They determined that CN^- and C_3N^- were the most abundant anions, with number densities of ~1 and 0.2 cm⁻³, respectively, at an altitude of ~1000 km. C_5N^- became the most abundant anion lower in the atmosphere, ≲850 km, because of the larger height of HC_5N. C_4H^- and C_6H^- also contributed significantly to the total anion abundance at lower altitudes (with densities of ~10^{-3}–10^{-2} cm⁻³), with all other anionic species being negligible. They found that CN^- was predominantly formed through dissociative electron attachment to HCN and HC_3N by solar photoelectrons, whereas C_3N^- was formed through proton transfer from HC_3N to CN^-. This is different from the findings of models of CSEs in which CN^- is formed through the reaction of bare carbon-chain anions and N atoms in the outer envelope and C_3N^- is formed through radiative attachment to the neutral and through the reaction of the larger bare carbon-chain anions ($n > 5$) and N atoms.[32,46,155,239] At the peak anion density, Vuitton et al. calculated anion-to-neutral ratios of 0.0024%, 0.016%, and 4.7% for C_2H^-, C_4H^-, and C_6H^-, respectively, and 1.9%, 0.19%, and 0.35% for CN^-, C_3N^-, and C_5N^-, respectively.[69] Interestingly, they saw a general increase in the ratio with increasing size of the hydrocarbon anions, as also observed in dark clouds and CSEs. However, they saw the opposite trend for the N-bearing anions, with a general decrease in the ratio with increasing anion size,

opposite to that observed in IRC+10216. The different behaviors reflect the different mechanisms by which the anions form. An increase in the anion-to-neutral ratio with increasing size under interstellar conditions is due to the increase in radiative attachment rates with molecule size. Also, interstellar conditions favor the production of unsaturated species and radicals, necessary for the formation of molecular anions through bare carbon-chain molecules.

More recent models have considered the role of rapid association reactions in forming hydrocarbons,[258] and the Bordeaux group has investigated hydrocarbon and O and N chemistry.[259,260] Loison et al.[261] discussed the complex gas-phase neutral chemistry of Titan's atmosphere in which reactive radicals are produced initially by photochemistry and high-energy electron collisions. These models have some success in reproducing observations but do not, as yet, describe a complete chemical model for the atmosphere, indicating a lack of accurate rate coefficients for some critical reactions, a lack of completeness in the reaction network, or a poor physical description of the gas.

In the most recent article from the Bordeaux group, Dobrijevic et al.[262] described a one-dimensional photochemical model that includes anions as well as neutral and cationic species. They also included a sensitivity analysis to identify key reactions for further study. In their model, anion chemistry is driven primarily by the dissociative electron attachment of CH_4 to produce H^-, which reacts with HCN to produce CN^- and with C_2H_2 to produce C_2H^-. The high abundance of HCN on Titan ensures that CN^- is the dominant anion. Here, the initial reaction with CH_4 requires high-energy (~10 eV) electrons, available on Titan but not in cold interstellar clouds, where H^- is produced inefficiently as a minor channel in the cosmic-ray ionization of H_2.

4.7. Cometary Comae

Cordiner and Charnley reported results of a model of the chemical structure of a cometary coma including the chemistry of the molecular anions discussed in this review.[263] They used a combined chemical and hydrodynamic model that follows the dynamical evolution of the gas following sublimation from the comet surface.[264] Using parameters applicable to comet Halley, they found that the hydrocarbon anions C_4H^- and C_6H^- are efficiently formed through radiative electron attachment to the neutral with C_6H^-, reaching a peak abundance of ~10^{-6} relative to gas-phase water between 100 and 1000 km from the comet nucleus. In the inner coma (<1000 km), they found that anions can exceed the electron abundance, thereby becoming the main charge carrier. This has implications for the physical structure of the coma, raising the ion abundances and reducing their average temperatures in the innermost region.

Farther out in the coma, beyond 2000 km, dissociative electron attachment of C_2H_2 and HCN dominates the production of C_2H^- and CN^-, respectively. In this region, the photoionization of H_2O produces electrons in a less dense environment where collisional energy loss is not as important as in the inner coma. As a result, the electron energies are large enough to overcome the endothermicities of these dissociative electron attachment reactions.

5. CONCLUSIONS

For many years, the presence of anions in the interstellar medium was simply the suggestion of theoreticians. However, with the provision of laboratory microwave spectra of a number

of polyynyl anions, it is now known that a few, presently three, carbon-chain molecular anions are present in cold, dark clouds. These anions are present in the cold circumstellar envelopes around carbon-rich AGB stars that also contain three cyanopolyynyl anions, essentially driven by the large abundance of HCN, which is created in high-temperature chemistry in the stellar photosphere. Most surprising of all was the detection of anions in Titan's atmosphere with mass-to-charge ratios from about 10 up to 10 000. Because these detections are mass spectroscopic in nature, with relatively low mass resolution, individual anions have not yet been detected, but models[69,262] indicate that the same type of circumstellar anions dominate on Titan, at least for small mass-to-charge ratios.

Models indicate that anions can have a larger abundance than free electrons in some sources and that they play an important role in the synthesis of very large hydrocarbon species. These results, together with the expectation that PAH molecules, which can contain up to 10% cosmic carbon, are predominantly negatively charged in regions shielded from UV radiation, indicate that anions might also play a role in regulating the interaction of magnetic fields with the gas. A better understanding of PAH chemistry is important because PAHs might provide most of the "particle" surface area in dense clouds. Furthermore, the importance of even larger-mass species, for example, fullerenes,[265,266] in contributing to the charge balance and anion chemistry in interstellar and circumstellar environments is yet to be quantified.[267−269]

A detailed knowledge of the properties and influence of anions will be possible only when the fundamental processes involved in their formation and destruction are better understood. These processes, including radiative attachment and dissociative electron attachment at low electron energies and photodetachment, all play important roles in determining anion abundances, and improved laboratory data and theoretical studies are needed. There is currently some uncertainty over rates of radiative electron attachment, which are key data for modeling anion abundances. Progress has been made in calculations of these attachment rates, but further work would be beneficial, particularly in trying to determine the importance of indirect electron attachment to larger poly-acetylenic-type molecules. Determining these rates is a serious challenge to both theory and experiment.

Given the presence of very large anions in Titan's atmosphere and potentially elsewhere, data on anion−cation collisions should be a major objective of experiments. It is particularly noticeable that models for C_4H^- chemistry all fail to give good agreement with observation, predicting anion-to-neutral ratios a factor of 10 larger, whereas the C_8H^-/C_8H abundance ratio is typically an order of magnitude too small using the best available data. In this particular case, the fact that formation is calculated to be dominated by radiative electron attachment at the collisional rate indicates that we are missing other, dominant routes to C_8H^-.

Although it appears that the detection of new molecular anions in space has stagnated in recent years, the theoretical community remains active in identifying potential targets for astrophysical observations (e.g., c-C_3H^- and C_3P^-).[270,271] Furthermore, there remains the possibility for new molecular anions to be identified through their electronic transitions.[20,22,140,272]

The current development of band 1 (31−45 GHz) receivers for the Atacama Large Millimeter/Submillimeter Array (ALMA) will make feasible sensitive searches for new large

hydrocarbon anions. The detectability of weak rotational lines of linear molecules such as $C_{10}H^-$ and $C_{12}H^-$ in cold dark clouds depends primarily on their abundance and permanent electric dipole moment. Models of dark cloud chemistry[43] show that abundances of hydrocarbon anions with six or more carbon atoms fall by a factor of 3−5 as the size of the chain increases by one C_2 unit. Because line intensity is proportional to the square of the electric dipole moment, this fall in abundance is partially offset by the fact that the dipole moment increases as the length of the chain increases. Botschwina and Oswald[273] calculated the dipole moments of C_8H^-, $C_{10}H^-$, and $C_{12}H^-$ to be 12.37, 15.71, and 19.28 D, respectively.

The polycarbon oxides C_nO, n = 2, 3, have been detected in interstellar clouds, and models of dark clouds indicate that larger analogues might be present. Cordiner and Charnley[42] considered the formation of the polycarbon oxides and related anions up to C_7O, C_7O^-, and HC_7O^-, showing that relatively large abundances of the anions could occur. Blanksby et al.[274] showed that the polycarbon oxides have large electron affinities and that their anions are linear with large dipole moments, up to 8.3 D for $C_{10}O^-$. Millimeter-wave spectra are needed for astronomical searches.

The additional sensitivity over current telescopes that ALMA will achieve in band 1 will also allow deeper searches to be made in photon-dominated regions (PDRs). As discussed in section 4.4, models predict relatively large anion-to-neutral abundance ratios for C_4H^-, C_6H^-, and C_8H^-, based on a "bottom-up" chemistry, despite the high rates for electron photodetachment in such sources. Hydrocarbon chains might also be produced in a "top-down" chemistry through, for example, the photodestruction of polycyclic aromatic hydrocarbons and fullerenes. A detailed model of such chemistries is needed using a time-dependent, rather than steady-state, chemical kinetic code.

At present, high-spatial-resolution observations of anion distributions are rare, although the Atacama Large Millimeter/Submillimeter Array (ALMA) is beginning to provide the necessary data, particularly for AGB stars, where observations are essentially limited to the nearest object, IRC+10216, and for which there are models that take into account the inhomogeneous nature of the circumstellar envelope.

Within PDRs and molecular clouds, mutual neutralization is an important destructive process for anions, but detailed rate coefficients are lacking, with models usually adopting a "standard" rate coefficient for all reactions. The determination of individual rate coefficients and associated branching ratios with double-ring storage experiments such as DESIREE will be an important step forward. Branching ratios are, in fact, missing for many important anion−neutral reactions: Their specific values can make observable differences to calculated anion−neutral abundances.[42] Examples for which such measurements would be welcome include O + C_5H^- and O + C_6H^-.

The presence of molecular anions can cause significant changes to the physics. In section 4.5, we showed how efficient formation of hydrocarbon anions can result in abundances greater than those of free electrons in certain parts of the circumstellar envelope. A similar result is found in cometary comae (section 4.7), where it leads to an increase in ion abundances and cooling in the inner comae. The relationship between anions and free electrons and its effect on dynamics must still be determined in models of protoplanetary disks (PPDs) and collapsing molecular clouds. In both objects, the presence of magnetic fields can affect the flow of the gas

through interactions with charged particles. In PPDs with weak magnetic fields, a magneto-rotational instability allows for the transfer of angular momentum outward while allowing mass to be transferred inwardly to the central star. The presence of the instability is directly linked to the ionization level of the gas: When it falls too low, the gas and the magnetic fields decouple, and the instability is quenched.[275] To date, there has been no investigation of the effect of anions on the presence of the instability, and this topic is worthy of future study.

AUTHOR INFORMATION

Corresponding Author

*E-mail: tom.millar@qub.ac.uk.

Notes

The authors declare no competing financial interest.

Biographies

Thomas J. Millar studied mathematics at the University of Manchester Institute of Science and Technology (UMIST) in 1973 before obtaining a Ph.D. in astrochemistry at the same institution in 1976. Following postdoctoral positions at York University (Toronto, Canada) and the University of Oxford, he moved as an SRC-funded Advanced Fellow back to UMIST in 1981. He was subsequently appointed to a lectureship in the Department of Mathematics. He was promoted to Professor of Astrophysics in 1995 and served subsequently as Head of the Department of Physics and Pro-Vice-Chancellor (Staffing) at UMIST. He moved to Queen's University Belfast in 2006 as Dean of the Faculty of Engineering and Physical Sciences and Professor of Astrophysics in the School of Mathematics and Physics. He has worked on most areas of astrochemistry during his career and has published more than 250 articles on the topic. He has managed the UMIST Database for Astrochemistry (www.udfa.net), a resource for the provision of data and codes for modeling chemical kinetics in various astronomical regions, since 1991. Although primarily a theoretician, he has a strong interest in observations and served as Chair of the International Board of the James Clerk Maxwell Telescope in Hawaii. He has also served as President of the International Astronomical Union's Division on Interstellar Matter and is currently President of the IAU Commission on Astrochemistry. He has been actively involved in gender issues for many years and is Director of the Queen's SWAN Initiative, which has primary responsibility for both institutional and school engagement with the Athena SWAN charter mark. In 2011, he was elected a member of the Royal Irish Academy.

Catherine Walsh obtained her Ph.D. in astrophysics from Queen's University Belfast (QUB) in 2010, with a thesis focussed on chemical processes in protoplanetary disks. She stayed at QUB for several years as a post-doctoral research fellow before moving to Leiden Observatory, Leiden, The Netherlands, in 2012. While at Leiden, she was awarded an early-career personal fellowship through the Innovational Research Incentives Scheme Veni, from the Netherlands Organisation for Scientific Research (NWO). This allowed her to conduct independent research exploring the connection between the chemical composition of protoplanetary disks and (exo)planetary systems. In September 2016, she moved to the University of Leeds as a University Academic Fellow. Although her early research focussed primarily on theoretical modeling of chemistry in star-forming regions, more recently, she has also worked with (sub)millimeter interferometric observations of dust and molecules in protoplanetary disks with ALMA (Atacama Large Millimeter/Submillimeter Array).

Thomas A. Field studied chemistry at the University of Oxford, where he completed his D.Phil. degree in 1996. He then obtained a postdoctoral position in Paris, France, based at L'Observatoire de Paris-Meudon and Université de Cergy-Pontoise. In 1997, he moved to a teaching fellow position in Chemistry at the University of Nottingham. He then moved to academic positions in the Physics departments at The University of Newcastle-upon-Tyne in 1999 and Queen's University Belfast in 2001, where he currently works in the School of Mathematics and Physics, Centre for Plasma Physics. His main research interests center on the behavior of molecular ions and particularly negative ions formed by electron attachment and the process of electron attachment; small time-of-flight mass spectrometers have featured heavily as an experimental research tool in these investigations. He also works on macroscopic plasmas and experiments to simulate the bombardment of astrophysical ices with ions having energies of a few kiloelectronvolts.

ACKNOWLEDGMENTS

REFERENCES

(1) Wildt, R. Negative Ions of Hydrogen and the Opacity of Stellar Atmospheres. *Astrophys. J.* **1939**, *90*, 611−620.

(2) McDowell, M. R. C. On the Formation of H_2 in H I Regions. *Observatory* **1961**, *81*, 240−243.

(3) Galli, D.; Palla, F. The Dawn of Chemistry. *Annu. Rev. Astron. Astrophys.* **2013**, *51*, 163−206.

(4) Dalgarno, A.; McCray, R. A. The Formation of Interstellar Molecules from Negative Ions. *Astrophys. J.* **1973**, *181*, 95−100.

(5) Sarre, P. J. On the Possible Detection of Negative Ions in the Interstellar Medium. *J. Chim. Phys.* **1980**, *77*, 769−771.

(6) Herbst, E.; Osamura, Y. Calculations on the Formation Rates and Mechanisms for C_nH Anions in Interstellar and Circumstellar Media. *Astrophys. J.* **2008**, *679*, 1670−1679.

(7) Herbst, E. Can Negative Molecular Ions be Detected in Dense Interstellar Clouds? *Nature* **1981**, *289*, 656−657.

(8) Bettens, R. P. A.; Herbst, E. The Abundance of Very Large Hydrocarbons and Carbon Clusters in the Diffuse Interstellar Medium. *Astrophys. J.* **1996**, *468*, 686−693.

(9) Terzieva, R.; Herbst, E. Radiative Electron Attachment to Small Linear Carbon Clusters and its Significance for the Chemistry of Diffuse Interstellar Clouds. *Int. J. Mass Spectrom.* **2000**, *201*, 135−142.

(10) Campbell, E. K.; Holz, M.; Gerlich, D.; Maier, J. P. Laboratory Confirmation of C_{60}^+ as the Carrier of two Diffuse Interstellar Bands. *Nature* **2015**, *523*, 322−323.

(11) Rudkjøbing, M. Tentative Identification of the Diffuse Interstellar Absorption Bands and of a Diffuse Interstellar Doublet Line. *Astrophys. Space Sci.* **1969**, *3*, 102−108.

(12) Millar, T. J.; Herbst, E.; Bettens, R. P. A. Large Molecules in the Envelope Surrounding IRC+10216. *Mon. Not. R. Astron. Soc.* **2000**, *316*, 195−203.

(13) McCarthy, M. C.; Gottlieb, C. A.; Gupta, H.; Thaddeus, P. Laboratory and Astronomical Identification of the Negative Molecular Ion C_6H^-. *Astrophys. J.* **2006**, *652*, L141−L144.

(14) Lepp, S.; Dalgarno, A. Polycyclic Aromatic Hydrocarbons in Interstellar Chemistry. *Astrophys. J.* **1988**, *324*, 553−556.

(15) Allamandola, L. J.; Tielens, A. G. G. M.; Barker, J. R. Interstellar Polycyclic Aromatic Hydrocarbons - The Infrared Emission Bands, the Excitation/Emission Mechanism, and the Astrophysical Implications. *Astrophys. J., Suppl. Ser.* **1989**, *71*, 733−775.

(16) Omont, A. Physics and Chemistry of Interstellar Polycyclic Aromatic Molecules. *Astron. Astrophys.* **1986**, *164*, 159−178.

(17) Schild, R.; Chaffee, F.; Frogel, J. A.; Persson, S. E. The Nature of Infrared Excesses in Extreme Be Stars. *Astrophys. J.* **1974**, *190*, 73−83.

(18) Snow, T. P., Jr. A Search for H⁻ in the Shell Surrounding Chi Ophiuchi. *Astrophys. J.* **1975**, *198*, 361−367.

(19) Ross, T.; Baker, E. J.; Snow, T. P.; Destree, J. D.; Rachford, B. L.; Drosback, M. M.; Jensen, A. G. The Search for H⁻ in Astrophysical Environments. *Astrophys. J.* **2008**, *684*, 358−363.

(20) Sarre, P. J. The Diffuse Interstellar Bands: A Dipole-Bound State Hypothesis. *Mon. Not. R. Astron. Soc.* **2000**, *313*, L14−L16.

(21) Tulej, M.; Kirkwood, D. A.; Pachkov, M.; Maier, J. P. Gas-Phase Electronic Transitions of Carbon Chain Anions Coinciding with Diffuse Interstellar Bands. *Astrophys. J.* **1998**, *506*, L69−L73.

(22) Cordiner, M. A.; Sarre, P. J. The CH_2CN^- Molecule: Carrier of the $\lambda 8037$ Diffuse Interstellar Band? *Astron. Astrophys.* **2007**, *472*, 537−545.

(23) Fortenberry, R. C.; Crawford, T. D.; Lee, T. J. The Possible Interstellar Anion CH_2CN^-: Spectroscopic Constants, Vibrational Frequencies, and Other Considerations. *Astrophys. J.* **2013**, *762*, 121.

(24) Kawaguchi, K.; Kasai, Y.; Ishikawa, S.-I.; Kaifu, N. A Spectral-Line Survey Observation of IRC + 10216 between 28 and 50 GHz. *Publ. Astron. Soc. Jpn.* **1995**, *47*, 853−876.

(25) Aoki, K. Candidates for U-lines at 1377 and 1394 MHz in IRC + 10216: Ab Initio Molecular Orbital Study. *Chem. Phys. Lett.* **2000**, *323*, 55−58.

(26) Brünken, S.; Gupta, H.; Gottlieb, C. A.; McCarthy, M. C.; Thaddeus, P. Detection of the Carbon Chain Negative Ion C_8H^- in TMC-1. *Astrophys. J.* **2007**, *664*, L43−L46.

(27) Gupta, H.; Brünken, S.; Tamassia, F.; Gottlieb, C. A.; McCarthy, M. C.; Thaddeus, P. Rotational Spectra of the Carbon Chain Negative Ions C_4H^- and C_8H^-. *Astrophys. J.* **2007**, *655*, L57−L60.

(28) Remijan, A. J.; Hollis, J. M.; Lovas, F. J.; Cordiner, M. A.; Millar, T. J.; Markwick-Kemper, A. J.; Jewell, P. R. Detection of C_8H^- and Comparison with C_8H toward IRC + 10216. *Astrophys. J.* **2007**, *664*, L47−L50.

(29) Cernicharo, J.; Guélin, M.; Agúndez, M.; Kawaguchi, K.; McCarthy, M.; Thaddeus, P. Astronomical Detection of C_4H^-, the Second Interstellar Anion. *Astron. Astrophys.* **2007**, *467*, L37−L40.

(30) Thaddeus, P.; Gottlieb, C. A.; Gupta, H.; Brünken, S.; McCarthy, M. C.; Agúndez, M.; Guélin, M.; Cernicharo, J. Laboratory and Astronomical Detection of the Negative Molecular Ion C_3N^-. *Astrophys. J.* **2008**, *677*, 1132−1139.

(31) Cernicharo, J.; Guélin, M.; Agúndez, M.; McCarthy, M. C.; Thaddeus, P. Detection of C_5N^- and Vibrationally Excited C_6H in IRC + 10216. *Astrophys. J.* **2008**, *688*, L83−L86.

(32) Agúndez, M.; Cernicharo, J.; Guélin, M.; Kahane, C.; Roueff, E.; Kłos, J.; Aoiz, F. J.; Lique, F.; Marcelino, N.; Goicoechea, J. R.; González García, M.; Gottlieb, C. A.; McCarthy, M. C.; Thaddeus, P. Astronomical Identification of CN^-, the Smallest Observed Molecular Anion. *Astron. Astrophys.* **2010**, *517*, L2.

(33) Sakai, N.; Sakai, T.; Yamamoto, S. Tentative Detection of C_4H^- toward the Low-Mass Protostar IRAS 04368 + 2557 in L1527. *Astrophys. J.* **2008**, *673*, L71−L74.

(34) Agúndez, M.; Cernicharo, J.; Guélin, M.; Gerin, M.; McCarthy, M. C.; Thaddeus, P. Search for Anions in Molecular Sources: C_4H^- Detection in L1527. *Astron. Astrophys.* **2008**, *478*, L19−L22.

(35) Sakai, N.; Sakai, T.; Hirota, T.; Yamamoto, S. Abundant Carbon-Chain Molecules toward the Low-Mass Protostar IRAS 04368 + 2557 in L1527. *Astrophys. J.* **2008**, *672*, 371−381.

(36) Sakai, N.; Shiino, T.; Hirota, T.; Sakai, T.; Yamamoto, S. Long Carbon-chain Molecules and Their Anions in the Starless Core, Lupus-1A. *Astrophys. J., Lett.* **2010**, *718*, L49−L52.

(37) Cordiner, M. A.; Charnley, S. B.; Buckle, J. V.; Walsh, C.; Millar, T. J. Discovery of Interstellar Anions in Cepheus and Auriga. *Astrophys. J., Lett.* **2011**, *730*, L18.

(38) Cordiner, M. A.; Buckle, J. V.; Wirström, E. S.; Olofsson, A. O. H.; Charnley, S. B. On the Ubiquity of Molecular Anions in the Dense Interstellar Medium. *Astrophys. J.* **2013**, *770*, 48.

(39) Gupta, H.; Gottlieb, C. A.; McCarthy, M. C.; Thaddeus, P. A Survey of C_4H, C_6H, and C_6H^- With the Green Bank Telescope. *Astrophys. J.* **2009**, *691*, 1494−1500.

(40) Millar, T. J.; Walsh, C.; Cordiner, M. A.; Ní Chuimín, R.; Herbst, E. Hydrocarbon Anions in Interstellar Clouds and Circumstellar Envelopes. *Astrophys. J.* **2007**, *662*, L87−L90.

(41) Walsh, C.; Harada, N.; Herbst, E.; Millar, T. J. The Effects of Molecular Anions on the Chemistry of Dark Clouds. *Astrophys. J.* **2009**, *700*, 752−761.

(42) Cordiner, M. A.; Charnley, S. B. Gas-Grain Models for Interstellar Anion Chemistry. *Astrophys. J.* **2012**, *749*, 120.

(43) McElroy, D.; Walsh, C.; Markwick, A. J.; Cordiner, M. A.; Smith, K.; Millar, T. J. The UMIST Database for Astrochemistry 2012. *Astron. Astrophys.* **2013**, *550*, A36.

(44) Sakai, N.; Sakai, T.; Osamura, Y.; Yamamoto, S. Detection of C_6H^- toward the Low-Mass Protostar IRAS 04368 + 2557 in L1527. *Astrophys. J.* **2007**, *667*, L65−L68.

(45) Harada, N.; Herbst, E. Modeling Carbon Chain Anions in L1527. *Astrophys. J.* **2008**, *685*, 272−280.

(46) Cordiner, M. A.; Millar, T. J. Density-Enhanced Gas and Dust Shells in a New Chemical Model for IRC+10216. *Astrophys. J.* **2009**, *697*, 68−78.

(47) Woods, P. M.; Walsh, C.; Cordiner, M. A.; Kemper, F. The Chemistry of Extragalactic Carbon Stars. *Mon. Not. R. Astron. Soc.* **2012**, *426*, 2689−2702.

(48) Kumar, S. S.; Hauser, D.; Jindra, R.; Best, T.; Roučka, Š.; Geppert, W. D.; Millar, T. J.; Wester, R. Photodetachment as Destruction Mechanism for CN^- and C_3N^- Anions in Circumstellar Envelopes. *Astrophys. J.* **2013**, *776*, 25.

(49) Millar, T. J. Chemistry in AGB Stars: Successes and Challenges. *J. Phys.: Conf. Ser.* **2016**, *728*, 052001.

(50) Lindal, G. F.; Wood, G. E.; Hotz, H. B.; Sweetnam, D. N.; Eshleman, V. R.; Tyler, G. L. The Atmosphere of Titan - An Analysis of the Voyager 1 Radio Occultation Measurements. *Icarus* **1983**, *53*, 348−363.

(51) Hanel, R.; Conrath, B.; Flasar, F. M.; Kunde, V.; Maguire, W.; Pearl, J.; Pirraglia, J.; Samuelson, R.; Herath, L.; Allison, M.; Cruikshank, D.; Gautier, D.; Gierasch, P.; Horn, L.; Koppany, R.; Ponnamperuma, C. Infrared Observations of the Saturnian System from Voyager 1. *Science* **1981**, *212*, 192−200.

(52) Kunde, V. G.; Aikin, A. C.; Hanel, R. A.; Jennings, D. E.; Maguire, W. C.; Samuelson, R. E. C_4H_2, HC_3N and C_2N_2 in Titan's Atmosphere. *Nature* **1981**, *292*, 686−688.

(53) Maguire, W. C.; Hanel, R. A.; Jennings, D. E.; Kunde, V. G.; Samuelson, R. E. C_3H_8 and C_3H_4 in Titan's Atmosphere. *Nature* **1981**, *292*, 683−686.

(54) Samuelson, R. E.; Hanel, R. A.; Kunde, V. G.; Maguire, W. C. Mean Molecular Weight and Hydrogen Abundance of Titan's Atmosphere. *Nature* **1981**, *292*, 688−693.

(55) Yung, Y. L.; Allen, M.; Pinto, J. P. Photochemistry of the Atmosphere of Titan - Comparison between Model and Observations. *Astrophys. J., Suppl. Ser.* **1984**, *55*, 465−506.

(56) Lutz, B. L.; de Bergh, C.; Owen, T. Titan - Discovery of Carbon Monoxide in its Atmosphere. *Science* **1983**, *220*, 1374−1375.

(57) Samuelson, R. E.; Maguire, W. C.; Hanel, R. A.; Kunde, V. G.; Jennings, D. E.; Yung, Y. L.; Aikin, A. C. CO_2 on Titan. *J. Geophys. Res.* **1983**, *88*, 8709−8715.

(58) Cravens, T. E.; Robertson, I. P.; Waite, J. H., Jr.; Yelle, R. V.; Kasprzak, W. T.; Keller, C. N.; Ledvina, S. A.; Niemann, H. B.; Luhmann, J. G.; McNutt, R. L.; Ip, W.-H.; De La Haye, V.; Mueller-Wodarg, I.; Wahlund, J.-E.; Anicich, V. G.; Vuitton, V. Composition of Titan's Ionosphere. *Geophys. Res. Lett.* **2006**, *33*, L07105.

(59) Vuitton, V.; Yelle, R. V.; Anicich, V. G. The Nitrogen Chemistry of Titan's Upper Atmosphere Revealed. *Astrophys. J.* **2006**, *647*, L175−L178.

(60) Waite, J. H.; Young, D. T.; Cravens, T. E.; Coates, A. J.; Crary, F. J.; Magee, B.; Westlake, J. The Process of Tholin Formation in Titan's Upper Atmosphere. *Science* **2007**, *316*, 870−875.

(61) Teanby, N. A.; Irwin, P. G. J.; de Kok, R.; Nixon, C. A.; Coustenis, A.; Bézard, B.; Calcutt, S. B.; Bowles, N. E.; Flasar, F. M.; Fletcher, L.; Howett, C.; Taylor, F. W. Latitudinal Variations of HCN, HC_3N, and C_2N_2 in Titan's Stratosphere Derived from Cassini CIRS Data. *Icarus* **2006**, *181*, 243−255.

(62) Vinatier, S.; Bézard, B.; Fouchet, T.; Teanby, N. A.; de Kok, R.; Irwin, P. G. J.; Conrath, B. J.; Nixon, C. A.; Romani, P. N.; Flasar, F. M.; Coustenis, A. Vertical Abundance Profiles of Hydrocarbons in Titan's Atmosphere at 15° S and 80° N Retrieved from Cassini/CIRS Spectra. *Icarus* **2007**, *188*, 120−138.

(63) Cui, J.; Galand, M.; Yelle, R. V.; Vuitton, V.; Wahlund, J.-E.; Lavvas, P. P.; Mueller-Wodarg, I. C. F.; Cravens, T. E.; Kasprzak, W. T.; Waite, J. H., Jr. Diurnal Variations of Titan's Ionosphere. *J. Geophys. Res.* **2009**, *114*, A06310.

(64) Coates, A. J.; Crary, F. J.; Lewis, G. R.; Young, D. T.; Waite, J. H., Jr.; Sittler, E. C. Discovery of Heavy Negative Ions in Titan's Ionosphere. *Geophys. Res. Lett.* **2007**, *34*, L22103.

(65) Coates, A. J.; Wellbrock, A.; Lewis, G. R.; Jones, G. H.; Young, D. T.; Crary, F. J.; Waite, J. H. Heavy Negative Ions in Titan's Ionosphere: Altitude and Latitude Dependence. *Planet. Space Sci.* **2009**, *57*, 1866−1871.

(66) Capone, L. A.; Whitten, R. C.; Dubach, J.; Prasad, S. S.; Huntress, W. T., Jr. The Lower Ionosphere of Titan. *Icarus* **1976**, *28*, 367−380.

(67) Borucki, W. J.; Levin, Z.; Whitten, R. C.; Keesee, R. G.; Capone, L. A.; Summers, A. L.; Toon, O. B.; Dubach, J. Predictions of the Electrical Conductivity and Charging of the Aerosols in Titan's Atmosphere. *Icarus* **1987**, *72*, 604−622.

(68) Molina-Cuberos, G. J.; López-Moreno, J. J.; Rodrigo, R. Influence of Electrophilic Species on the Lower Ionosphere of Titan. *Geophys. Res. Lett.* **2000**, *27*, 1351−1354.

(69) Vuitton, V.; Lavvas, P.; Yelle, R. V.; Galand, M.; Wellbrock, A.; Lewis, G. R.; Coates, A. J.; Wahlund, J.-E. Negative Ion Chemistry in Titan's Upper Atmosphere. *Planet. Space Sci.* **2009**, *57*, 1558−1572.

(70) Chaizy, P.; Reme, H.; Sauvaud, J. A.; D'Uston, C.; Lin, R. P.; Larson, D. E.; Mitchell, D. L.; Anderson, K. A.; Carlson, C. W.; Korth, A.; Mendis, D. A. Negative Ions in the Coma of Comet Halley. *Nature* **1991**, *349*, 393−396.

(71) Chutjian, A.; Garscadden, A.; Wadehra, J. M. Electron Attachment to Molecules at Low Electron Energies. *Phys. Rep.* **1996**, *264*, 393−470.

(72) Burrow, P. D.; Howard, A. E.; Johnston, A. R.; Jordan, K. D. Temporary Anion States of Hydrogen Cyanide, Methyl Cyanide, and Methylene Dicyanide, Selected Cyanoethylenes, Benzonitrile, and Tetracyanoquinodimethane. *J. Phys. Chem.* **1992**, *96*, 7570−7578.

(73) Graupner, K.; Merrigan, T. L.; Field, T. A.; Youngs, T. G. A.; Marr, P. C. Dissociative Electron Attachment to HCCCN. *New J. Phys.* **2006**, *8*, 117.

(74) Schramm, A.; Weber, J. M.; Kreil, J.; Klar, D.; Ruf, M. W.; Hotop, H. Laser Photoelectron Attachment to Molecules in a Skimmed Supersonic Beam: Diagnostics of Weak Electric Fields and Attachment Cross Sections down to 20 mu eV. *Phys. Rev. Lett.* **1998**, *81*, 778−781.

(75) Field, D.; Jones, N. C.; Ziesel, J. P. Cold Electron Scattering in SF_6 and C_6F_6: Bound and Virtual State Channels. *Phys. Rev. A: At., Mol., Opt. Phys.* **2004**, *69*, 052716.

(76) Graupner, K.; Field, T. A.; Mauracher, A.; Scheier, P.; Bacher, A.; Denifl, S.; Zappa, F.; Märk, T. D. Fragmentation of Metastable SF_6^-* Ions with Microsecond Lifetimes in Competition with Autodetachment. *J. Chem. Phys.* **2008**, *128*, 104304.

(77) Compton, R. N.; Christophorou, L. G.; Hurst, G. S.; Reinhardt, P. W. Nondissociative Electron Capture in Complex Molecules and Negative Ion Lifetimes. *J. Chem. Phys.* **1966**, *45*, 4634.

(78) Harland, P. W.; Thynne, J. C. J. Autodetachment Lifetimes, Attachment Cross Sections, and Negative Ions formed by Sulfur Hexafluoride and Sulfur Tetrafluoride. *J. Phys. Chem.* **1971**, *75*, 3517−3523.

(79) Odom, R. W.; Smith, D. L.; Futrell, J. H. A Study of Electron Attachment to SF_6 and Auto-Detachment and Stabilization of SF_6^-. *J. Phys. B: At. Mol. Phys.* **1975**, *8*, 1349−1366.

(80) Rajput, J.; Lammich, L.; Andersen, L. H. Measured Lifetime of SF_6^-. *Phys. Rev. Lett.* **2008**, *100*, 153001.

(81) Graupner, K.; Field, T. A.; Saunders, G. C. Experimental Evidence for Radiative Attachment in Astrochemistry from Electron Attachment to NCCCCN. *Astrophys. J.* **2008**, *685*, L95−L98.

(82) Barsotti, S.; Ruf, M.-W.; Hotop, H. Clear Experimental Evidence for p-Wave Attachment-Threshold Behavior in Electron Attachment to Chlorine Molecules. *Phys. Rev. Lett.* **2002**, *89*, 083201.

(83) Jordan, K. D.; Burrow, P. D. Studies of the Temporary Anion States of Unsaturated Hydrocarbons by Electron Transmission Spectroscopy. *Acc. Chem. Res.* **1978**, *11*, 341−348.

(84) Sanche, L.; Schulz, G. J. Electron Transmission Spectroscopy: Rare Gases. *Phys. Rev. A: At., Mol., Opt. Phys.* **1972**, *5*, 1672−1683.

(85) Asfandiarov, N.; Nafikova, E.; Pshenichnyuk, S. Interpreting Electron Transmission Spectroscopy and Negative Ion Mass Spectrometry Data using a Spherical Potential Well Model. *J. Exp. Theor. Phys.* **2007**, *104*, 357−362.

(86) Zecca, A.; Karwasz, G. P.; Brusa, R. S. One Century of Experiments on Electron-Atom and Molecule Scattering: A Critical Review of Integral Cross-Sections. *Riv. Nuovo Cim.* **1996**, *19*, 1−146.

(87) Ferch, J.; Raith, W.; Schroder, K. Total Cross Section Measurements for Electron Scattering from Molecular Hydrogen at Very Low Energies. *J. Phys. B: At. Mol. Phys.* **1980**, *13*, 1481−1490.

(88) Allan, M. Selectivity in the Excitation of Fermi-Coupled Vibrations in CO_2 by Impact of Slow Electrons. *Phys. Rev. Lett.* **2001**, *87*, 033201.

(89) Cížek, M.; Horáček, J.; Sergenton, A.-C.; Popović, D. B.; Allan, M.; Domcke, W.; Leininger, T.; Gadéa, F. X. Inelastic Low-Energy Electron Collisions with the HBr and DBr Molecules: Experiment and Theory. *Phys. Rev. A: At., Mol., Opt. Phys.* **2001**, *63*, 062710.

(90) Ingolfsson, O.; Weik, F.; Illenberger, E. The Reactivity of Slow Electrons with Molecules at Different Degrees of Aggregation: Gas Phase, Clusters and Condensed Phase. *Int. J. Mass Spectrom. Ion Processes* **1996**, *155*, 1−68.

(91) Braun, M.; Marienfeld, S.; Ruf, M.-W.; Hotop, H. High-resolution Electron Attachment to the Molecules CCl_4 and SF_6 over Extended Energy Ranges with the (EX)LPA Method. *J. Phys. B: At, Mol. Opt. Phys.* **2009**, *42*, 125202.

(92) Mayhew, C. A.; Critchley, A. D.; Howse, D. C.; Mikhailov, V.; Parkes, M. A. Measurements of Thermal Electron Attachment Rate Coefficients to Molecules using an Electron Swarm Technique. *Eur. Phys. J. D* **2005**, *35*, 307−312.

(93) Smith, D.; Spanel, P. The SIFT and FALP Techniques; Applications to Ionic and Electronic Reactions Studies and Their Evolution to the SIFT-MS and FA-MS Analytical Methods. *Int. J. Mass Spectrom.* **2015**, *377*, 467−468.

(94) Tennyson, J. Electron−Molecule Collision Calculations Using the R-Matrix Method. *Phys. Rep.* **2010**, *491*, 29−76.

(95) Lucchese, R. R.; Takatsuka, K.; McKoy, V. Applications of the Schwinger Variational Principle to Electron-Molecule Collisions and Molecular Photoionization. *Phys. Rep.* **1986**, *131*, 147.

(96) Chourou, S. T.; Orel, A. E. Dissociative Electron Attachment to HCN and HNC. *Phys. Rev. A: At., Mol., Opt. Phys.* **2009**, *80*, 032709.

(97) Feuerbacher, S.; Sommerfeld, T.; Cederbaum, L. S. Extrapolating Bound State Data of Anions into the Metastable Domain. *J. Chem. Phys.* **2004**, *121*, 6628−6633.

(98) Sommerfeld, T.; Knecht, S. Electronic Interaction between Valence and Dipole-Bound States of the Cyanoacetylene Anion. *Eur. Phys. J. D* **2005**, *35*, 207−216.

(99) Sebastianelli, F.; Gianturco, F. A. Metastable Anions of Polyynes: Dynamics of Fragmentation/Stabilization in Planetary Atmospheres after Electron Attachment. *Eur. Phys. J. D* **2012**, *66*, 41.

(100) Gilmore, T. D.; Field, T. A. Corrigendum: Absolute Cross Sections for Dissociative Electron Attachment to HCCCN. *J. Phys. B: At., Mol. Opt. Phys.* **2015**, *48*, 179501.

(101) Illenberger, E.; Momigny, J. *Gaseous Molecular Ions: An Introduction to Elementary Processes Induced by Ionization*; Topics in Physical Chemistry; Steinkopff Verlag: Darmstadt, Germany, 1992; Vol. 2.

(102) Pelc, A.; Sailer, W.; Scheier, P.; Probst, M.; Mason, N. J.; Illenberger, E.; Märk, T. D. Dissociative Electron Attachment to Formic Acid (HCOOH). *Chem. Phys. Lett.* **2002**, *361*, 277−284.

(103) McLaughlin, B. M.; Sadeghpour, H. R.; Stancil, P. C.; Dalgarno, A.; Forrey, R. C. New H⁻ Photodetachment and Radiative Attachment Computations for Astrophysical Environments. *J. Phys.: Conf. Ser.* **2012**, *388*, 022034.

(104) Douguet, N.; Fonseca dos Santos, S.; Raoult, M.; Dulieu, O.; Orel, A. E.; Kokoouline, V. Theory of Radiative Electron Attachment to Molecules: Benchmark Study of CN⁻. *Phys. Rev. A: At., Mol., Opt. Phys.* **2013**, *88*, 052710.

(105) Douguet, N.; Fonseca dos Santos, S.; Raoult, M.; Dulieu, O.; Orel, A. E.; Kokoouline, V. Theoretical Study of Radiative Electron Attachment to CN, C₂H, and C₄H Radicals. *J. Chem. Phys.* **2015**, *142*, 234309.

(106) Khamesian, M.; Douguet, N.; Fonseca dos Santos, S.; Dulieu, O.; Raoult, M.; Brigg, W. J.; Kokoouline, V. Formation of CN⁻, C₃N⁻, and C₅N⁻ Molecules by Radiative Electron Attachment and Their Destruction by Photodetachment. *Phys. Rev. Lett.* **2016**, *117*, 123001.

(107) Carelli, F.; Gianturco, F. A.; Wester, R.; Satta, M. Formation of Cyanopolyyne Anions in the Interstellar Medium: The Possible Role of Permanent Dipoles. *J. Chem. Phys.* **2014**, *141*, 054302.

(108) Sebastianelli, F.; Gianturco, F. Stabilizing Dicyanoacetylene Anions in Planetary Atmospheres: Quantum Dynamics of its Transient Negative Ions. *Eur. Phys. J. D* **2010**, *59*, 389−398.

(109) Carelli, F.; Grassi, T.; Gianturco, F. Electron Attachment Rates for PAH Anions in the ISM and Dark Molecular Clouds: Dependence on their Chemical Properties. *Astron. Astrophys.* **2013**, *549*, A103.

(110) Carelli, F.; Satta, M.; Grassi, T.; Gianturco, F. Carbon-Rich Molecular Chains in Protoplanetary and Planetary Atmospheres: Quantum Mechanisms and Electron Attachment Rates for Anion Formation. *Astrophys. J.* **2013**, *774*, 97.

(111) Langer, W. D.; Velusamy, T.; Kuiper, T. B. H.; Peng, R.; McCarthy, M. C.; Travers, M. J.; Kovács, A.; Gottlieb, C. A.; Thaddeus, P. First Astronomical Detection of the Cumulene Carbon Chain Molecule H₂C₆ in TMC-1. *Astrophys. J.* **1997**, *480*, L63−L66.

(112) Cernicharo, J.; Heras, A. M.; Tielens, A. G. G. M.; Pardo, J. R.; Herpin, F.; Guélin, M.; Waters, L. B. F. M. Infrared Space Observatory's Discovery of C₄H₂, C₆H₂, and Benzene in CRL 618. *Astrophys. J.* **2001**, *546*, L123−L126.

(113) Field, T. A.; Slattery, A. E.; Adams, D. J.; Morrison, D. D. Experimental Observation of Dissociative Electron Attachment to S₂O and S₂O₂ with a New Spectrometer for Unstable Molecules. *J. Phys. B: At., Mol. Opt. Phys.* **2005**, *38*, 255−264.

(114) May, O.; Fedor, J.; Ibănescu, B. C.; Allan, M. Absolute Cross Sections for Dissociative Electron Attachment to Acetylene and Diacetylene. *Phys. Rev. A: At., Mol., Opt. Phys.* **2008**, *77*, 040701.

(115) May, O.; Fedor, J.; Allan, M. Absolute Dissociative Electron Attachment Cross Sections in Acetylene and its Deuterated Analogue. *Chimia* **2010**, *64*, 173−176.

(116) May, O.; Kubala, D.; Allan, M. Absolute Cross Sections for Dissociative Electron Attachment to HCN and DCN. *Phys. Rev. A: At., Mol., Opt. Phys.* **2010**, *82*, 010701.

(117) Gilmore, T.; Field, T. Absolute Cross Sections for Dissociative Electron Attachment to HCCCN. *J. Phys. B: At., Mol. Opt. Phys.* **2015**, *48*, 035201.

(118) Haxton, D. J.; McCurdy, C. W.; Rescigno, T. N. Dissociative Electron Attachment to the H₂O molecule I. Complex-Valued Potential-Energy Surfaces for the ²B₁, ²A₁, and ²B₂ Metastable States of the Water Anion. *Phys. Rev. A: At., Mol., Opt. Phys.* **2007**, *75*, 012710.

(119) Haxton, D. J.; Rescigno, T. N.; McCurdy, C. W. Dissociative Electron Attachment to the H₂O molecule. II. Nuclear Dynamics on Coupled Electronic Surfaces within the Local Complex Potential Model. *Phys. Rev. A: At., Mol., Opt. Phys.* **2007**, *75*, 012711.

(120) Tarana, M.; Houfek, K.; Horáček, J.; Fabrikant, I. I. Dissociative Electron Attachment and Vibrational Excitation of CF₃Cl: Effect of Two Vibrational Modes Revisited. *Phys. Rev. A: At., Mol., Opt. Phys.* **2011**, *84*, 052717.

(121) Chourou, S. T.; Orel, A. E. Dissociative Electron Attachment to HCN, HCCH and HCCCN. *J. Phys.: Conf. Ser.* **2011**, *300*, 012014.

(122) Sebastianelli, F.; Carelli, F.; Gianturco, F. Forming NCCN⁻ by Quantum Scattering: A Modeling for Titans Atmosphere. *Chem. Phys.* **2012**, *398*, 199−205.

(123) Baccarelli, I.; Sebastianelli, F.; Nestmann, B. M.; Gianturco, F. A. Forming Metastable Carbon-Rich Anions in Planetary Atmospheres: the Case of Diacetylene. *Eur. Phys. J. D* **2013**, *67*, 93.

(124) Carelli, F.; Grassi, T.; Sebastianelli, F.; Gianturco, F. Electron-Attachment Rates for Carbon-Rich Molecules in Protoplanetary Atmospheres: The Role of Chemical Differences. *Mon. Not. R. Astron. Soc.* **2013**, *428*, 1181−1184.

(125) Simpson, M. J.; Tuckett, R. P. Vacuum-UV Negative Photoion Spectroscopy of Gas-Phase Polyatomic Molecules. *Int. Rev. Phys. Chem.* **2011**, *30*, 197−273.

(126) Szymańska, E.; Čadež, I.; Krishnakumar, E.; Mason, N. J. Electron Impact Induced Anion Production in Acetylene. *Phys. Chem. Chem. Phys.* **2014**, *16*, 3425−3432.

(127) Wexler, S. Associative and Non-Associative Ion Pair Formation by Fast Atoms. *Ber. Bunsen-Ges. Phys. Chem.* **1973**, *77*, 606−627.

(128) Wexler, S.; Parks, E. Molecular Beam Studies of Collisional Ionization and Ion-Pair Formation. *Annu. Rev. Phys. Chem.* **1979**, *30*, 179−213.

(129) Andersen, T.; Haugen, H. K.; Hotop, H. Binding Energies in Atomic Negative Ions: III. *J. Phys. Chem. Ref. Data* **1999**, *28*, 1511−1533.

(130) Pegg, D. J. Structure and Dynamics of Negative Ions. *Rep. Prog. Phys.* **2004**, *67*, 857−905.

(131) Simons, J. Theoretical Study of Negative Molecular Ions. *Annu. Rev. Phys. Chem.* **2011**, *62*, 107−128.

(132) Simons, J. Molecular Anions. *J. Phys. Chem. A* **2008**, *112*, 6401−6511.

(133) Dzhonson, A.; Gerlich, D.; Bieske, E. J.; Maier, J. P. Apparatus for the Study of Electronic Spectra of Collisionally Cooled Cations: Para-Dichlorobenzene. *J. Mol. Struct.* **2006**, *795*, 93−97.

(134) Mulin, D.; Roučka, Š; Jusko, P.; Zymak, I.; Plašil, R.; Gerlich, D.; Wester, R.; Glosík, J. H/D Exchange in reactions of OH⁻ with D₂ and of OD⁻ with H₂ at Low Temperatures. *Phys. Chem. Chem. Phys.* **2015**, *17*, 8732−8739.

(135) Jusko, P.; Roučka, Š; Mulin, D.; Zymak, I.; Plašil, R.; Gerlich, D.; Čížek, M.; Houfek, K.; Glosík, J. Interaction of O⁻ and H₂ at Low Temperatures. *J. Chem. Phys.* **2015**, *142*, 014304.

(136) Smith, I. W.; Rowe, B. R. Reaction Kinetics at Very Low Temperatures: Laboratory Studies and Interstellar Chemistry. *Acc. Chem. Res.* **2000**, *33*, 261−268.

(137) Quemener, G.; Julienne, P. S. Ultracold Molecules under Control! *Chem. Rev.* **2012**, *112*, 4949−5011.

(138) Andersen, T. Atomic Negative Ions: Structure, Dynamics and Collisions. *Phys. Rep.* **2004**, *394*, 157−313.

(139) Génévriez, M.; Urbain, X. Animated-Beam Measurement of the Photodetachment Cross Section of H⁻. *Phys. Rev. A: At., Mol., Opt. Phys.* **2015**, *91*, 033403.

(140) Pino, T.; Tulej, M.; Güthe, F.; Pachkov, M.; Maier, J. P. Photodetachment Spectroscopy of the C₂ₙH⁻ (n = 2−4) Anions in the Vicinity of their Electron Detachment Threshold. *J. Chem. Phys.* **2002**, *116*, 6126−6131.

(141) Neumark, D. M. Probing Chemical Dynamics with Negative Ions. *J. Chem. Phys.* **2006**, *125*, 132303.

(142) Best, T.; Otto, R.; Trippel, S.; Hlavenka, P.; von Zastrow, A.; Eisenbach, S.; Jézouin, S.; Wester, R.; Vigren, E.; Hamberg, M.;

Geppert, W. D. Absolute Photodetachment Cross-Section Measurements for Hydrocarbon Chain Anions. *Astrophys. J.* **2011**, *742*, 63.

(143) Douguet, N.; Kokoouline, V.; Orel, A. E. Photodetachment Cross Sections of the C_2nH^- (n= 1−3) Hydrocarbon-Chain Anions. *Phys. Rev. A: At., Mol., Opt. Phys.* **2014**, *90*, 063410.

(144) Robicheaux, F. Electron-Impact Detachment of Weakly Bound Negative ions: Threshold and Scaling Laws. *Phys. Rev. A: At., Mol., Opt. Phys.* **1999**, *60*, 1206−1215.

(145) Rost, J. M. Threshold Detachment of Negative Ions by Electron Impact. *Phys. Rev. Lett.* **1999**, *82*, 1652−1655.

(146) Wannier, G. H. The Threshold Law for Single Ionization of Atoms or Ions by Electrons. *Phys. Rev.* **1953**, *90*, 817−825.

(147) Andersen, L.; Mathur, D.; Schmidt, H.; Vejby-Christensen, L. Electron-Impact Detachment of D^-: Near-Threshold Behavior and the Nonexistence of D_2-Resonances. *Phys. Rev. Lett.* **1995**, *74*, 892−895.

(148) Vejby-Christensen, L.; Kella, D.; Mathur, D.; Pedersen, H. B.; Schmidt, H. T.; Andersen, L. H. Electron-Impact Detachment from Negative Ions. *Phys. Rev. A: At., Mol., Opt. Phys.* **1996**, *53*, 2371−2378.

(149) Fritioff, K.; Sandström, J.; Andersson, P.; Hanstorp, D.; Hellberg, F.; Thomas, R.; Geppert, W.; Larsson, M.; Österdahl, F.; Collins, G. F.; Pegg, D. J.; Danared, H.; Källberg, A.; Gibson, N. D. Single and Double Detachment from H^-. *Phys. Rev. A: At., Mol., Opt. Phys.* **2004**, *69*, 042707.

(150) Svendsen, A.; Lammich, L.; Sanggaard, M.; Andersen, L. H. Electron-Impact Detachment from PO_n^- (n = 0−3). *Phys. Rev. A: At., Mol., Opt. Phys.* **2007**, *76*, 032707.

(151) Bruhns, H.; Kreckel, H.; Miller, K.; Lestinsky, M.; Seredyuk, B.; Mitthumsiri, W.; Schmitt, B. L.; Schnell, M.; Urbain, X.; Rappaport, M. L.; Havener, C. C.; Savin, D. W. A Novel Merged Beams Apparatus to Study Anion-Neutral Reactions. *Rev. Sci. Instrum.* **2010**, *81*, 013112.

(152) Miller, K. A.; Bruhns, H.; Eliášek, J.; Čížek, M.; Kreckel, H.; Urbain, X.; Savin, D. W. Associative Detachment of H^- + H → H_2 + e^-. *Phys. Rev. A: At., Mol., Opt. Phys.* **2011**, *84*, 052709.

(153) Miller, K. A.; Bruhns, H.; Čížek, M.; Eliášek, J.; Cabrera-Trujillo, R.; Kreckel, H.; O'Connor, A. P.; Urbain, X.; Savin, D. W. Isotope Effect for Associative Detachment: $H(D)^- + H(D) \rightarrow H_2(D_2)+e^-$. *Phys. Rev. A: At., Mol., Opt. Phys.* **2012**, *86*, 032714.

(154) Eichelberger, B.; Barckholtz, C.; Stepanovic, M.; Bierbaum, V.; Snow, T. Laboratory Anion Chemistry: Implications for the DIBs, and a Potential Formation Mechanism for a Known Interstellar Molecule. In *Proceedings of the NASA Laboratory Astrophysics Workshop*; NASA/CP-2002-211863; Salama, F., Ed.; NASA: Washington, DC, 2002; pp 120−123.

(155) Eichelberger, B.; Snow, T. P.; Barckholtz, C.; Bierbaum, V. M. Reactions of H, N, and O Atoms with Carbon Chain Anions of Interstellar Interest: An Experimental Study. *Astrophys. J.* **2007**, *667*, 1283−1289.

(156) Jusko, P.; Roučka, Š; Plašil, R.; Glosík, J. Determining the Energy Distribution of Electrons Produced in Associative Detachment: The electron spectrometer with multipole trap. *Int. J. Mass Spectrom.* **2013**, *352*, 19−28.

(157) Gerlich, D.; Jusko, P.; Roučka, Š; Zymak, I.; Plašil, R.; Glosík, J. Ion Trap Studies of H^- + H → H_2 + e^- between 10 and 135 K. *Astrophys. J.* **2012**, *749*, 22.

(158) Phelps, A. Laboratory Studies of Electron Attachment and Detachment Processes of Aeronomic Interest. *Can. J. Chem.* **1969**, *47*, 1783−1793.

(159) Ranjan, R.; Goodyear, C. Collisional Detachment from Atmospheric Negative Ions. *J. Phys. B: At. Mol. Phys.* **1973**, *6*, 1070−1078.

(160) Champion, R. Collisional Detachment of Negative Ions. In *Advances in Electronics and Electron Physics*; Marton, C., Ed.; Academic Press, 1982; Vol. *58*; pp 143−189.

(161) Čížek, M.; Horáček, J.; Thiel, F. A. U.; Hotop, H. Associative Detachment in Low-Energy Collisions between Hydrogen Atoms and Atomic Halogen Anions. *J. Phys. B: At., Mol. Opt. Phys.* **2001**, *34*, 983−1004.

(162) Zivanov, S.; Čížek, M.; Horáček, J.; Allan, M. Electron Spectra for Associative Detachment in Low-Energy Collisions of Cl^- and Br^- with H and D. *J. Phys. B: At., Mol. Opt. Phys.* **2003**, *36*, 3513−3531.

(163) Koike, F. Theory of Electron Detachment in Slow Anion Impact on Atoms. *J. Phys. B: At. Mol. Phys.* **1987**, *20*, 1965−1982.

(164) Luque, A.; Gordillo-Vázquez, F. Mesospheric Electric Breakdown and Delayed Sprite Ignition Caused by Electron Detachment. *Nat. Geosci.* **2012**, *5*, 22−25.

(165) Ard, S.; Garrett, W.; Compton, R.; Adamowicz, L.; Stepanian, S. Rotational States of Dipole-Bound Anions of Hydrogen Cyanide. *Chem. Phys. Lett.* **2009**, *473*, 223−226.

(166) Suess, L.; Liu, Y.; Parthasarathy, R.; Dunning, F. Dipole-Bound Negative Ions: Collisional Destruction and Blackbody-Radiation-Induced Photodetachment. *J. Chem. Phys.* **2003**, *119*, 12890−12894.

(167) Desfrançois, C.; Abdoul-Carime, H.; Khelifa, N.; Schermann, J. From $1/r$ to $1/r^2$ Potentials: Electron Exchange Between Rydberg Atoms and Polar Molecules. *Phys. Rev. Lett.* **1994**, *73*, 2436−2439.

(168) Glover, S. C.; Savin, D. W.; Jappsen, A.-K. Cosmological Implications of the Uncertainty in H^- Destruction Rate Coefficients. *Astrophys. J.* **2006**, *640*, 553−568.

(169) Smith, D.; Adams, N. G.; Alge, E. Ion−Ion Mutual Neutralization and Ion−Neutral Switching Reactions of Some Stratospheric Ions. *Planet. Space Sci.* **1981**, *29*, 449−454.

(170) Adams, N. G.; Smith, D. Laboratory Studies of Dissociative Recombination and Mutual Neutralisation and Their Relevance to Interstellar Chemistry. *Astrophys. Space Sci. Libr.* **1988**, *146*, 173−192.

(171) Hickman, A. P. Approximate Formula for Ion−Ion Mutual Neutralization Rates. *J. Chem. Phys.* **1979**, *70*, 4872−4878.

(172) Urbain, X.; Lecointre, J.; Mezdari, F.; Miller, K. A.; Savin, D. W. Merged-Beam Study of Mutual Neutralization of H^- and H^+. *J. Phys.: Conf. Ser.* **2012**, *388*, 092004.

(173) Stenrup, M.; Larson, Å.; Elander, N. Mutual Neutralization in Low-Energy H^+ + H^- Collisions: A Quantum Ab Initio Study. *Phys. Rev. A: At., Mol., Opt. Phys.* **2009**, *79*, 012713.

(174) Croft, H.; Dickinson, A. S.; Gadéa, F. X. Rate Coefficients for the Li^+/H^- and Li^-/H^+ Mutual Neutralization Reactions. *Mon. Not. R. Astron. Soc.* **1999**, *304*, 327−329.

(175) Miller, T. M.; Shuman, N. S.; Viggiano, A. Behavior of Rate Coefficients for Ion−Ion Mutual Neutralization, 300−550 K. *J. Chem. Phys.* **2012**, *136*, 204306.

(176) Shuman, N. S.; Wiens, J. P.; Miller, T. M.; Viggiano, A. A. Kinetics of Ion−Ion Mutual Neutralization: Halide Anions with Polyatomic Cations. *J. Chem. Phys.* **2014**, *140*, 224309.

(177) Wiens, J. P.; Shuman, N. S.; Viggiano, A. A. Dissociative Recombination and Mutual Neutralization of Heavier Molecular Ions: $C_{10}H_8^+$, WF_5^+, and $C_nF_m^+$. *J. Chem. Phys.* **2015**, *142*, 114304.

(178) Mezei, J. Z.; Roos, J. B.; Shilyaeva, K.; Elander, N.; Larson, Å. Mutual Neutralization in Low-Energy H^+ + F^- Collisions. *Phys. Rev. A: At., Mol., Opt. Phys.* **2011**, *84*, 012703.

(179) Liu, C. L.; Wang, J. G.; Janev, R. K. Mutual Neutralization in Slow H_2^+−H^- Collisions. *J. Phys. B: At., Mol. Opt. Phys.* **2006**, *39*, 1223−1229.

(180) Mikosch, J.; Weidemüller, M.; Wester, R. On the Dynamics of Chemical Reactions of Negative Ions. *Int. Rev. Phys. Chem.* **2010**, *29*, 589−617.

(181) DePuy, C. H. An Introduction to the Gas Phase Chemistry of Anions. *Int. J. Mass Spectrom.* **2000**, *200*, 79−96.

(182) Geppert, W. D.; Larsson, M. Experimental Investigations into Astrophysically Relevant Ionic Reactions. *Chem. Rev.* **2013**, *113*, 8872−8905.

(183) Larsson, M.; Geppert, W. D.; Nyman, G. Ion Chemistry in Space. *Rep. Prog. Phys.* **2012**, *75*, 066901.

(184) Ervin, K. M. Experimental Techniques in Gas-Phase Ion Thermochemistry. *Chem. Rev.* **2001**, *101*, 391−444.

(185) Mirsaleh-Kohan, N.; Bass, A. D.; Cloutier, P.; Massey, S.; Sanche, L. Low Energy Electron Stimulated Desorption from DNA Films Dosed with Oxygen. *J. Chem. Phys.* **2012**, *136*, 235104.

(186) Böhler, E.; Warneke, J.; Swiderek, P. Control of Chemical Reactions and Synthesis by Low-Energy Electrons. *Chem. Soc. Rev.* **2013**, *42*, 9219–9231.

(187) Pirim, C.; Gann, R.; McLain, J.; Orlando, T. Electron-Molecule Chemistry and Charging Processes on Organic Ices and Titan's Icy Aerosol Surrogates. *Icarus* **2015**, *258*, 109–119.

(188) Balog, R.; Cicman, P.; Jones, N.; Field, D. Spontaneous Dipole Alignment in Films of N$_2$O. *Phys. Rev. Lett.* **2009**, *102*, 073003.

(189) Plekan, O.; Cassidy, A.; Balog, R.; Jones, N. C.; Field, D. A New form of Spontaneously Polarized Material. *Phys. Chem. Chem. Phys.* **2011**, *13*, 21035–21044.

(190) Jensen, E. T.; Sanche, L. Electron Transfer Reactions for Image and Image-Derived States in Dielectric Thin Films. *J. Chem. Phys.* **2008**, *129*, 074703.

(191) Fabrikant, I. I. Dissociative Electron Attachment to CH$_3$I on Surfaces and in Bulk Media: Vibrational Feshbach Resonance Suppression. *J. Phys. B: At., Mol. Opt. Phys.* **2011**, *44*, 225202.

(192) Fabrikant, I. I.; Caprasecca, S.; Gallup, G. A.; Gorfinkiel, J. D. Electron Attachment to Molecules in a Cluster Environment. *J. Chem. Phys.* **2012**, *136*, 184301.

(193) Lu, Q.-B.; Sanche, L. Enhanced Dissociative Electron Attachment to CF$_2$Cl$_2$ by Transfer of Electrons in Precursors to the Solvated State in Water and Ammonia Ice. *Phys. Rev. B: Condens. Matter Mater. Phys.* **2001**, *63*, 153403.

(194) van Broekhuizen, F. A.; Pontoppidan, K. M.; Fraser, H. J.; van Dishoeck, E. F. A 3–5 μm VLT Spectroscopic Survey of Embedded Young Low Mass Stars II. Solid OCN$^-$. *Astron. Astrophys.* **2005**, *441*, 249–260.

(195) Iskandarov, I.; Gianturco, F. A.; Carelli, F.; Yurtsever, E.; Wester, R. Exploring a Dynamical Path for C$_2$H$^-$ and NCO$^-$ Formation in Dark Molecular Clouds. *Eur. Phys. J. D* **2016**, *70*, 38.

(196) Yurtsever, E.; Gianturco, F. A.; Wester, R. Forming NCO$^-$ in Dense Molecular Clouds: Possible Gas-Phase Chemical Paths From Quantum Calculations. *J. Phys. Chem. A* **2016**, *120*, 4693–4701.

(197) Martinez, R.; Bordalo, V.; da Silveira, E. F.; Boechat-Roberty, H. M. Production of NH$_4^+$ and OCN$^-$ Ions by the Interaction of Heavy-Ion Cosmic Rays with CO-NH$_3$ Interstellar Ice. *Mon. Not. R. Astron. Soc.* **2014**, *444*, 3317–3327.

(198) Mispelaer, F.; Theule, P.; Duvernay, F.; Roubin, P.; Chiavassa, T. Kinetics of OCN$^-$ Formation from the HNCO + NH$_3$ Solid-State Thermal Reaction. *Astron. Astrophys.* **2012**, *540*, A40.

(199) Hecht, T.; Winter, H.; Borisov, A. G.; Gauyacq, J. P.; Kazansky, A. K. Role of the 2D Surface State Continuum and Projected Band Gap in Charge Transfer in Front of a Cu(111) Surface. *Phys. Rev. Lett.* **2000**, *84*, 2517–2520.

(200) Obreshkov, B.; Thumm, U. H$^-$ Formation in Collisions of Hydrogen Atoms with Al(100) Surfaces. *Phys. Rev. A: At., Mol, Opt. Phys.* **2013**, *87*, 022903.

(201) Lienemann, J.; Blauth, D.; Wethekam, S.; Busch, M.; Winter, H.; Wurz, P.; Fuselier, S.; Hertzberg, E. Negative Ion Formation During Scattering of Fast Ions from Diamond-Like Carbon Surfaces. *Nucl. Instrum. Methods Phys. Res., Sect. B* **2011**, *269*, 915–918.

(202) Millar, T. J.; Bennett, A.; Rawlings, J. M. C.; Brown, P. D.; Charnley, S. B. Gas Phase Reactions and Rate Coefficients for Use in Astrochemistry - The UMIST Ratefile. *Astron. Astrophys. Suppl. Ser.* **1991**, *87*, 585–619.

(203) Millar, T. J.; Farquhar, P. R. A.; Willacy, K. The UMIST Database for Astrochemistry 1995. *Astron. Astrophys., Suppl. Ser.* **1997**, *121*, 139–185.

(204) Le Teuff, Y. H.; Millar, T. J.; Markwick, A. J. The UMIST Database for Astrochemistry 1999. *Astron. Astrophys., Suppl. Ser.* **2000**, *146*, 157–168.

(205) Woodall, J.; Agúndez, M.; Markwick-Kemper, A. J.; Millar, T. J. The UMIST database for Astrochemistry 2006. *Astron. Astrophys.* **2007**, *466*, 1197–1204.

(206) Wakelam, V.; et al. A Kinetic Database for Astrochemistry (KIDA). *Astrophys. J., Suppl. Ser.* **2012**, *199*, 21.

(207) Prasad, S. S.; Tarafdar, S. P. UV Radiation Field inside Dense Clouds - Its Possible Existence and Chemical Implications. *Astrophys. J.* **1983**, *267*, 603–609.

(208) Bettens, R. P. A.; Lee, H.-H.; Herbst, E. The Importance of Classes of Neutral-Neutral Reactions in the Production of Complex Interstellar Molecules. *Astrophys. J.* **1995**, *443*, 664–674.

(209) Terzieva, R.; Herbst, E. The Sensitivity of Gas-Phase Chemical Models of Interstellar Clouds to C and O Elemental Abundances and to a New Formation Mechanism for Ammonia. *Astrophys. J.* **1998**, *501*, 207–220.

(210) Smith, I. W. M.; Herbst, E.; Chang, Q. Rapid Neutral-Neutral Reactions at Low Temperatures: A New Network and First Results for TMC-1. *Mon. Not. R. Astron. Soc.* **2004**, *350*, 323–330.

(211) Harada, N.; Herbst, E.; Wakelam, V. A New Network for Higher-temperature Gas-phase Chemistry. I. A Preliminary Study of Accretion Disks in Active Galactic Nuclei. *Astrophys. J.* **2010**, *721*, 1570–1578.

(212) Wakelam, V.; et al. The 2014 KIDA Network for Interstellar Chemistry. *Astrophys. J. Suppl. Ser.* **2015**, *217*, 20.

(213) Bettens, R. P. A.; Herbst, E. The Formation of Large Hydrocarbons and Carbon Clusters in Dense Interstellar Clouds. *Astrophys. J.* **1997**, *478*, 585–593.

(214) Petrie, S. Novel Pathways to CN$^-$ within Interstellar Clouds and Circumstellar Envelopes: Implications for IS and CS Chemistry. *Mon. Not. R. Astron. Soc.* **1996**, *281*, 137–144.

(215) Ruffle, D. P.; Bettens, R. P. A.; Terzieva, R.; Herbst, E. The Abundance of C$_7^-$ in Diffuse Clouds. *Astrophys. J.* **1999**, *523*, 678–682.

(216) Szczepanski, J.; Ekern, S.; Vala, M. Vibrational Spectroscopy of Small Matrix-Isolated Linear Carbon Cluster Anions. *J. Phys. Chem. A* **1997**, *101*, 1841–1847.

(217) Mathis, J. S.; Mezger, P. G.; Panagia, N. Interstellar Radiation Field and Dust Temperatures in the Diffuse Interstellar Matter and in Giant Molecular Clouds. *Astron. Astrophys.* **1983**, *128*, 212–229.

(218) Barckholtz, C.; Snow, T. P.; Bierbaum, V. M. Reactions of C$_n^-$ and C$_n$H$^-$ with Atomic and Molecular Hydrogen. *Astrophys. J.* **2001**, *547*, L171–L174.

(219) Güthe, F.; Tulej, M.; Pachkov, M. V.; Maier, J. P. Photodetachment Spectrum of l-C$_3$H$_2^-$: The Role of Dipole Bound States for Electron Attachment in Interstellar Clouds. *Astrophys. J.* **2001**, *555*, 466–471.

(220) Wakelam, V.; Herbst, E. Polycyclic Aromatic Hydrocarbons in Dense Cloud Chemistry. *Astrophys. J.* **2008**, *680*, 371–383.

(221) Adams, N. G.; Smith, D.; Viggiano, A. A.; Paulson, J. F.; Henchman, M. J. Dissociative Attachment Reactions of Electrons with Strong Acid Molecules. *J. Chem. Phys.* **1986**, *84*, 6728–6731.

(222) Bierbaum, V. University of Colorado, Boulder, Colorado. Personal communication, 2008.

(223) Hasegawa, T. I.; Herbst, E. New Gas-Grain Chemical Models of Quiescent Dense Interstellar Clouds - The Effects of H$_2$ Tunnelling Reactions and Cosmic Ray Induced Desorption. *Mon. Not. R. Astron. Soc.* **1993**, *261*, 83–102.

(224) Willacy, K.; Rawlings, J. M. C.; Williams, D. A. Molecular Desorption from Dust in Star-Forming Regions. *Mon. Not. R. Astron. Soc.* **1994**, *269*, 921–927.

(225) Yang, Z.; Cole, C. A.; Martinez, O., Jr.; Carpenter, M. Y.; Snow, T. P.; Bierbaum, V. M. Experimental and Theoretical Studies of Reactions between H atoms and Nitrogen-Containing Carbanions. *Astrophys. J.* **2011**, *739*, 19.

(226) Shu, F. H.; Adams, F. C.; Lizano, S. Star Formation in Molecular Clouds - Observation and Theory. *Annu. Rev. Astron. Astrophys.* **1987**, *25*, 23–81.

(227) Hollenbach, D. J.; Tielens, A. G. G. M. Dense Photo-dissociation Regions (PDRs). *Annu. Rev. Astron. Astrophys.* **1997**, *35*, 179–215.

(228) Le Petit, F.; Nehmé, C.; Le Bourlot, J.; Roueff, E. A Model for Atomic and Molecular Interstellar Gas: The Meudon PDR Code. *Astrophys. J., Suppl. Ser.* **2006**, *164*, 506–529.

(229) Teyssier, D.; Fossé, D.; Gerin, M.; Pety, J.; Abergel, A.; Roueff, E. Carbon Budget and Carbon Chemistry in Photon Dominated Regions. *Astron. Astrophys.* **2004**, *417*, 135−149.

(230) Papadopoulos, P. P.; Thi, W.-F.; Viti, S. Molecular Gas in Spiral Galaxies: A New Warm Phase at Large Galactocentric Distances? *Astrophys. J.* **2002**, *579*, 270−274.

(231) Bell, T. A.; Roueff, E.; Viti, S.; Williams, D. A. Molecular Line Intensities as Measures of Cloud Masses - I. Sensitivity of CO Emissions to Physical Parameter Variations. *Mon. Not. R. Astron. Soc.* **2006**, *371*, 1865−1872.

(232) Smith, D.; Church, M. J.; Miller, T. M. Mutual Neutralization of Simple and Clustered Positive and Negative Ions. *J. Chem. Phys.* **1978**, *68*, 1224−1229.

(233) Schmidt, H. T.; Johansson, H. A. B.; Thomas, R. D.; Geppert, W. D.; Haag, N.; Reinhed, P.; Rosén, S.; Larsson, M.; Danared, H.; Rensfelt, K.-G.; Liljeby, L.; Bagge, L.; Björkhage, M.; Blom, M.; Löfgren, P.; Källberg, A.; Simonsson, An.; Paál, A.; Zettergren, H.; Cederquist, H. DESIREE as a New Tool for Interstellar Ion Chemistry. *Int. J. Astrobiol.* **2008**, *7*, 205−208.

(234) Gatchell, M.; et al. First Results from the Double ElectroStatic Ion-Ring ExPeriment, DESIREE. *J. Phys.: Conf. Ser.* **2014**, *488*, 092003.

(235) Kasai, Y.; Kagi, E.; Kawaguchi, K. Analysis of Radio Astronomical Data of the Negative Ion C_6H^- in IRC + 10 216. *Astrophys. J.* **2007**, *661*, L61−L64.

(236) Jura, M.; Morris, M. Model for the Circumstellar Gas around Alpha Orionis. *Astrophys. J.* **1981**, *251*, 181−189.

(237) Li, X.; Millar, T. J.; Walsh, C.; Heays, A. N.; van Dishoeck, E. F. Photodissociation and Chemistry of N_2 in the Circumstellar Envelope of Carbon-Rich AGB Stars. *Astron. Astrophys.* **2014**, *568*, A111.

(238) Agúndez, M.; Cernicharo, J. Oxygen Chemistry in the Circumstellar Envelope of the Carbon-Rich Star IRC + 10216. *Astrophys. J.* **2006**, *650*, 374−393.

(239) Petrie, S.; Herbst, E. Some Interstellar Reactions Involving Electrons and Neutral Species: Attachment and Isomerization. *Astrophys. J.* **1997**, *491*, 210−215.

(240) Brünken, S.; Gottlieb, C. A.; Gupta, H.; McCarthy, M. C.; Thaddeus, P. Laboratory Detection of the Negative Molecular Ion CCH^-. *Astron. Astrophys.* **2007**, *464*, L33−L36.

(241) Gottlieb, C. A.; Brünken, S.; McCarthy, M. C.; Thaddeus, P. The Rotational Spectrum of CN^-. *J. Chem. Phys.* **2007**, *126*, 191101.

(242) Amano, T. Extended Negative Glow and "Hollow Anode" Discharges for Submillimeter-Wave Observation of CN^-, C_2H^-, and C_4H^-. *J. Chem. Phys.* **2008**, *129*, 244305.

(243) Prasad, S. S.; Huntress, W. T., Jr. A Model for Gas Phase Chemistry in Interstellar Clouds. I - The Basic Model, Library of Chemical Reactions, and Chemistry among C, N, and O Compounds. *Astrophys. J., Suppl. Ser.* **1980**, *43*, 1−35.

(244) Mackay, G.; Tanaka, K.; Bohme, D. Rate Constants at 297 K for Proton-Transfer Reactions with C_2H_2: An Assessment of the Average Quadrupole Orientation Theory. *Int. J. Mass Spectrom. Ion Phys.* **1977**, *24*, 125−136.

(245) Gianturco, F. A.; Satta, M.; Mendolicchio, M.; Palazzetti, F.; Piserchia, A.; Barone, V.; Wester, R. Exploring a Chemical Path for the Formation of Stable Anions of Polyynes in Molecular Clouds. *Astrophys. J.* **2016**, *830*, 2.

(246) Mauron, N.; Huggins, P. J. Multiple Shells in IRC+10216: Shell Properties. *Astron. Astrophys.* **2000**, *359*, 707−715.

(247) Brown, J. M.; Millar, T. J. Modelling Enhanced Density Shells in the Circumstellar Envelope of IRC + 10216. *Mon. Not. R. Astron. Soc.* **2003**, *339*, 1041−1047.

(248) Li, X.; Heays, A. N.; Visser, R.; Ubachs, W.; Lewis, B. R.; Gibson, S. T.; van Dishoeck, E. F. Photodissociation of Interstellar N_2. *Astron. Astrophys.* **2013**, *555*, A14.

(249) Decin, L.; et al. Warm Water Vapour in the Sooty Outflow from a Luminous Carbon Star. *Nature* **2010**, *467*, 64−67.

(250) Agúndez, M.; Cernicharo, J.; Guélin, M. Photochemistry in the Inner Layers of Clumpy Circumstellar Envelopes: Formation of Water in C-rich Objects and of C-bearing Molecules in O-rich Objects. *Astrophys. J., Lett.* **2010**, *724*, L133−L136.

(251) Satta, M.; Gianturco, F. A.; Carelli, F.; Wester, R. A Quantum Study of the Chemical Formation of Cyano Anions in Inner Cores and Diffuse Regions of Interstellar Molecular Clouds. *Astrophys. J.* **2015**, *799*, 228.

(252) Capone, L. A.; Dubach, J.; Whitten, R. C.; Prasad, S. S.; Santhanam, K. Cosmic Ray Synthesis of Organic Molecules in Titan's Atmosphere. *Icarus* **1980**, *44*, 72−84.

(253) Borucki, W. J.; Whitten, R. C.; Bakes, E. L. O.; Barth, E.; Tripathi, S. Predictions of the Electrical Conductivity and Charging of the Aerosols in Titan's Atmosphere. *Icarus* **2006**, *181*, 527−544.

(254) Lebonnois, S.; Bakes, E. L. O.; McKay, C. P. Transition from Gaseous Compounds to Aerosols in Titan's Atmosphere. *Icarus* **2002**, *159*, 505−517.

(255) Bakes, E. L. O.; McKay, C. P.; Bauschlicher, C. W. Photoelectric Charging of Submicron Aerosols and Macromolecules in the Titan Haze. *Icarus* **2002**, *157*, 464−475.

(256) Vuitton, V.; Yelle, R. V.; McEwan, M. J. Ion Chemistry and N-Containing Molecules in Titan's Upper Atmosphere. *Icarus* **2007**, *191*, 722−742.

(257) Vuitton, V.; Yelle, R. V.; Cui, J. Formation and Distribution of Benzene on Titan. *J. Geophys. Res.* **2008**, *113*, E05007.

(258) Vuitton, V.; Yelle, R. V.; Lavvas, P.; Klippenstein, S. J. Rapid Association Reactions at Low Pressure: Impact on the Formation of Hydrocarbons on Titan. *Astrophys. J.* **2012**, *744*, 11.

(259) Hébrard, E.; Dobrijevic, M.; Loison, J. C.; Bergeat, A.; Hickson, K. M.; Caralp, F. Photochemistry of C_3H_p Hydrocarbons in Titan's Stratosphere Revisited. *Astron. Astrophys.* **2013**, *552*, A132.

(260) Dobrijevic, M.; Hébrard, E.; Loison, J. C.; Hickson, K. M. Coupling of Oxygen, Nitrogen, and Hydrocarbon Species in the Photochemistry of Titan's Atmosphere. *Icarus* **2014**, *228*, 324−346.

(261) Loison, J. C.; Hébrard, E.; Dobrijevic, M.; Hickson, K. M.; Caralp, F.; Hue, V.; Gronoff, G.; Venot, O.; Bénilan, Y. The Neutral Photochemistry of Nitriles, Amines and Imines in the Atmosphere of Titan. *Icarus* **2015**, *247*, 218−247.

(262) Dobrijevic, M.; Loison, J. C.; Hickson, K. M.; Gronoff, G. 1D-Coupled Photochemical Model of Neutrals, Cations and Anions in the Atmosphere of Titan. *Icarus* **2016**, *268*, 313−339.

(263) Cordiner, M. A.; Charnley, S. B. Negative Ion Chemistry in the Coma of Comet 1P/Halley. *Meteoritics and Planetary Science* **2014**, *49*, 21−27.

(264) Rodgers, S. D.; Charnley, S. B. A Model of the Chemistry in Cometary Comae: Deuterated Molecules. *Mon. Not. R. Astron. Soc.* **2002**, *330*, 660−674.

(265) Kroto, H. W.; Heath, J. R.; O'Brien, S. C.; Curl, R. F.; Smalley, R. E. C_{60}: Buckminsterfullerene. *Nature* **1985**, *318*, 162−163.

(266) Cami, J.; Bernard-Salas, J.; Peeters, E.; Malek, S. E. Detection of C_{60} and C_{70} in a Young Planetary Nebula. *Science* **2010**, *329*, 1180−1182.

(267) Elhamidi, O.; Pommier, J.; Abouaf, R. Low-energy Electron Attachment to Fullerenes C_{60} and C_{70} in the Gas Phase. *J. Phys. B: At., Mol. Opt. Phys.* **1997**, *30*, 4633−4642.

(268) Amusia, M. Y.; Baltenkov, A. S.; Krakov, B. G. Photodetachment of Negative C_{60}^- Ions. *Phys. Lett. A* **1998**, *243*, 99−105.

(269) Huang, D.-L.; Dau, P. D.; Liu, H.-T.; Wang, L.-S. High-Resolution Photoelectron Imaging of Cold C_{60}^- Anions and Accurate Determination of the Electron Affinity of C_{60}. *J. Chem. Phys.* **2014**, *140*, 224315.

(270) Fortenberry, R. C.; Huang, X.; Crawford, T. D.; Lee, T. J. Quantum Chemical Rovibrational Data for the Interstellar Detection of c-C_3H^-. *Astrophys. J.* **2014**, *796*, 139.

(271) Fortenberry, R. C.; Lukemire, J. A. Electronic and Rovibrational Quantum Chemical Analysis of C_3P^-: The Next Interstellar Anion? *Mon. Not. R. Astron. Soc.* **2015**, *453*, 2824−2829.

(272) Güthe, F.; Tulej, M.; Pachkov, M. V.; Maier, J. P. Photodetachment Spectrum of l-$C_3H_2^-$: The Role of Dipole Bound States for Electron Attachment in Interstellar Clouds. *Astrophys. J.* **2001**, *555*, 466−471.

(273) Botschwina, P.; Oswald, R. Coupled Cluster Calculations for (Potential) Interstellar Anions: The $C_{2n}H^-$ Series (n = 2−6). *Int. J. Mass Spectrom.* **2008**, *277*, 180−188.

(274) Blanksby, S. J.; McAnoy, A. M.; Dua, S.; Bowie, J. H. Cumulenic and Heterocumulenic Anions: Potential Interstellar Species? *Mon. Not. R. Astron. Soc.* **2001**, *328*, 89−100.

(275) Armitage, P. J. Dynamics of Protoplanetary Disks. *Annu. Rev. Astron. Astrophys.* **2011**, *49*, 195−236.

AE